NONCOVALENT INTERACTIONS IN PERFLUORINATED MEDIA

by

Kristi L. O'Neal

BS, Frostburg State University, 2004

Submitted to the Graduate Faculty of

Arts and Sciences in partial fulfillment

of the requirements for the degree of

Doctor of Philosophy

University of Pittsburgh

2009

UNIVERSITY OF PITTSBURGH

GRADUATE ARTS AND SCIENCES

This dissertation was presented

by

Kristi L. O'Neal

It was defended on

June 2, 2009

and approved by

Dr. Stephen G. Weber, Department of Chemistry

Dr. Sunil Saxena, Professor, Department of Chemistry

Dr. Craig S. Wilcox, Professor, Department of Chemistry

Dr. Robert M. Enick, Professor, Department of Chemical and Petroleum Engineering

Reproduced with permission from:

O'Neal, K.; Geib, S.; Weber, S. G. *Analytical Chemistry,* **2007**, *79*, 3117-3125; O'Neal, K. L. Weber, S. G., *The Journal of Physical Chemistry B,* **2009**, *113*, 149-158; and O'Neal, K. L. Weber, S. G., *The Journal of Physical Chemistry B,* **2009**, *113*, 7449-7456.

NONCOVALENT INTERACTIONS IN PERFLUORINATED MEDIA

Kristi L. O'Neal, PhD

University of Pittsburgh, 2009

Molecular receptors enhance extraction efficacy when incorporated into a receiving phase. Extraction selectivity is defined as the ratio of the relative concentrations of analyte and interfering species in each phase. Recognition-based extractions are highly selective if target/receptor interactions dominate the free energy change for the extraction process. As the receiving phase becomes a poorer solvent, selectivity increases. Noncovalent interactions between target and receptor are strengthened while the solubility of interfering compounds is decreased. Perfluorinated (fluorous) liquids are exceptionally non-polar, poor solvents that should increase the extraction selectivity by reducing the extraction of interfering species. Synthetic chemists have focused on fluorous biphasic separations of catalysts, reactants, and products based on fluorophilicity using covalently attached perfluoroalkyl tags. Until recently, noncovalent approaches had not been explored. This work is focused on developing a fundamental understanding of noncovalent interactions in fluorous environments. Quantification of the strength of such associations should have application reaching far beyond the synthetic community.

The application of perfluoropolyether carboxylic acid receptors to fluorous biphasic extractions of pyridine-like bases, including porphyrins, is explored. UV, IR, X-ray crystallography, and quantitative continuous variations plots leads to an understanding of complex formation in the fluorous phase. We quantified free energy of formation of the hydrogen bond between the receptor and pyridine (-39 kJ mol^{-1}) in perfluorohexanes at room temperature. This is the first reported hydrogen bond strength in a fluorous environment.

The solvent environment affects complex formation significantly. We wondered if nonpolar fluorous liquids could support proton transfer. We show that the protonated pyridine is 'solvated' by carboxylic acids, making the local environment more polarizable than the bulk solvent. Investigations of complexation between N-heterocyclic bases and carboxylic acids in a range of solvents showed that proton transfer occurs in fluorous environments when both the acid/base ratio and the ΔpK_a between the acid and conjugate acid of the base are sufficiently high. Remarkably, we have observed solvation of a hexavalent porphyrin cation in the fluorous phase. The fundamental understanding of molecular recognition in fluorous liquids should provide opportunities for development in sensing and separation applications.

TABLE OF CONTENTS

LIST OF TABLES

LIST OF FIGURES

LIST OF EQUATIONS

LIST OF SCHEMES

PREFACE

I would like to take a moment to acknowledge those people in my life who have contributed to my success in graduate school, without whom, this dissertation could not have been completed.

I will be forever indebted to my parents for teaching me the value of a good education and supporting my dreams throughout this long process (not to mention the extra spending money). Thanks Mom and Dad!

I would like to express my gratitude to my advisor and mentor, Dr. Stephen Weber, who has given me the autonomy to choose the direction of my project and the opportunity to grow into an independent scientist. I have learned a great deal from his guidance and expertise. It will be a bittersweet day when I leave the group but fortunately, I won't be going far.

I am tremendously grateful for the friends that I have made along the way, especially Amy Hamsher. We have shared so many memories. You have encouraged me through frustrating times and been there to celebrate the good times. I feel very fortunate to have the support of such a good friend; I could not have made it through this program without you.

I would also like to express my appreciation to the entire Weber group (past and present) for their helpful comments and insights on my many practice presentations. And thank you for participating in and contributing to the group's social activities and making a more enjoyable work environment.

Last, but certainly not least, I would like to thank Douglas Kauffman for showing me that everything I have always wanted was right here all along. If it hadn't been for you, I would have never found the job that is everything I could have asked for. Now I will get stay close to my friends and family and be just as happy with my family life as with my professional life. For that, I cannot thank you enough.

1.0 INTRODUCTION

1.1 SAMPLE PREPARATION

Over the past few decades, rapidly advancing technology and increasingly powerful computing has led unprecedented advances in measurement techniques and scientific instrumentation. Even with these advances in instrumentation and automation, most systems of interest still require some pretreatment steps, collectively known as sample preparations. Sample preparation methods have been developed to clean up the sample matrix and preconcentrate the target analyte with the overall goal to enhance the measurement signal. Despite the significant impact that sample preparation methods have on the success of the overall analytical process, they have traditionally been laborious, time consuming, waste generating, and practically neglected by the research community.[4] However, because of developments in high-throughput measurements, sample preparations are often the rate-determining step in the analytical process, thus driving the need for improvement. In addition, increasing awareness of our impact on the environment has placed a greater emphasis on analytical methods that produce less waste.

Extractions are the most widely used sample preparation techniques. The goal of any extraction is the selective removal of a target analyte from the sample matrix. Liquid-liquid

extraction (LLE) is a method to separate compounds based on their partitioning between two immiscible liquid phases.[5] LLE is an equilibrium process, thermodynamically driven by a difference in chemical potential of the solute in each phase. Sample clean up is achieved through designing the system to have a high selectivity for analyte partitioning and preconcentration is achieved when the analyte has a high distribution coefficient (D_c) between phase *a* and *b*. D_c, given by **Equation 1-1**, is the ratio of concentrations in each phase multiplied by the volume (V) phase ratio ($\Phi = V_b/V_a$).

$$D_c = \frac{C_{x,b}}{C_{x,a}}\Phi$$

Equation 1-1

D_C is distinguished from a partition coefficient (K_c) in that D_c includes all forms of the sample component (ie. free, complexed, ionized, dimerized, etc.) while K_c only considers one particular form (ie. only the free form).

Solid-phase extraction (SPE) was originally developed as a solvent-free alternative to LLE and is now one of the most common sampling techniques in environmental, pharmaceutical, clinical, and food chemistry.[6] In SPE, analytes are exhaustively removed from a flowing sample matrix by transfer and sorption to a solid phase. SPE methods are distinct from filtration methods because, in SPE, the molecules become associated with the solid phase through sorption. Solid phase microextraction (SPME) is another widely accepted sorbent technique that was later developed by the Pawliszyn group.[7,8] SPME involves non-equilibrium removal of chemical

constituents from a sample matrix via retention on a sorbent with subsequent desorption of target analytes. SPME differs from SPE in that the sorbent material is coated on a fine rod, allowing rapid mass transfer during extraction/desorption that results in fast, simple separations in a solvent-free system. Two main processes are involved, (1) partitioning of analytes between the sample matrix and sorbent, and (2) desorption of concentrated analytes for analysis.[8] Therefore, selection of the sorbent material can be crucial to the success of the separation. It must be able to sorb sample constituents rapidly and reproducibly[9] yet components must be easily eluted from the sorbent,[10] meaning that the sorption process must be reversible. Although silica is commonly applied as the solid phase in SPE and SPME, there is no universal sorbent for all applications[11] and retention behaviors can vary dramatically between sorbent materials. Therefore, it is necessary to continue to explore new materials for SPE and SPME applications and design sorbents for specific analyte/matrix systems.

The selectivity of an extraction is defined as the ratio of the relative concentrations of the analyte and interfering species in the two phases. High selectivity is commonly achieved through choice of extraction solvent, manipulation of the physical properties of the extracting solvent (i.e. temperature and pressure), or by the application of restricted access media (RAM) and molecularly imprinted polymers (MIPs).[12] It has also been shown that extraction selectivity is enhanced through incorporating an artificial molecular receptor into the receiving phase.[13,14]

1.2 MOLECULAR RECOGNITION

Molecular recognition is a chemical phenomenon involving three-dimensional interactions between a receptor and substrate and is one of the most fundamental processes in chemistry,

biology, and physics. Selectivity is largely driven by non-covalent forces, including hydrogen bond, hydrophobicity, ionic, and π–π interactions. These selective interactions play an essential role in many life processes, including DNA complementary base pairing, t-RNA binding to amino acids, enzyme-substrate binding, neurotransmitter and neuropeptide binding at receptors, cell organelle self-assembly, and pheromone-mediated chemical communication.[15] The lock-and-key model, proposed by Emil Fischer over a century ago, is still one of the most widely accepted models. It involves 1:1 complexation between substrate and receptor with binding sites that are complementary in size, shape and spatial arrangement of functional groups, in many ways similar to a lock and key.

The application of molecular recognition to current technologies is limited only by the imagination and numerous receptors have been designed to bind targeted substrates of chemical or biological significance. A greater understanding of these interactions would have many applications in supramolecular chemistry, where host-guest chemistry, molecular recognition, and self-assembly are collectively applied to develop multi-molecular complexes possesing magnetic properties, light responsiveness, and catalytic activity that a single molecule cannot. Supramolecular research has been applied to the development of chemical sensors, self-healing polymers, processes to treat radioactive waste, compact information storage devices for computers, high-performance catalysis for industrial processes, and contrast agents for CAT scans.[16] Artificial receptors have also been used to design synthetic recognition scaffolds that reproduces econdary structure features at protein-protein interfaces, and have promising applications in identifying inhibitors of protein-protein interactions.[17]

Our group has done a great deal of work combining molecular recognition processes with separation and sample preparation methods, specifically on analytical applications of barbital

receptors. Valenta *et al.*[18] observed a 40-fold increase in extraction efficiency when they incorporated an artificial molecular receptor (**Figure 1-1**) into a chloroform receiving phase in the extraction of phenobarbital from human control serum compared with receptor-free. This work was pivotal in demonstrating the effectiveness of artificial receptors in analytical applications.

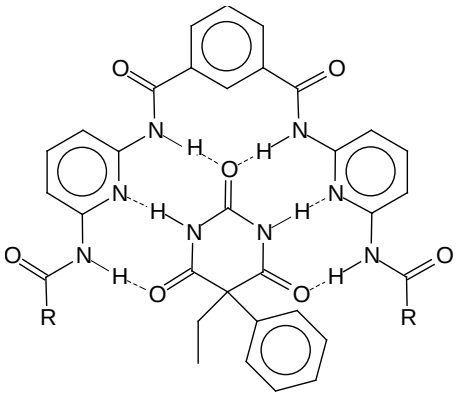

Figure 1-1. Artificial molecular receptor (R = 1-propyl) binding with phenobarbital.

A study of extractions based on molecular recognition in plasticizer/chloroform solutions was later performed. This set up the groundwork for Li *et al.*[14] to develop a plasticized poly(vinyl chloride) (PVC) extraction medium coated on a fine rod for SPME with capillary electrophoresis (CE) detection of barbiturates (**Figure 1-2**).

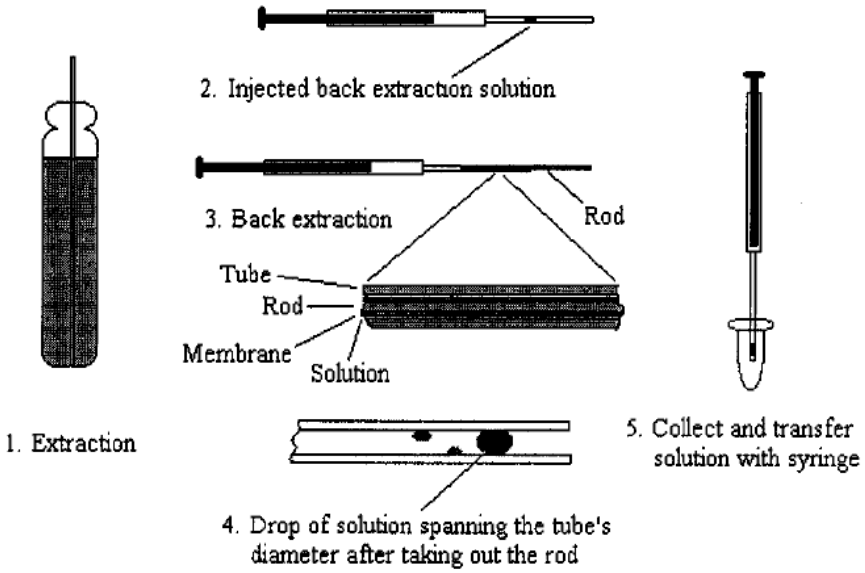

Figure 1-2. Reproduced with permission from Li *et al.,*[14] SPME device and operation. (1) Place rod in sample solution for a designated amount of time. (2) Inject 5 μL of backextraction solution into the Teflon tube. (3) Remove rod, wipe clean, place in Teflon tube, and (4) remove after a set time. (5) Collect the solution by moving the droplet spanning the diameter as a piston and transfer the drop to an injecton vial.

In molecular recognition-based extractions, selectivity for a target is high if non-covalent intermolecular interactions between receptor and target dominate the standard-state free energy change for the extraction process. These interactions become less important in competitive solvents,[19] thus a matrix that is a poor solvent will provide a more selective environment for molecular recognition interactions.[14,20]

1.3 FLUOROUS SOLVENTS

Fluorous liquids are highly non-polar and notoriously poor solvents[21] that have been particularly useful for increasing selectivity in liquid-liquid extractions by reducing the unintentional extraction of interfering matrix species.[22-24] An appealing property to the field of separation science is the simultaneous hydrophobic and oleophobic nature of these materials, often leading to the exclusion of non-fluorinated molecules.[14] Horvath[23] first suggested that the affinity of a molecule for a fluorous phase can be manipulated by attaching varying numbers and lengths of 'pony tails' in the form of $(CH_2)_m(CF_2)_{n-1}$. This led to interest in the field of fluorous biphasic chemistry for synthesis and purification. Curran[25,26] and Wipf[27] developed fluorous tagging strategies to selectively isolate target analytes from complicated sample matricies. Curran and coworkers[28] also developed the fluorous triphasic reaction in which a liquid-liquid separation is directly coupled with a chemical reaction to produce a pure product from impure starting material. In addition to separations and derivitization, recent innovations suggest a wide range of potential applicatons of fluorous tags for identification resulting from distinctive signatures in mass spectrometry and ^{19}F NMR.[29]

Synthetic fluorous separations, made possible by covalent labeling of a product precursor or catalyst with a fluorous tag, result in easy separation of the labeled entities through extraction with fluorous liquids. However, non-covalent approaches based on non-covalent complex formation are more straightforward and have wider applicability outside of the synthetic community. Molecular recognition in combination with fluorous matrices should improve the selectivity of extractions by 1) reducing the amount of interfering species extracted and 2) eliminating solute-solvent competition, effectively increasing the strength of substrate-receptor interactions.[22,23] Thus, a fluorous-solvent or polymer-based extraction with a molecular receptor

component should be quite selective. Although considerable research has recently been devoted to understanding the properties of highly fluorinated systems, little is known about the interactions that take place in them.

The general problem exists to develop receptors that are moderate-to-highly soluble in such poor solvents, yet retain functional groups with the ability to participate in molecular recognition interactions. These criteria are met by highly fluorinated receptors with carboxylic-acid end groups. Depending on the length and nature of the perfluorinated chain, the resulting receptor-substrate complex can be rendered exclusively soluble in the highly non-polar fluorous liquid, thus achieving an excellent separation. The ability of the receptor to realize separations by enticing the polar substrate into the highly non-polar fluorous phase through hydrogen bonding should be a promising alternative to the covalently linked ponytails previously used in fluorous biphasic extractions.

1.4 THE EXTRACTION SYSTEM

1.4.1 Fluorous Receptor

A 'good' receptor will bind strongly with the target analyte (i.e. have a high formation constant) and enhance the selectivity of an extraction while a 'poor' solvent will decrease the extraction of interfering or unwanted matrix species. The required properties for good receptors in fluorous biphasic extractions generally include moderate solubility in the non-polar fluorous phase, low solubility in the organic phase to prevent back extraction of the receptor and/or the complex, and a high formation constant with the substrate. Among the limited number of perfluorinated

compounds available, perflurocarboxylic acids fit these criteria well. Carboxylic acids play an important role in molecular recognition and have been used as receptors for aminopyridines[30] and for the self-assembly of pyrazine carboxylic acid.[31] A wide variety of perfluoroalkanoic acids of varying lengths are commercially available; however, the rigidity of the perfluorinated chain results in low solubility in both fluorous and organic liquids. Krytox 157FSx (where x = L, M, or H) is a perfluoropolyether whose ether oxygens offer much more flexibility than the straight perfluroalkanoic chains and, abundant ether oxygens non-withstanding, is extremely hydrophobic and soluble only in highly fluorinated solvents.[32] Krytox is available in molecular weights ranging from 2500 to 7500 g/mol (designated by L, M or H) and can be obtained terminated with almost any functional group imaginable. A carboxylic acid terminated Krytox 157FSH (**1**) at the high molecular weight range would be an excellent choice for a fluorous receptor; the high molecular weight (longer fluorous chain) would ensure that the receptor stays in the fluorous phase and the carboxylic acid end group has been demonstrated to have superior hydrogen bonding capabilities toward amide-like hydrogen bond acceptors.

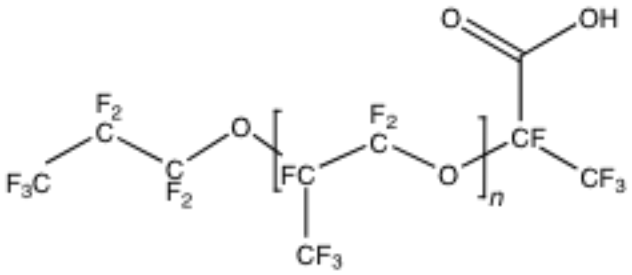

1

1.4.2 Fluorous Receiving Phase

As mentioned earlier, a nonpolar, poorly-solvating matrix strenghtens noncovalent molecular-recognition interactions by reducing solvent competition. We chose 3M's FC-72 Fluorinert Electronic Liquid, a mixture of perfluorohexanes, as the nonpolar receiving phase in fluorous biphasic LLEs. **Figure 1-3**[33] shows that FC-72 is the most nonpolar, highly fluorous solvent commonly used in fluorous biphasic separations, therefore, it is logical to begin the study of noncovalent interaction in this liquid.

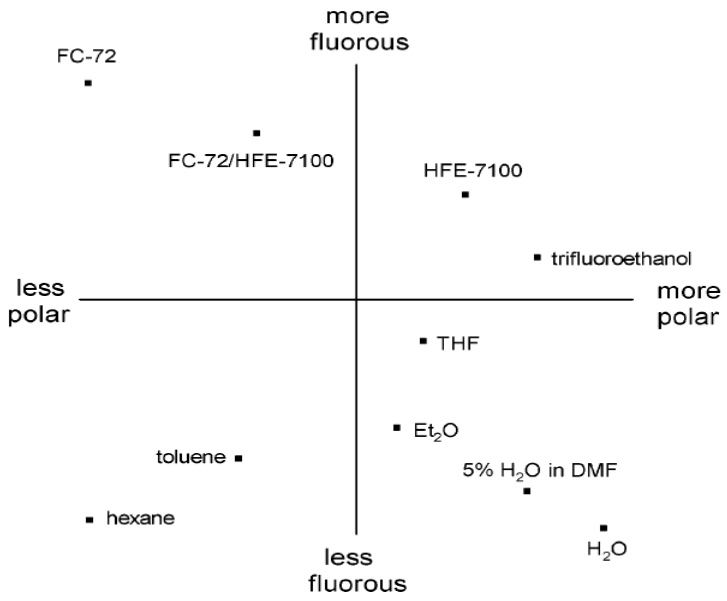

Figure 1-3. Reproduced with permission from Yu *et al.*[33] A qualitative representation of various solvent systems commonly used in fluorous biphasic separations.

FC-72 is clear and colorless, thermally and chemically stable, compatible with sensitive materials, nonflammable, non-toxic, and leaves no residue upon evaporation. This unique

combination of properties makes FC-72 ideal for many electronics applications and it's inertness makes it a useful reaction medium.[34] In addition, the boiling point (56 °C) is very close to that of chloroform (61 °C), which we have used as the source phase in fluorous biphasic extractions.

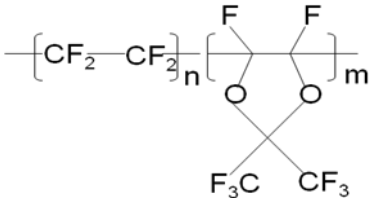

Teflon AF2400

2

Teflon AF2400 (**2**) is a chemically inert and thermally stable amorphous fluorinated polymer used as the sorbent phase in our flurous-SPEs. It is a copolymer of tetrafluoroethylene (13%) and 2,2-bistrifluoromethyl-4,5-difluoro-1,3 dioxole (87%). Thin films are easily prepared through solvent casting and are transparent through a wide UV-Vis and IR range, making them ideal for studying intermolecular interactions in films. Sorption and permeation studies of light gases,[35,36] C_1-C_{12} hydrocarbons,[36,37] C_1-C_7 perfluorocarbons,[36] chlorinated hydrocarbons,[37] and small alcohols,[37] in Teflon AF films have revealed high permeabilites and large fractional free volumes (FFVs). Recently, Lai *et al.*[38] have developed ion-selective electrodes (ISEs) for pH measurements with membranes composed of **2** containing a linear perfluorooligoether plasticizer, sodium tetrakis[3,5-bis(perfluorohexyl)phenyl]borate for ionic sites, and bis[(perfluorooctyl)propyl]-2,2,2-trifluoroethylamine as an H^+ ionophore. Although the

electrodes exhibited high potentiometric selectivities, Nernstian responses to H^+ over a wide pH range, and enhanced mechanical stability, potentiometric and spectroscopic evidence showed that **2** contains COOH functional groups formed by hydrolysis of carboxylic acid fluoride groups originally present in Teflon AF2400, resulting in undesirable side effects. Fortunately, for their application, the use of higher ionophore concentrations removed any such undesirable effects of these COOH groups almost completely.

Transport studies of organic solutes from a chloroform source through **2** films to a chloroform receiving phase have shown that the solute permeability is proportional to the size of the solute.[39] In addition, the films demonstrated selectivity for fluorinated solutes in comparison to the hydrogen-containing control. **1** can easily be incorporated into **2** and was found to plasticize the films, for 50% **1** (w/w), T_g = -40 °C compared to intitial T_g = 240 °C.[39,40] However, it was also found that **1**-plasticized thin films reduce the permeability of organic solutes by decreasing their diffusivity in the films.[39] The opposite effect is expected for solutes that exhibit a favorable interaction with the carboxylic acid functional group of **1**.

1.5 OBJECTIVE

This work is aimed at improving extractions through the use of artificial receptors in fluorous liquids and thin films. The influence of a fluorous matrix on the binding strength and selectivity of non-covalent interactions is also investigated. A greater understanding of the specific interactions between receptor and substrate in fluorous matricies will add an element of predictability to fluorous biphasic extractions and thus increase the applicability of such techniques. Understanding non covalent interactions in fluorous liquids will lead to greater

advances in sensor development, research for biomedical applications, and create new avenues to self-assembly. To our knowledge, there are no previously reported systematic and quantitative studies of host/guest chemistry in fluorous media.

Chapter 2.0 details a study on the effectiveness of a carboxylic acid end-capped perfluoropolyether (PFPE) receptor (**1**) on the extraction of a series of polar substituted pyridines into a fluorous liquid (FC-72). We found that fluorous receptors enhance the selective partitioning of N-heterocyclic substrates, resulting in cleaner samples and faster separations with lower cost than the fluorous biphasic separations that employ covalently attached fluorous ponytails. Surprisingly, we observed proton transfer from **1** to pyridine, leading to a quantitative investigation of pyridine-**1** interactions. Chapter 3.0 takes a closer look at molecular and ionic hydrogen bond formation in fluorous solvents. Literature and experimental data on complexes between N-heterocyclic bases and carboxylic acids in a range of solvents were compiled to compare solvent effects on proton transfer. It becomes clear that polar solvents support ionic hydrogen bonds at a 1:1 mol ratio while ionic hydrogen bonds in nonpolar organic solvents are only observed in complexes with 1:2 (base/acid) stoichiometries. In fluorous solvents, a larger excess of acid (1:3) is necessary to facilitate proton transfer. In Chapter 4.0, our pyridine extraction study is extended to larger, more complex porphyrin substrates to develop a fundamental understanding of porphyrin-**1** interactions in a highly fluorinated matrix. This study should lead to the development of more robust and selective porphyrin-based sensors. We observed reversible extraction of 5, 10, 15, 20 -tetra(4-phenyl)porphyrin (TPhP) and 5, 10, 15, 20-tetra(4-pyridyl)porphyrin (TPyP) from $CHCl_3$ with excess **1** in FC-72. Two protons are donated from **1** to the central pyrrole ring of TPhP to create the dication (H_2TPhP^{2+}) in FC-72. The interaction between **1** and TPyP, however, is primarily on the more basic pyridyl-nitrogens

and protonation of the central pyrrole ring is a secondary interaction that only occurs with additional **1**. This chapter also examines the extraction of metalloporphyrins, common in biological and sensor applications, and the effect of competitive binding on extraction efficacy. And finally, in chapter 5.0 we study the equilibrium distribution of pyridine-like solutes between a buffered aqueous phase into **1**-receptor doped **2** thin films. In general, it was found that the presence of **1** in the fluorous film effectively increases the film/aqueous distribution coefficient for pyridine-like bases that have shown favorable interaction with **1** in FC-72 liquid-liquid extractions (LLEs) from chloroform. Primed optical fibers were then dip-coated with receptor-doped films to create a fluorous molecular recognition-based SPME device for aqueous extractions followed by direct GC thermal desorption. When compared to commercially available polydimethylsiloxane (PDMS) SPME fibers, **1**-doped Teflon AF showed greater selectivity for pyridine-like bases over their non-heterocyclic counterparts. To our knowledge, this is the first report coupling receptor-doped fluorous membrane extraction with SPME.

2.0 EXTRACTION OF PYRIDINES INTO FLUOROUS SOLVENTS BASED ON HYDROGEN BOND COMPLEX FORMATION WITH CARBOXYLIC ACID RECEPTORS

Abstract

A molecular receptor embedded in a 'poor-solvent' receiving phase, such as a fluorous phase, should offer the ideal medium for selective extraction and sensing. The limited solubility of most solutes in fluorous phases enhances selectivity by reducing the extraction of unwanted matrix material. In this work, fluorous carboxylic acids (a carboxylic-acid terminated perfluoropolypropylene oxide called Krytox and perfluorodecanoic acid (PFDA)) were used as receptors and substituted pyridines as substrates to show that the fluorous receptor dramatically enhances the liquid-liquid extraction of the polar substrates from chloroform into perfluorohexanes. The method of continuous variations was used to determine the receptor-pyridine complex stoichiometry of 3:1. The free energies of formation of the 3:1 complexes from one pyridine and 3/2 H-bonded cyclic dimers of the fluorous carboxylic acid are -30.4 kJ mol^{-1} (Krytox) and -37.3 kJ mol^{-1} (PFDA). The free energy required to dissociate the dimer in perfluorohexanes is +16.5 kJ mol^{-1} (Krytox). The crystal structure of the complex showed a 1:1 stoichiometry with a mixed strong-weak hydrogen bonded motif. Based on the stoichiometry, crystal structure, and UV and IR spectroscopic shifts, we propose that the 3:1 complex has 4

hydrogen bonds and the carboxylic acid transfers a proton to pyridine. The resulting pyridinium -carboxylate N^+H---O^- hydrogen bond is accompanied by a weak pyridine ring CH---O bond and is supported by two more carboxylic acid H-bond donors. We estimate that the free energy of formation of the pyridinium-carboxylate ion pair from a free acid, pyridine, and a carboxylic acid dimer to be about -39 kJ mol^{-1}; this is the first reported hydrogen bond strength in a fluorous environment.

2.1 INTRODUCTION

Solvent extraction, or the related more modern approaches such as supercritical fluid extraction, and pressurized fluid extractions as well as solid phase extraction and solid phase microextraction,[41] are at the heart of an extraordinary number and variety of analytical, synthetic and production operations. Despite this, the selectivity of extractions is generally quite poor. Molecular recognition or host/guest chemistry, can enhance extractions significantly.[18] Artificial receptors have been used to improve extractions of creatinine,[42] honokiol,[43] tryptophan,[44] hydrocarbons,[45] pyrimidines and xanthenes,[46] picric acid,[47] saccharides,[48] fullerenes,[49] barbiturates,[14] and even cytochrome c.[50] Ultimately, the selectivity of an extraction based on a molecular receptor dissolved in a matrix will always be limited by the solvent power of the matrix. A matrix that is a poor solvent will provide better selectivity than a matrix that is a good solvent because the poor solvent will dissolve fewer unwanted compounds while the desired compound is extracted by the receptor.

The synthetic community has recognized the value of poor solvents, namely fluorous solvents, to improve purification.[22-24] While this typically involves covalent labeling with a

fluorous functional group, host/guest chemistry has recently been shown to improve fluorous synthesis. Perfluoroalkanoic acids can act as hosts for ureas[51] and metals.[52-54] Amine[55] and phosphine[53] ligands also support metals in fluorous environments. Pyridyl tags can be used in conjunction with perfluorocarboxylate-supported copper to extract porphyrins and fullerenes.[56] Recently,[57,58] fluorous liquid-membrane cation-selective electrodes doped with tetrakis[3,5-bis(perfluorohexyl)phenyl]borate salts have shown increased selectivity with respect to conventional organic membranes. Thus, in both synthetic and analytical endeavors, molecular recognition in fluorous solvents appears to be potentially very powerful. Yet, to our knowledge, there are no systematic and quantitative studies of host/guest chemistry in fluorous media.

Fluorous liquids are highly non-polar and notoriously poor solvents.[21 22-24] An appealing property to the field of separation science is the simultaneous hydrophobic and oleophobic nature of these liquids.[14] The biological inertness, high gas solubility and ability to form micro- and nanophases has also lead to research on highly fluorinated molecules for biomedical applications such as injectible O_2 carriers, contrast agents, and drug delivery systems.[59] A significant quantity of research has been devoted to understanding the properties of highly fluorinated systems but little is known about the interactions that take place in them.

This work is aimed at improving extractions using artificial receptors in fluorous liquids. The influence of fluorous solvents on the binding strength and selectivity of non-covalent interactions is also addressed. A greater understanding of the specific interactions between receptor and substrate in fluorous liquids will add an element of predictability to fluorous biphasic extractions and thus increase the applicability of such techniques. In this study, the receptors are commercially available fluorous carboxylic acids. The substrates are highly polar substituted pyridines. We have found that pyridines are effectively extracted into a fluorous

solvent in the presence of fluorous carboxylic acids, but hardly at all in the absence of the acids. UV spectroscopy, IR spectroscopy and crystallography as well as quantitative evaluation of Job's plots leads to the understanding that, at practical laboratory concentrations (10 mM), pyridine exists in the fluorous carboxylic acid-containing fluorous phase as a complex containing 2 carboxylic acids, one carboxylate and pyridinium ion.

2.2 EXPERIMENTAL

All of the hydroxy- and amino- substituted pyridines, as well as aniline, nicotinamide (NTA), and perflurodecanoic acid (PFDA) were obtained from Aldrich (Milwaukee, WI). Phenol was obtained from EM Science (Cherry Hill, NJ) and chloroform was purchased from Fisher Scientific (Fair Lawn, NJ) and dried over molecular sieves. FC-72 Fluoroinert Electronic Liquid (a mixture of perfluorohexanes) was obtained from 3M (St. Paul, MN) and was used throughout as the 'fluorous phase'. Krytox, a perfluoropolyether (PFPE) oil (shown below), is synthesized through base-catalyzed polymerization of hexafluoropropylene oxide and is used mainly as a lubricant in high-performance applications.[32] Krytox 157FSH (**1**) with a carboxylic acid end group (present only on the propagation side of the chain) was obtained from Miller-Stephenson Chemical Co. (Morton Grove, IL). ^{19}F NMR analysis of **1** yielded a number averaged molecular weight of 5840 g mol^{-1} with an average of 33 polymer repeat units.

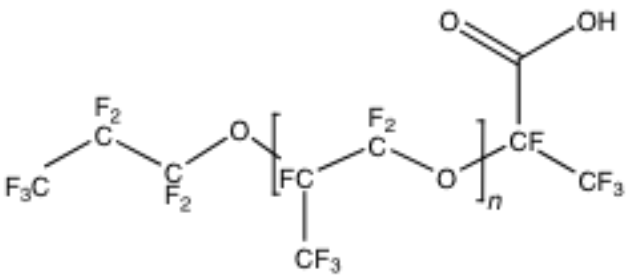

1

A Hewlett-Packard 8452A UV-Vis diode array spectrophotometer was used for all UV absorbance measurements. A quartz cell with a 0.1 cm path length was purchased from Fisher Scientific (Pittsburgh, PA) and used for all measurements.

The UV titration data were obtained by titrating 0.50 mL of **1** in FC-72 (2.15, 8.00, and 15.07 mM) with pyridine in FC-72 (1.72, 3.74, and 5.75 mM respectively). All samples were diluted to a constant volume of 1.00 mL to maintain uniformity in the extent of acid dimerization. The UV difference absorbance, as discussed by Valenta,[18] at 255 nm is related to the amount of **1**-substrate complex present in solution and was measured as a function of added pyridine. All absorbance values were measured under ambient conditions (22.0 ± 1 °C) and baseline corrected.

The UV continuous variation data were obtained by creating a series of solutions of a 1.075 mM pyridine solution in FC-72 with 2.15 mM **1** in FC-72 (or 1.075 mM $\mathbf{1}_2$) so that the molar sum of pyridine and $\mathbf{1}_2$ remained constant according to Connors.[60] All samples were shaken for 10 minutes on a mechanical shaker to ensure homogeneity and allowed to rest 10 minutes before UV measurements were made. All errors are reported as standard deviations of the mean. Likussar[61] has developed a general method for determining formation constants from

continuous variations data by normalizing all absorbances to a value corresponding to the absorbance of the complex being studied. This maximum absorbance is obtained by measuring the absorbance of a solution containing a definite excess of receptor and a substrate concentration equal to that corresponding to the maximum on the continuous variations plot. The reader is referred to his publication for a more detailed explanation, including derivation of generalized equations to describe the continuous variations plots.

For the extractions, a series of standard solute solutions were prepared in chloroform that had been dried over molecular sieves. A Cole-Parmer ultra-sonicator bath (Chicago, IL) was used to aid in the dissolution of the solid substituted pyridines. The UV absorbance of each was measured and the concentration determined according to Beer's Law. A series of solutions increasing in [**1**] were prepared in FC-72 and the containers placed in the ultra-sonicator bath for 10 minutes to ensure dissolution of the oil. Equal volumes of solute/$CHCl_3$ solution and each **1**/FC-72 solution were placed in separate GC-autosampler vials, shaken with a mechanical shaker for 10 minutes, and allowed to rest for 10 minutes. A series of samples of equal volumes each solute and FC-72 containing no **1** were prepared as controls. The layers were physically separated using a syringe and the UV absorbance of each layer was measured against a solvent blank and baseline corrected.

The IR titration data were obtained by titrating 0.25 mL of 20.0 mM **1** in FC-72 with 20.0 mM pyridine in FC-72 in increments of 0.05 mL and diluting to a constant volume of 0.50 mL to maintain uniform **1** activity. The IR spectra were measured in a KBr flow cell with a path length of 0.05 cm against an FC-72 background.

To study receptor dimerization, 119.0 mM **1** in FC-72 was diluted to create a series of solutions ranging from 0.08 – 119.0 mM **1**. The IR spectra of the resulting solutions were measured in a KBr flow cell with a path length of 0.05 cm against a FC-72 background.

For crystal growth, the mixed solvent method was used to slow the precipitation of the PFDA-pyridine crystals. PFDA (27.1 mg) was placed in 5.0 mL FC-72 (in which it is only slightly soluble) followed by 5 minutes in the ultrasonicator bath to aid in dissolution. 5.0 mL of HFE-7100 (in which PFDA is much more soluble) was added followed by 5 more minutes in the ultrasonicator bath. 20.0 μL of liquid pyridine (12.48 M) was added to the solution and ultrasonicated for 10 more minutes before being filtered and poured into a small Petri dish where it was lightly covered and allowed to cool and evaporate slowly.

2.3 RESULTS AND DISCUSSION

2.3.1 Fluorous Biphasic Extractions

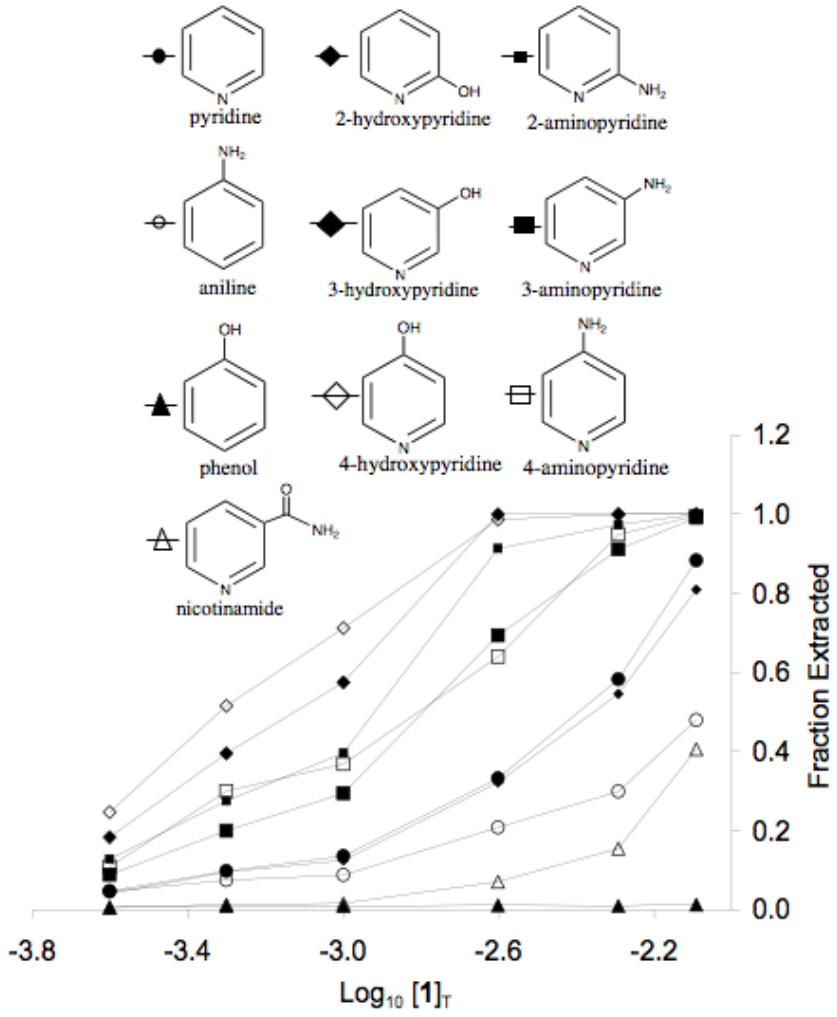

Figure 2-1. The fraction of solute extracted into a FC-72 receiving phase containing **1** is plotted against the $\log_{10}$ of the concentration of **1**. The solutes shown are: (•) 2-, (●) 3-, and (○) 4-hydroxypyridine, (■) 2-, (■) 3-, and (□) 4-aminopyridine, (◆) pyridine, (◇) aniline, (▲) nicotinamide, and (△) phenol. The data shown are from measurements of the fluorous receiving phase.

Addition of **1** to a fluorous phase is effective at enhancing the extraction of a series of highly polar substituted pyridines from chloroform (**Figure 2-1**). It has been suggested[14] that the lower the polarity of the solvent, the more the partitioning of the polar solute will be dependent on the formation of a complex. The data show that the extraction efficiency into the fluorous phase, and hence the complex formation, increases with increasing receptor concentration (see **Figure 2-1**). An increase in **1** concentration has very little effect on the extraction of phenol, a small but noticeable effect on the extraction of aniline, a significant effect on the extraction of pyridine and an even greater effect on the extraction of amino- and hydroxy- substituted pyridines. Thus, the pyridyl nitrogen is primarily responsible for binding to the carboxylic acid functional group, with the amino substituent acting as a weak hydrogen bond donor to the carbonyl group and the alcohol substituent having only a small interaction with **1**.

Table 2-1. A list of the fraction of solute extracted from a 2.0 mM solute/$CHCl_3$ solution into an equal volume of 2.0 mM **1**/FC-72 solution (**1**:solute molar ratio = 1).

Solute	Fraction Extracted
2-Hydroxypyridine	0.41
3-Hydroxypyridine	0.96
4-Hydroxypyridine	0.82
2-Aminopyridine	0.98
3-Aminopyridine	0.98
4-Aminopyridine	0.99
Pyridine	0.72
Aniline	0.05
Nicotinamide	0.09
Phenol	0.01

Values of the fraction of solute extracted into the fluorous phase containing equimolar **1** are shown in **Table 2-1**. The variance in extraction efficiency of the hydroxypyridine isomers confirms the significance of structure and tautomerism in molecular recognition interactions. **Scheme 2-1** summarizes the tautomerism of the hydroxypyridine isomers. 2HP exists predominately in the pyridone form and readily forms a H-bonded cyclic dimer,[62,63] thus the formation of the dimer stabilizes 2HP in the chloroform phase. 4HP also readily tautomerizes to the pyridone form[62] and is able to form intermolecular H-bonds with other 4HP or 4-pyridone molecules. While it is possible for 3HP to tautomerize, it is not favorable[62] and 3HP is free to interact with **1** in the pyridine form. The aminopyridine isomers all share similar extraction profiles because all three prefer the aminopyridine form. In fact, no detectable amount of pyridonimine form has been found for any of the aminopyridine isomers in a variety of solvents.[62]

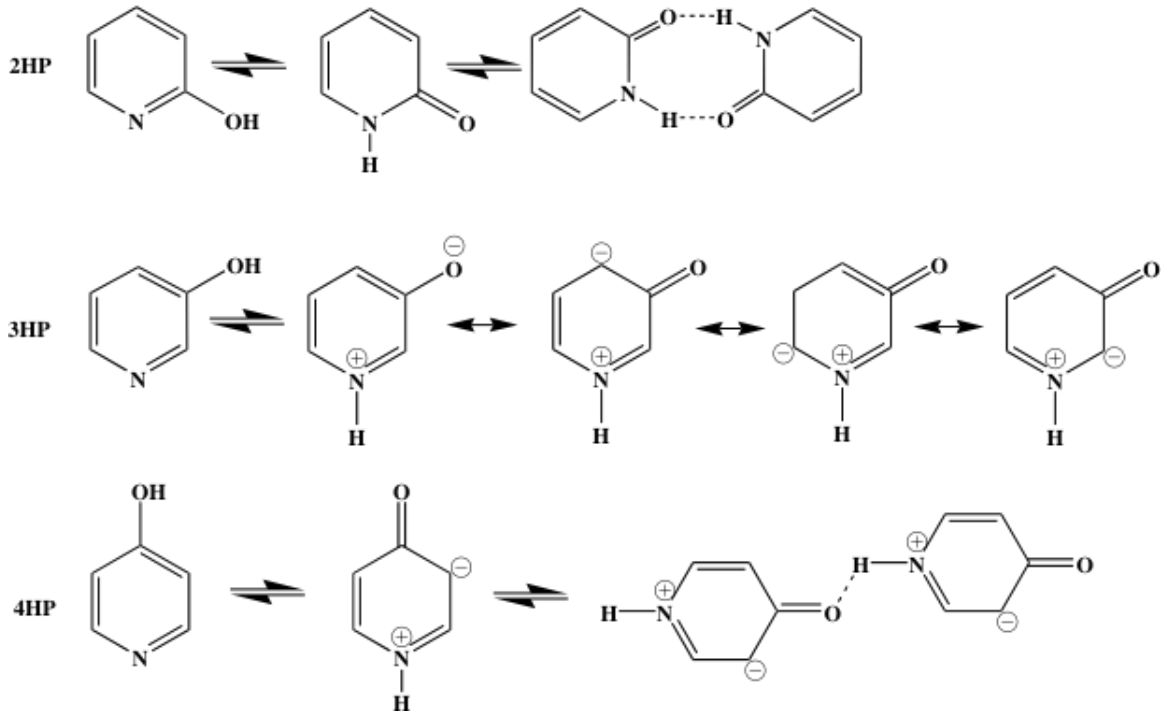

Scheme 2-1. Hydroxypyridine tautomerism.

It is well established that a pair of carboxylic acids can exist as a cyclic dimer in organic solvents.[64,65] Self-association in poor solvents should decrease the efficacy of **1** as an artificial receptor; however, it has been shown that –OH---N hydrogen bonds are more stable than the -OH---O hydrogen bonds found in cyclic carboxylic acid dimers[66]. In fact, a study of the 2001 Cambridge Structural Database (CSD) by Vishweshwar *et al.*[31] has shown that –COOH–pyridine association is found ten times more frequently (through the -OH---N hydrogen bond) than –COOH–HOOC– associations. Another CSD study by Steiner[67] has shown that most N H-bond acceptors are more successful at competing for the carboxylic acid H-bonds than the carboxylic acids themselves. In the crystalline state, both the H-bonded form, -OH---N, and the proton transfer hydrogen-bonded form, $N^{+}H$---O^{-}, are possible, the likelihood of each dependent on the acidity of the –COOH group and the basicity of the substituted pyridine.[62]

Pyridine has a distribution coefficient (D_c) of 4 x 10^{-3} (fluorous:pyridine) from pure liquid pyridine (12.48 M) to FC-72 calculated according to **Equation 2-1**

$$D_c = \frac{(1-q)}{q\Phi}$$

Equation 2-1

where q is the fraction of pyridine remaining following extraction and Φ is the volume phase ratio. However, extraction of a pyridine solution in chloroform with FC-72 resulted in no detectable pyridine in the fluorous phase. Pyridine is the structural core of all solutes that were well extracted and it is the only solute in the series that exhibits any measurable solubility in FC-72. Zhao *et al.*[40] were able to measure the partition ratio of 3-hydroxypyridine between FC-72 and chloroform as 6.7 x 10^{-5} but found it necessary to employ preconcentration coupled with capillary electrophoresis to measure the low concentrations found in the fluorous phase. Stoichiometries and formation constants for all solutes with **1** would be valuable in understanding the extractions results; however, the lack of solubility in a fluorous environment makes difficult the study of these solute complexes. Therefore, the body of this work focuses on the specific interactions between **1** and pyridine.

2.3.2 Stoichiometry and Formation Constant

The stoichiometry of the **1**-pyridine complex was determined by continuous variations methods,[60,61,68] and confirmed using the mole ratio method[69] (spectrophotometric titration) and Specfit software, to be 3:1 (**1**:pyridine) in FC-72. At higher overall concentrations (> 2 mM), photometric titrations (see supplemental material) indicate that the stoichiometry of the complex exceeds 3:1 and may become a function of receptor concentration. The UV spectra of the

fluorous receiving phase following liquid-liquid extraction (not shown) display a hypsocromic (blue) shift as the initial concentration of receptor is increased. This indicates stabilization of the ground state through hydrogen bonding and suggests a change in complex stoichiometry, and possibly even proton transfer, under excess **1**, agreeing with the photometric titrations.

Golubev *et al.*[70] have used low temperature ^{1}H-NMR experiments to reach the slow hydrogen bond exchange regime. They have used this method to identify various H-bonded acetic acid-pyridine complexes in a $CDClF_2/CDF_3$ solvent system. This group reports a 1:1 (acetic acid:pyridine) stoichiometry that changes to 2:1 and finally 3:1 with increasing acid concentration. They suggest a H-bonded relay chain in which the proton donating power of the acid increases with increasing relay chain length and the hydrogen bond strength increases as the proton is transferred from the acid to the pyridine. Nibu *et al.*[71] have recently studied water-2-fluoropyridine clusters experimentally and with molecular orbital calculations to find mainly 2:1 and 3:1 clusters. Our results of a 3:1 (**1**:pyridine) complex formed through a H-bonded network are further supported by the fact that pyridine forms a constant-boiling azeotrope with water of the form $3H_2O\bullet C_5H_5N$.[62]

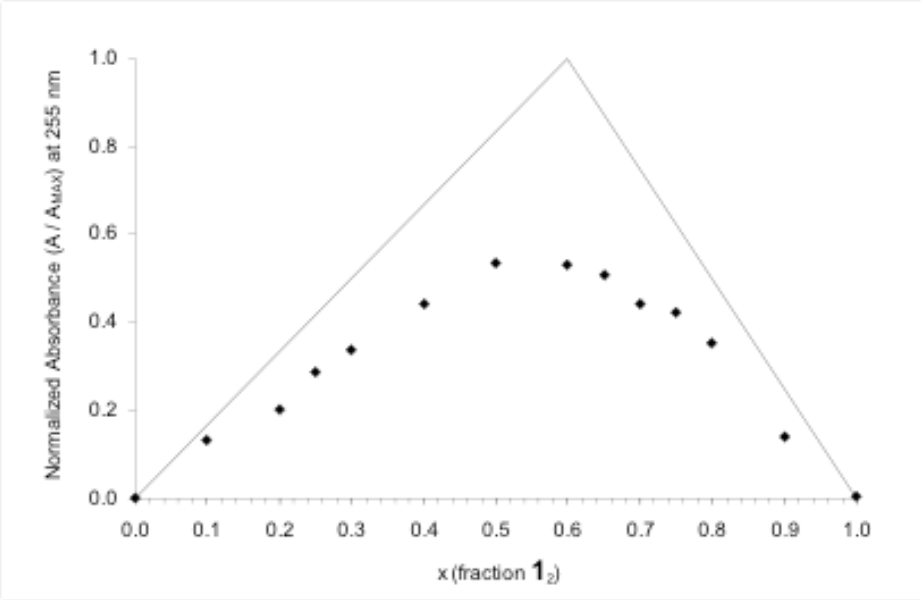

Figure 2-2. A normalized Job's plot of a **1**-pyridine complex in FC-72 shown as a function of sample composition. The diamonds represent normalized absorbance data points and the solid line represents the absorbance for 'maximum' complex formation at x = 0.6 to which all data points were normalized. $\mathbf{1}_2$ corresponds to the cyclic carboxylic acid dimer of **1**.

Because **1** is initially a H-bonded dimer, it is logical to determine the formation constant assuming a stoichiometry of 3/2 **1** dimer ($\mathbf{1}_2$) to 1 pyridine rather than 3:1 using **Equation 2-2**. **Figure 2-2** shows the continuous variations results considering the receptor dimer as a single 'reagent'. The formation constant (K_f, **Equation 2-2**) of the 3/2:1 ($\mathbf{1}_2$:pyridine) complex was found to be (2.1 ± 0.44) x 10^5 $M^{-3/2}$ using the method described by Likussar[61] and verified using Specfit software.

$$K_f = \frac{\left[\frac{3}{2}:1\ \text{complex}\right]}{[\text{pyridine}][1]^{\frac{3}{2}}}$$

Equation 2-2

The stoichiometry of a PFDA-pyridine complex was also determined to be 3:1 (PFDA:pyridine) using the same methods as above. The formation constant of a 3/2:1 ($PFDA_2$:pyridine) complex was found to be (3.4 ± 0.27) x 10^6 $M^{-3/2}$. Although PFDA exhibits a slightly stronger association with pyridine, the rigidity of the perfluoroalkyl chain lowers its solubility in fluorous liquids and limits its application as a fluorous receptor. In fact, the PFDA-pyridine complex shows a lower solubility than the PFDA alone. Perfluoropolyethers are much more flexible than perfluoroalkanes and are almost exclusively soluble in fluorous liquids, making them more viable candidates for such purposes. Despite differences in the perfluorinated chains, the PFDA-pyridine complex and the **1**-pyridine complex exhibit identical stoichiometries and comparable formation constants in FC-72 solvent.

The low solubility of perfluoroalkyl carboxylic acids makes them suitable candidates for crystal growth. The single crystal structure of a PFDA-pyridine complex (**Figure 2-3**) has a 1:1 stoichiometry and exhibits the heterodimer ring motif (**3**) described by Vishweshwar.[31] A summary of the crystallographic data and full details of the structure solution are given in **Appendix A**.

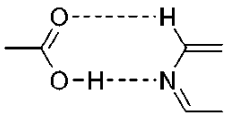

3

A titration of **1** with pyridine followed with IR spectroscopy was performed to gain more insight into the structure(s) of the complex(es) in solution. **Figure 2-4** shows a series of spectra from the titration (front to back: 1.0 to 10.0 mM pyridine in 1.0 mM steps with 10.0 mM **1** in each). **Table 2-2** shows the peak assignments.

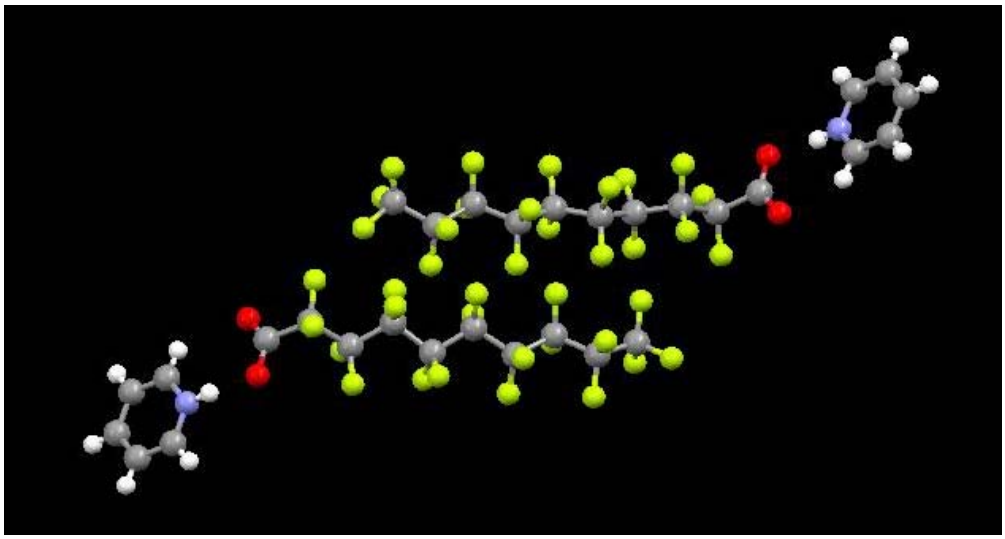

Figure 2-3. PFDA-Pyridine crystal structure. Crystallographic data and details of the solution are given in Appendix A.

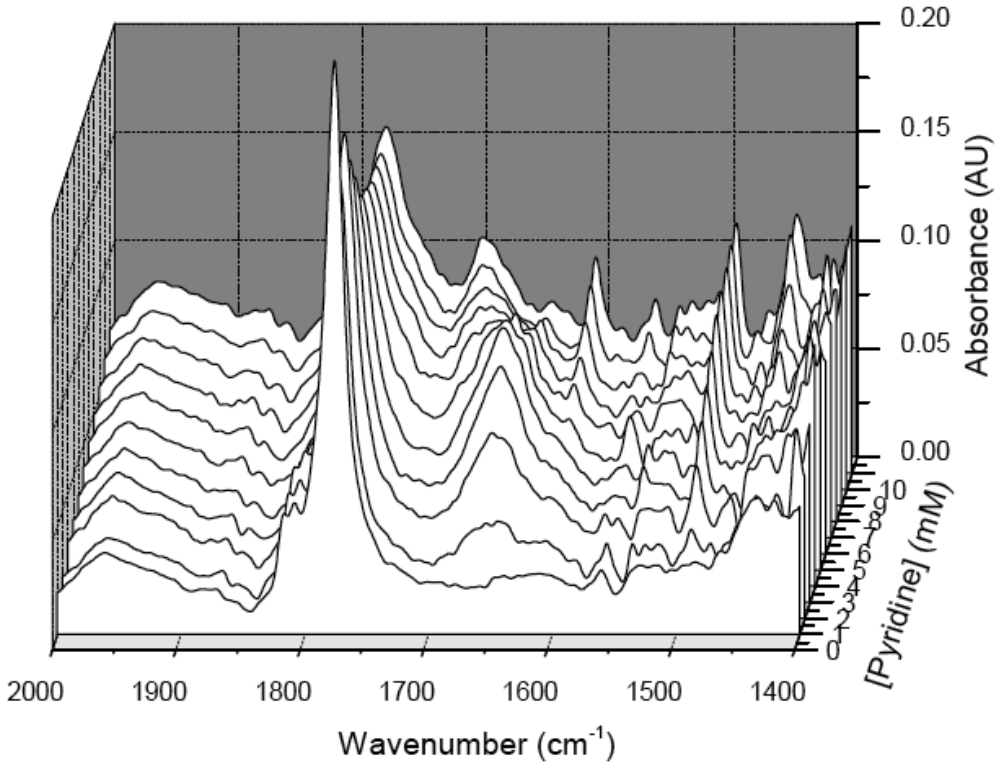

Figure 2-4. IR spectra resulting from a titration of 10 mM **1** in FC-72 with 0.05 mL increments of 20.0 mM Pyridine in FC-72 (constant volume). Only the carbonyl-stretching region is shown (see **Appendix A** for –OH region).

Table 2-2. Summary of IR bands and assignments in the 2000 – 1400 cm^{-1} spectral region resulting from titration of **1** with pyridine in FC-72. Pyridine is abbreviated as 'Py' and pyridinium is referred to as 'PyH^+'. The term 'solvated' means that the COO^- group in the ionic complex is associated with additional **1** molecules. The term 'complex' refers to acid/pyridine in association with one another. The term 'secondary' refers to molecules that are participating in the complex through hydrogen bonding to the complex but that are not directly associated with the pyridine.

Compound	Band	Assignment	
1	1817	C=O	monomer
	1808	C=O	polymer
	1775	C=O	dimer
Pyridine	1590	Py	free
	1440	Py	free
(3:1) **1**-PyH^+	1770	C=O	secondary
	1650	COO^-	'solvated'ionic complex
	1492	PyH^+	ionic complex
(2:1) **1**-PyH^+	1750	C=O	secondary
	1650	COO^-	'solvated'ionic complex
	1492	PyH^+	ionic complex
(1:1) **1**-PyH^+	1700	COO^-	ionic complex
	1492	PyH^+	ionic complex
(1:1) **1**-Py	1740	C=O	complex
	1609	Py	complex

The vibration centered at 1775 cm^{-1} in the front spectrum (10 mM **1** only) is characteristic of the carbonyl stretch of the cyclic **1** dimer.[32] A trifluoroacetic acid monomer is known to produce a distinctive sharp peak in the 1800 cm^{-1} region[72,73] and a corresponding peak in the OH stretch region near 3600 cm^{-1}.[32] The experimental spectra show two small peaks at 1817 and 1808 cm^{-1} and two at 3700 and 3558 cm^{-1} (see supporting information). These we

attribute to the C=O and –OH stretches of a small amount carboxylic acid monomer and the H-bonded polymeric form, respectively.

Turning now to the remaining spectra in **Figure 2-4** in which both **1** and pyridine are present; under conditions of excess **1** (low pyridine concentrations) a band appears at 1658 cm^{-1} that is assigned to the carboxylate stretch in the 3:1 ionic complex (PyH^+•**A^-**•HA•HA, Py = pyridine, PyH^+ = pyridinium, A^- = **1**$^-$, HA = **1** and the component designated in bold is the one assigned to the peak). Under the same conditions, the carbonyl dimer band at 1775 cm^{-1} decreases in intensity, broadens, and exhibits a shoulder at approximately 1770 cm^{-1} that can be attributed to the hydrogen-bonded carbonyl stretch of the second and third acids (PyH^+•A^- •**HA**•**HA**) of the complex combined with a small amount of **1**-dimer. The secondary acids effectively solvate the ionic complex. The spectra in this concentration range also show a pyridinium band at 1492 cm^{-1} that increases as **1** is titrated. **Figure 2-5** shows that this peak increases, begins to level of f at near 3:1 stoichiometry, and then increases again to 2:1 stoichiometry.

As the concentration of pyridine increases and reaches a 2:1 (**1**:pyridine) molar ratio ([pyridine] = 5 mM), the 2:1 ionic complex (PyH^+•A^-•HA**)** is the predominant species as evidenced by the 'solvated' carboxylate band at 1658 cm^{-1} along with the hydrogen-bonded carbonyl band that broadens even further and shows a shoulder at ~1740 cm^{-1} in strong agreement with Dega-Szafran[73] and Barrow.[72] At this point in the titration, the pyridinium band reaches a maximum absorbance, indicating that there is no additional pyridinium formed as the titration continues beyond a 2:1 molar ratio. At pyridine concentrations just above the 2:1 molar ratio a new band characteristic of hydrogen-bonded pyridine[72,74,75] appears at 1609 cm^{-1}. Meanwhile, the band attributed to the pyridinium ion (1492 cm^{-1}) levels off (see **Figure 2-5**).

At a 1:1 molar ratio, the solution is comprised of two main components. One species is a 1:1 ionic complex ($PyH^+ \bullet A^-$) as shown by the 'unsolvated' carboxylate band at 1700 cm^{-1} and the persisting pyridinium peak at 1492 cm^{-1}. The other species is a 1:1 hydrogen-bonded complex (Py•HA) that exhibits a hydrogen-bonded carbonyl band at ~ 1740 cm^{-1} and the hydrogen-bonded pyridine band at 1609 cm^{-1}. These peak assignments are also in good agreement with Lee,[74] Gill,[75] Barrow,[72] and Dega-Szafran.[73] The data show evidence that both pyridinium ions and carboxylate groups co-exist with hydrogen-bonded pyridine and carbonyl groups in the FC-72 solutions; the relative amount of each one changes as **1** is titrated with pyridine.

These assignments are bolstered by the literature. **Table 2-3** summarizes the published peak assignments and in the bottom row shows our assignments. The IR spectrum of pyridine contains a ring mode at 1590 cm^{-1} that is sensitive to changes in the electronic structure of the ring nitrogen. Upon hydrogen bonding[72,74] or when coordinated to a metal,[75] the pyridine mode at 1590 cm^{-1} is perturbed and shifts to 1600 cm^{-1}. Gill[75] studied the pyridinium-$CoCl_4$ salt and observed strong pyridinium bands at approximately 1640 and 1490 cm^{-1}. Barrow[72] reports the same pyridinium bands in the study of a trifluroacetic acid-pyridine complex in $CHCl_3$. Barrow also observed a hydrogen-bonded carbonyl band at approximately 1710 cm^{-1} and a carboxylate band at 1666 cm^{-1}, showing that proton transfer can occur to create an ionic hydrogen-bonded complex in a non-polar solvent like chloroform. Dega-Szafran *et al.*[73] have studied the proton equilibrium position in complexes of trifluoroacetic acid and pyridine in dichloromethane. They have assigned bands at 1740 and 1780 cm^{-1} to the carbonyl vibrations of each of the two acids in a 2:1 trifluoroacetic acid:pyridine hydrogen-bonded complex (Py•HA•HA). They also report the presence of a 1:1 ($PyH^+ \bullet A^-$) and 2:1 ($PyH^+ \bullet A^- \bullet HA$) hydrogen-bonded ion-pair showing

carboxylate peaks at 1690 and 1671 cm^{-1}, respectively. Fernandez-Berridi *et al.*[76] have used the hybrid density functional theory procedure to calculate the optimized geometries of a formic acid-pyridine complex 'solvated' with additional formic acid molecules. They have found that solvation of the complexed carbonyl group substantially decreases the N-H distance in the N---HO- hydrogen bond and increases the strength of such interactions. As a result, the carbonyl stretching frequency of the 'solvated' complex is predicted to be ~65 cm^{-1} lower than that of the unsolvated complex.

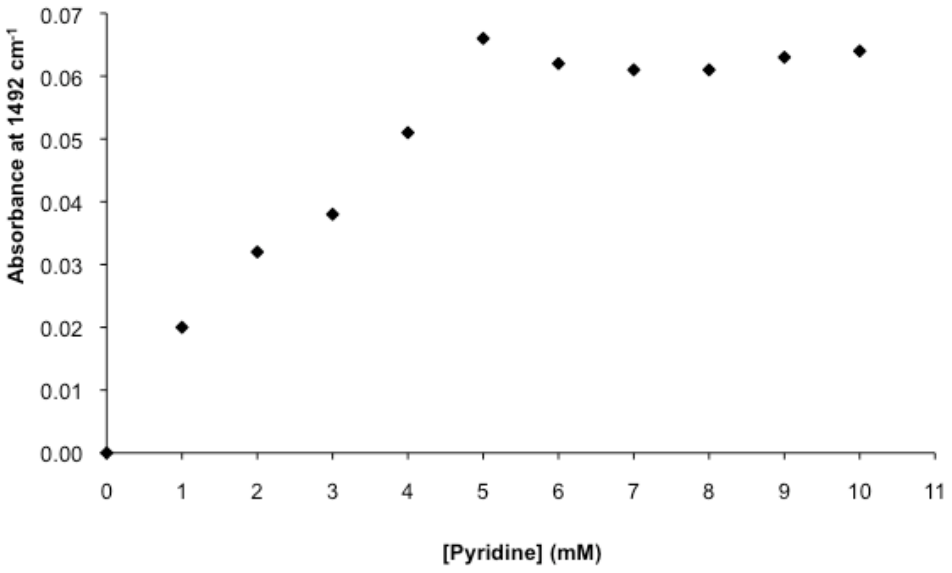

Figure 2-5. The absorbance of the IR pyridinium peak (1492 cm^{-1}) plotted against the concentration of pyridine in a solution of 10 mM **1** in FC-72.

Table 2-3. Summary of published IR peaks and their assignments for pyridine/pyridinium complexes in the 2000-1400 cm^{-1} spectral region. Pyridine is abbreviated as 'Py' and pyridinium is referred to as 'PyH^+'.

Compound	Solvent	C=O Monomer	C=O Dimer	C=O Complex	C=O Ionic	Py H-bonded	PyH^+
1[32]	None		1775		1696/1665[a]		
PyH^+ - BF_4^- salt[75]	KBr pellet					1600	1540
CF_3COOH-Py[73]	CH_2Cl_2	1804	1781	1780 1740	1690 1670		
CF_3COOH-Py[72]	$CHCl_3$		1782	1710	1666		1639 1488
CF_3COOH-Py[77]	KBr pellet		1780		1662		1600 1545 1489

For comparison with the complex spectra in FC-72, titrations were performed in a solvent-free environment in which **1**-oil was added to a constant volume of liquid pyridine (12.48 M) to create a series of pastes with varying molar ratios. The IR spectra of the resulting pastes (see Appendix A) are similar to the spectra shown in **Figure 2-4**, differing mainly in the virtual disappearance of the bands in the 1780 – 1750 cm^{-1} range at equimolar ratios. Another significant difference lies in the carbonyl/carboxylate peaks: one broad, tailing peak is seen in the paste spectra instead of two distinct peaks as shown in **Figure 2-4**. This heterogeneous peak

broadening is most likely a result of the increased number of carbonyl/carboxlate environments in the sample. Despite these differences, the pyridinium peaks (~1640 and 1490 cm^{-1}) remain in the spectra as well as a hint of the hydrogen-bonded pyridine peak (1609 cm^{-1}) on the shoulder of the broad carbonyl/carboxylate peak at higher pyridine concentrations, leading to the conclusion that similar complex forms exist in both the fluorous liquid and the perfluoropolyether environment. The titration spectra were also compared to the IR spectrum of 1:1 PFDA-pyridine crystals (see **Appendix A**) for which the structure is known (**Figure 2-3**). Pyridinium ion peaks at 1641 and 1496 cm^{-1} are also quite evident in this spectrum although the hydrogen-bonded pyridine peak at 1609 cm^{-1} is missing.

Factor analysis (Specfit:[78] Model-free evolving factor analysis or EFA) is able to determine of the number of absorbing components for a series of spectra.[79] Analysis of the carbonyl and, independently, the hydroxyl stretching regions of the titration spectra both give rise to 3 significant eigenvectors corresponding to three different components (see **Appendix A**). The EFA of both the carbonyl and hydroxyl regions resulted in nearly identical concentration profiles for each of the three components. One component is maximum at [pyridine] = 0.0, and decreases to zero at [pyridine] = 4.0 or 5.0 mM. This component's spectrum and behavior are recognizable as **1**. The second component is maximal at **1**:Py = 2:1 ([pyridine] = 5.0 mM). It corresponds to **1**-solvated pyridinium-carboxylate. The third component is maximal at **1**:Py = 1:1 ([pyridine] = 10.0 mM). The spectrum corresponds to a mixture of a pyridinium-carboxylate complex, and a pyridine-carboxylic acid complex.

Based on the foregoing discussion, we propose a structure for the 3/2:1 complex (**4**). It contains a hydrogen-bonded relay 'chain' as suggested by Golubev for the acetic acid-pyridine complex,[70] the -OH---N and CH---O hydrogen-bonded motif[31,76] that also appears in the crystal

structure, and it supports the EFA results. Although a proton-transfer seems unexpected in such a non-polar fluorous environment, it is clear from the IR spectra that the pyridinium is solvated by carboxylic acid functional groups, and thus does not perceive a low polarity medium.

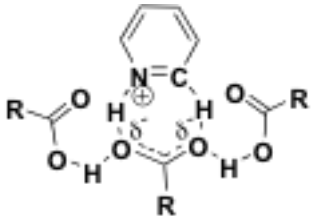

$CF_3CF_2CF_2O[CF(CF_3)CF_2O]_{33}CF(CF_3)$ = R

4

2.3.3 Thermodynamics

The self-association of **1** can be seen in the IR spectra of solutions of **1** in FC-72 at various concentrations. The equilibrium constant for the formation of the cyclic dimer was found to be 775 M^{-1} using methods described by Gonzalez[80] (see **Appendix A**). The IR absorbances were normalized to the path length so that data from the low concentration range could be combined with data taken at higher concentrations.

It follows that the free energy of formation for the cyclic dimer in FC-72 is equal to –16.5 kJ mol^{-1}or –8.24 kJ mol^{-1}per hydrogen bond. The thermodynamic cycle for the formation of the **1**-pyridine complex is shown in **Appendix A**. For the formation of the 3/2:1 **1**:pyridine complex, three dimer hydrogen bonds must be broken, costing a total of +24.7 kJ mol^{-1}. From the equilibrium constant, the free energy of formation of the complex from receptor dimer is determined to be –30.4 kJ mol^{-1} (-37.3 kJ mol^{-1} for the PFDA complex). Therefore, the overall

free energy for the hypothetical process in which free carboxylic acids combine with pyridine must be –55.1 kJ mol^{-1}. In the proposed structure (**4**), four hydrogen bonds are formed, resulting in an average hydrogen bond energy of –13.8 kJ mol^{-1}. To assign this value to the free energy of formation of the C—O^{-} · · · $^{+}$HN is conservative because the hydrogen bonds in the proposed complex are not of equal strength. The N---H hydrogen bond should be the strongest, resulting in a larger energy than this estimate shows, where as the CH---O hydrogen bond is expected to be significantly weaker. Fernandez-Berridi *et al.*[76] have reported the presence of a C-H---O hydrogen bond between formic acid and pyridine, as described by Vishweshwar[31] (**3**) and as suggested in **4**, with a second order interaction energy equal to only 3.8 % that of the N---HO-hydrogen bond energy. Thus, the free energy involved in the association of a single pyridine with a single 1 is virtually all attributed to the O—H—N hydrogen bond. Unfortunately, we do not have enough information for a confident estimate of the free energy of that H-bond, however we can estimate a related quantity. Consider the following set of reactions in **Scheme 2-2**:

½ $(AH)_2$		→	AH	ΔG_3^o = + 8.2 kJ/mol
Py	+ AH	→	Py•HA	ΔG_4^o
$(AH)_2$	+ Py•HA	→	PyH^+•A^-•HA•HA	ΔG_5^o
3/2 AH_2	+ Py	→	PyH^+•A^-•HA•HA	ΔG_6^o = - 30.4 kJ/mol

Scheme 2-2

From the data, it is clear that, in solutions at mM concentrations, solvation by **1** is necessary for formation of the ionic complex. The sum of the free energies of the second and third reactions in **Scheme 2-2** is about. –39 kJ mol-1. This energy includes the formation of a complex from a pyridine and an acid as well as the difference in free energy between an H-bonded carboxylic dimer and a pair of carboxylic acid H-bonds stabilizing the ionic complex. To our knowledge, these are the first reported estimates of hydrogen bond strengths in a fluorous solvent.

It is important to note that, while the extraction of pyridine is significantly affected by the presence of **1**, it is not the most strongly bound of the substrates studied (refer to **Figure 2-1**). The hydrogen bond energies between **1** and the aminopyridine and hydroxypyridine isomers are expected to be even greater.

Horvath and coworkers[23] first introduced the use of fluorous 'ponytails' of the form $(CH_2)_m(CF_2)_{n-1}CF_3$ to render high fluorous affinities to common catalysts and reagents. The fluorous affinity of a fluorous ponytail-tagged organic molecule is a direct function of the number of CF_2 groups in the ponytail. Rocaboy *et al.*[81] found that large numbers of CF_2 groups were required to immobilize benzene derivatives effectively in a fluorous liquid, it ultimately proving to be a challenging task. The average free energy of transfer of a CF_2 group from an organic solvent to a fluorous solvent is -2.44 ± 0.07 kJ mol^{-1} K^{-1}.[22] Thus, partitioning of a pyridine, or pyridine-containing molecule, into a fluorous phase is favored equally by incorporating receptor **1** into the fluorous phase or by covalently attaching approximately 12 CF_2 groups to the pyridine. Clearly, the non-covalent nature of the interactions allows for more efficient sample clean up and a reusability of **1** that is highly economical.

2.4 CONCLUSIONS

Non-covalent associations improve the extraction of non-fluorinated organic bases into a fluorous phase. The presence of receptor **1** dramatically enhances the extraction of a series of highly polar substituted pyridines from chloroform into FC-72, with virtually no extraction of solute in the absence of the receptor. The shapes of the extraction curves indicate higher order binding. Our studies of one particular complex have shown a (3/2):1 ($\mathbf{1}_2$:pyridine) stoichiometry in FC-72 solution and a (1/2):1 stoichiometry in the crystalline state. The equilibrium formation constant for the 3/2:1 complex in solution is $(2.1 \pm 0.44) \times 10^5$ $M^{-3/2}$.

Analysis of the infrared carbonyl and hydroxyl stretching vibration region of **1** in FC-72 shows bands corresponding to the monomeric and hydrogen-bonded cyclic dimer form of receptor. The self-association constant is 755 M^{-1} corresponding to a free energy of formation of -16.5 kJ mol^{-1} for the cyclic dimer ($\mathbf{1}_2$).

A structure has been proposed for the Krytox-pyridine complex in FC-72 solution based on IR spectroscopic evidence and known chemical phenomena.[31,32,82] Using this model, an estimate of the hydrogen bond free energy for the formation of **3** from pyridine and a free carboxylic acid in a fluorous environment containing **1** is approximately -39 kJ mol^{-1}

2.5 ACKNOWLEDGEMENTS

This research was funded by the National Science Foundation (NSF) through grants CHE 0315188 and CHE 0615952.

2.6 SUPPORTING INFORMATION

Supporting information for chapter 2.0 'Hydrogen Bond Complex Formation and Proton Transfer Between Carboxylic Acids and Pyridines in a Fluorous Solvent' can be found in **Appendix A**. The data available includes single-crystal X-ray crystallographic data for 1:1 PFDA-pyridine in CIF format (**Table A-1**) as well as Figures showing: (**Figure A-1**) the UV spectroscopic results of titrations of **1** with pyridine in FC-72, (**Figure A-2**) spectra showing the IR OH stretching region of **1** with various concentrations of pyridine in FC-72, (**Figure A-3**) spectra showing the IR carbonyl stretching region of pyridine with various concentrations of **1** in the absence of any solvent, (**Figure A-4**) factor analysis (EFA) results on the IR carbonyl stretching region of a titration of **1** with pyridine in FC-72, (**Figure A-5**) EFA results on the IR OH stretching region of a titration of **1** with pyridine in FC-72, and (**Figure A-6.** The IR carbonyl stretching region of PFDA (thick line) and 1:1 PFDA-pyridine crystal (thin line) KBr pellets.

3.0 MOLECULAR AND IONIC HYDROGEN BOND FORMATION IN FLUOROUS SOLVENTS

Abstract

There are only a few studies of noncovalent association in fluorous solvents and even fewer that are quantitative. A full understanding, particularly of stoichiometry and binding strength of noncovalent interactions in fluorous solvents could be very useful in improved molecular-receptor based extractions, advancements in sensor technologies, crystal engineering, and supramolecular chemistry. This work investigates hydrogen bonding between heterocyclic bases and a perfluoropolyether with a terminal carboxylic acid group (Krytox 157FSH (**1**)), chiefly in FC-72 (a mixture of perfluorohexanes). In particular, we were interested in whether or not proton transfer occurs, and if so, under what conditions in H-bonded complexes.

Continuous variations experiments show that in FC-72, weaker bases (pyrazine, pyrimidine, and quinazoline) form 1:1 complexes with **1**, while stronger bases (quinoline, pyridine, and isoquinoline) form 1:3 complexes. UV and IR spectral signatures reveal that the 1:1 complexes are molecular (B•HA) while the 1:3 complexes are ionic (BH^+•A^- HAHA). Infrared spectra of 1:3 ionic complexes are discussed in detail. Literature and experimental data on complexes between N-heterocyclic bases and carboxylic acids in a range of solvents are compiled to compare solvent effects on proton transfer. Polar solvents support ionic hydrogen bonds at a 1:1

mole ratio. In non-polar organic solvents, ionic hydrogen bonds are only observed in complexes with 1: 2 (base:acid) s toichiometries. In f luorous s olvents, a l arger e xcess of a cid, 1: 3, i s necessary to facilitate proton transfer in hydrogen bonds between carboxylic acids and the bases studied.

3.1 INTRODUCTION

Noncovalent interactions facilitate a remarkable range of applications of chemistry.[83-85] Artificial molecular receptors have been used to enhance selectivity and minimize solvent consumption for the extraction of a wide variety of target molecules.[18,42,44,48-50] Selectivity is high if non-covalent intermolecular interactions between receptor and target dominate the standard-state free energy change f or t he ex traction process. These i nteractions be come l ess i mportant i n competitive solvents,[19] thus a m atrix t hat i s a poor s olvent will pr ovide a m ore s elective e nvironment f or molecular recognition interactions.[14,20]

Poorly s olvating, highly non -polar fluorous l iquids are pr actically immis cible with both aqueous and organic phases[22] and non-fluorous solutes, with the exception of a few small gases, are in general vi rtually ins oluble in them. Thus, f luorous l iquids ha ve be come us eful f or purification and reaction clean-up[22-24] by reducing t he uni ntentional extraction of i nterfering species. Fluorous s eparations become pos sible b y covalent l abeling of a pr oduct pr ecursor or catalyst with a f luorous tag f or e asy s eparation of the la beled entities through e xtraction with fluorous l iquids. H owever, non -covalent a pproaches based on non -covalent c omplex formation are more desirable because they are more straightforward and have applications where selective, covalent la beling of a t arget mol ecule is impos sible, impractical, or unde sirable. Molecular

recognition in combination with fluorous matrices should improve the selectivity of molecular extraction by reducing the number and amount of interfering species extracted and increasing the strength of the substrate-receptor interactions by eliminating solute-solvent competition.[22,23,86] Perfluoroalkane based amine[55] and phosphine[53] ligands have been shown to support metals in fluorous liquids. Pyridyl tags can be used in conjunction with perfluorocarboxylate-supported copper to extract porphyrins and fullerenes.[56,87] Boswell *et al*.[57,58,88] have used fluorous liquids to provide a medium for more stable ion-ionophore complexes, thereby creating exceptionally selective sensor membranes. We have recently reported that a carboxylic acid terminated poly-hexafluoropropylene oxide, Krytox 157 FSH (**1**), significantly enhances the extraction of pyridine (100-fold with excess **1** as compared to **1**-free) and substituted pyridines from chloroform into a mixture of perfluorohexanes (FC-72).[20]

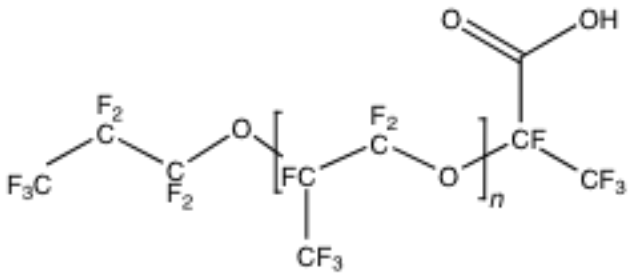

1

1 is a suitable molecular receptor for the fluorous phase because the ether oxygens are not basic[58] and it is soluble only in highly fluorinated solvents.[32] We have previously found that **1** extracts pyridine into the fluorous solvent FC-72. A 1:3 (pyridinium:$\mathbf{1}^-$) H-bonded complex is formed. We estimated the free energy of formation of the complex from a free acid, pyridine, and a carboxylic acid dimer to be -39 kJ mol^{-1}; thus reporting the first hydrogen bond strength in a fluorous environment.[20]

Complexes between pyridine and HF also form molecular and ionic hydrogen bonds depending on the stoichiometry. In the crystalline state, 1:1 complexes exhibit molecular hydrogen bonds (N---HF) whereas higher order 1:2 and 1:3 (pyridine:HF) complexes contain ionic hydrogen bonds.[89] Low-temperature NMR studies of pyridine-acetic acid complexes in a 2:1 mixture of $CDClF_2$ and CDF_3 show that 1:1, 1:2, and 1:3 complexes are formed.[70] The hydrogen bond is strengthened and the proton is transferred from acetic acid to pyridine as the order of the complex increases.

It is known that the pyridine nitrogen interacts strongly with carboxylic acids. Both hydrogen-bonded molecular complexes (N---HO) and ionic complexes (NH^+---O^-) in which the proton is transferred are possible. There has been a great deal of interest in the degree of proton transfer in acid-pyridine complexes under various conditions, thus relevant UV/Vis, IR, and NMR spectroscopic signals of pyridines in the presence of acids are well documented.[70,72,90-99] A study of the state of proton transfer in hydrogen-bonded pyridine complexes shows a gradual shift of the proton towards the nitrogen atom with increasing H-bond donor acidity and, for a given complex, the N-H distance falls with *increasing* solvent dielectric constant.[93] Changes in the IR spectrum show that in going from the gas phase to the condensed phase, as well as upon increasing solvent polarity, the hydrogen bond in a pyridine-acetic acid complex is strengthened

and the proton is transferred to the nitrogen atom.[96] The body of work on carboxylic acid-pyridine complexes agrees that *polar* environments strengthen hydrogen bonds and support proton transfer through ordering and polarization of the solvent in the vicinity of the hydrogen bond.[93,95,96,100-102] Thus the question arises, to what extent can nonpolarizable fluorous liquids support proton transfer?

It is evident from this collection of work that proton transfer is sensitive to the environment beyond the immediate configuration of the hydrogen bond. Here, we investigate the proton transfer phenomenon in fluorous matrices to gain insight into non-covalent interactions in such environments. This study is specifically aimed at providing a fundamental understanding of the influence had by fluorous solvents on the stoichiometry and binding strength of non-covalent interactions and ultimately improving extractions through the use of artificial receptors in fluorous liquids. A better understanding of non-covalent interactions in a fluorous matrix will also have potential applications in new sensor technologies, crystal engineering, and supramolecular chemistry.

3.2 EXPERIMENTAL

3.2.1 Chemicals and Instrumentation

Pyrazine, pyrimidine, quinazoline, quinoline, isoquinoline, dichloroacetic acid and perfluorodecanoic acid (PFDA) were obtained from Aldrich (Milwaukee, WI), pyridine and cyclohexane were purchased from J.T. Baker (Phillipsburg, NJ), and benzene was obtained from EMD Chemicals Inc. (Gibbstown, NJ). Monochloroacetic acid was purchased from Mallinckrodt

(St. Louis, MO) and trichloroacetic acid from Fisher Scientific (Pittsburgh, PA). Mono-, di-, and tri-fluoroacetic acids were purchased from Acros (NJ). FC-72 Fluororoinert Electronic Liquid (a mixture of perfluorohexanes) was obtained from 3M (St. Paul, MN). HFE-7100 (a mixture of perfluoro-*n*-butyl and perfluoroisobutyl methyl ether) and Krytox 157 FSH (**1**) were purchased from Miller-Stephenson Chemical Co., Inc. (Danbury, CT). All the compounds listed above were used as received. Chloroform was purchased from Fisher Scientific (Fair Lawn, NJ), dried over molecular sieves, and treated with potassium carbonate (EM Science, Cherry Hill, NJ) to neutralize any HCl that may have formed due to photosensitivity. Note that perfluorocarboxylates are known to be environmentally persistent and should be handled accordingly. ^{19}F-NMR analysis of **1** resulted a number-averaged molecular weight of 5150 g mol^{-1} with an average of 29 polymer repeat units. It should be noted that we previously reported[20] a number-averaged molecular weight of 5840 g mol^{-1} with 33 repeat units for Krytox 157 FSH. The difference lies in variability between batches.

A Hewlett-Packard 8452A UV-visible diode array spectrophotometer was used for all the UV absorbance measurements. A quartz cell with a path length of 0.1 cm was purchased from Fisher Scientific (Pittsburgh, PA) and used for all measurements.

A Varian Excalibur FT-IR spectrophotometer was used for all IR measurements and all spectra were analyzed using Varian Resolutions Pro 4.2 software package. An amalgamated KBr liquid sample cell with a 1.0 mm path length and holder was purchased from International Crystal Laboratories (Garfield, NJ) and used for liquid samples. Liquid samples were measured against a solvent background at resolution = 2 cm^{-1} with 50 scans averaged. 'Solvent-free' samples were measured against a blank background in KBr salt plates with a 0.1 mm lead spacer obtained from Wilmad (Buena, NJ) at resolution = 2 cm^{-1} with 50 scans averaged. A titration of **1**

with quinoline in FC-72 was measured at resolution = 0.25 cm^{-1} with 500 scans averaged, smoothed using a 49-point boxcar, and baseline corrected to achieve a higher signal-to-noise ratio. All other IR spectra were smoothed using a 5-point boxcar and baseline corrected. A Jouan A12 centrifuge was used for the solvent-free samples.

The mixed solvent method was used for slow precipitation of PFDA-quinoline crystals. 1.0 mL of 5.0 mM PFDA in FC-72 was mixed with 1.0 mL of quinoline-saturated HFE-7100 in a 20 mL scintillation vial and placed in a mechanical shaker (in-house construction) for 10 minutes followed by 10 minutes in the ultra-sonicator bath. The solution was transferred to a small Petri dish where it was lightly covered with weighing paper and allowed to cool and evaporate slowly overnight. 1.9 mg of crystalline material was then mixed with 99.0 mg of KBr in a mortar and pestle and transferred to a pellet press obtained from International Crystal Laboratories (Garfield, NJ). IR spectra of the resulting pellets were measured at a resolution = 4 cm^{-1} with 20 scans averaged.

3.2.2 Spectroscopy-Based Determination of Stoichiometry and Formation Constants

The UV continuous variations data were obtained by creating a series of solutions from 1.00 mM base and 1.00 mM acid so that the molar sum of base and acid remained constant according to Connors.[60] All stock solutions were placed in a Cole-Parmer (Chicago, IL) ultrasonicator bath for 10-30 minutes to ensure dissolution of the materials in their respective solvents. The method for normalized continuous variations plots was derived based on the general method developed by Likussar.[61] See **Appendix B** for the derivation. The UV titration data were obtained by titrating 0.50 mL of 2.00 mM base with 5.00 mM acid and diluting to a constant volume of 1.00 mL with a final base concentration of 1.00 mM. All samples were shaken for 10 minutes on a

mechanical shaker (in-house construction) to ensure homogeneity and allowed to rest for 10 minutes before measurements were made. All absorbance values were measured under ambient conditions (22.0 ± 1 °C) and baseline corrected. The UV difference absorbance as discussed by Valenta[18] is related to the amount of acid-base complex present in solution and was measured as a function of the fraction acid for continuous variations experiments and acid:base ratio for titrations. Specfit/32[78] software package distributed by Spectrum Software Associates (Marlborough, MA) was used for two separate treatments of spectroscopic data. In one, a nonlinear regression approach estimates binding constants based on a set of spectra and assumed complex stoichiometries. In the other, there are no chemical assumptions. Evolving Factor Analysis (EFA) of the experimental and difference spectra lead directly to the number of individual spectra (i.e., chemical species) contributing to the observed set of spectra.

IR solution titration data were obtained by titrating 0.25 mL of 10.00 mM **1** in FC-72 with 10.00 mM base and diluting to a constant volume of 0.50 mL, resulting in 5.00 mM final **1** concentration in each sample. For solvent-free IR titrations, precisely weighed aliquots of **1** were added to 1.0 μL neat base, stirred, and centrifuged for 10 minutes.

3.3 RESULTS AND DISCUSSION

No single experimental result tells the entire story. For the most part we have relied on electronic absorption spectra (actually, difference spectra as there are typically no new bands associated with the complexes formed) for stoichiometry and estimates of formation constants. For some complexes, there is literature on electronic spectroscopic changes accompanying proton transfer (BH^+---A^-, where B and HA are the initial base and acids) vs. those in which it

has not occurred (B---HA). While useful, those changes are often subtle, so infrared spectra are then used for distinguishing complexes in which proton transfer has occurred.

3.3.1 Stoichiometry and Formation Constant

We used the method of continuous variations[61] (see **Appendix B**) based on difference absorbance spectra to determine the stoichiometric ratio in complexes of **1** with pyridine, quinoline, isoquinoline, quinazoline, pyrazine, and pyrimidine in FC-72. These substrates were chosen because they demonstrated some solubility in **1**-free FC-72, allowing separate solutions of receptor and substrate to be prepared. However, despite the apparent solubility in FC-72, there is no measurable partitioning of any of the six bases listed above from 1.0 mM chloroform solutions into FC-72 at room temperature with a phase ratio of 1.0.

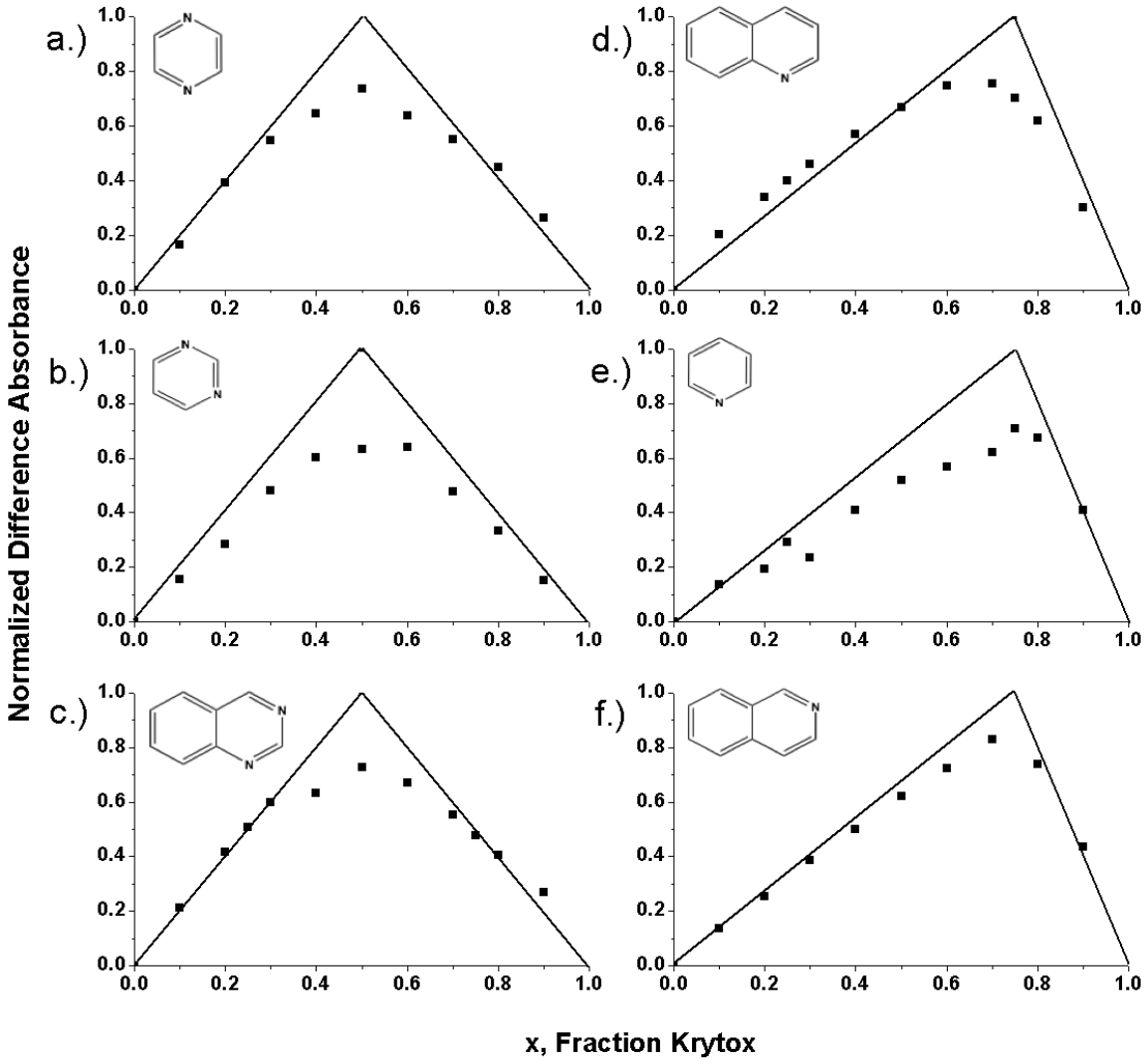

Figure 3-1. Representative normalized continuous variations plots for a.) pyrazine, b.) pyrimidine, c.) quinazoline, d.) quinoline, e.) pyridine, and f.) isoquinoline with **1** in FC-72 shown as a function of sample composition. The data points represent absorbances normalized relative to a solution containing a definite excess of acid in which all base is associated with acid. Lines correspond to the expected difference absorbance if the complexation reaction goes to completion at each concentration ratio.

The continuous variations plots (**Figure 3-1**) reveal 1:1 stoichiometries for **1** complexes with pyrazine, pyrimidine, and quinazoline and 1:3 (base:acid) stoichiometries with quinoline, pyridine, and isoquinoline in FC-72. From the continuous variations data, we applied the normalized absorbance method[61,103] to determine the formation constant (K_f) and hence the free energy of formation, ΔG°_f (1), of complexes with **1**, where R is the gas constant and T is temperature.

$$\Delta G^\circ_f = -RT \ln(K_f)$$

Equation 3-1

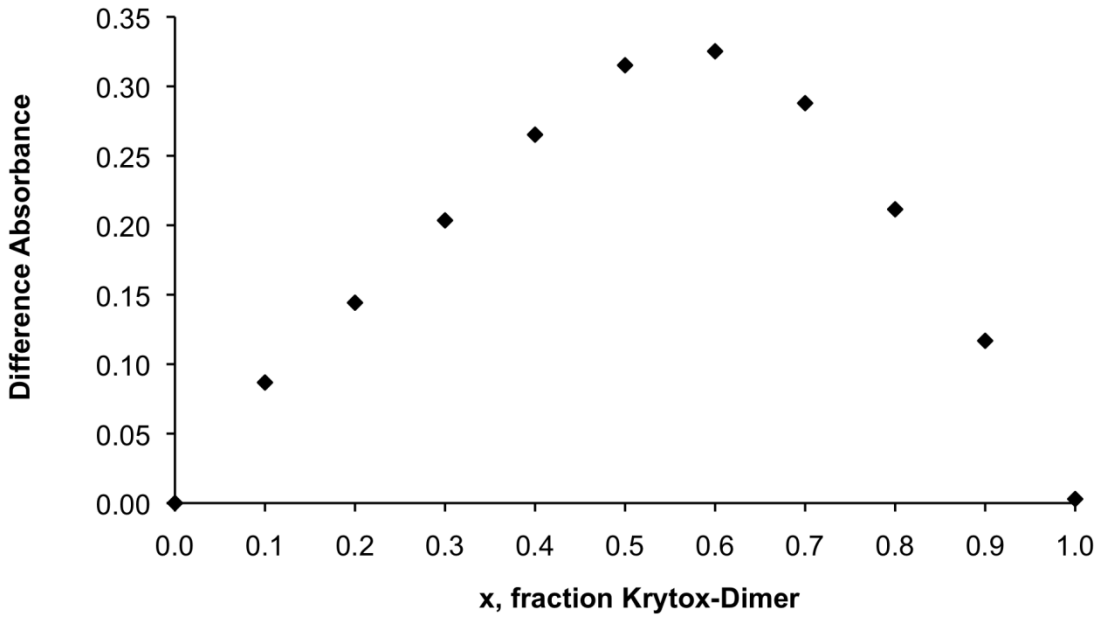

Figure 3-2. Continuous variations plot for a quinoline-$\mathbf{1}_2$ (dimer) complex. A complex composition of x = 0.6 for a quinoline-$\mathbf{1}_2$ corresponds to a complex composition of x = 0.75 for a quinoline-**1** complex, confirming the 1:3 (base:acid) stoichiometry of the complex.

In this method, absorbances are normalized to the absorbance obtained from a solution containing excess **1**. In such a solution there is effectively no free base, thus the absorbance measured represents only complex (see **Appendix B** for derivation). The lines in **Figure 3-1** correspond to the expected difference absorbance if the complexation reaction goes to completion at each concentration ratio. Hypochromic effects from base self-association were not observed in the experimental concentration range (0.1 – 1.0 mM). Nonetheless, in the continuous variations plot of quinoline (**Figure 3-1**, d) that the data points for $x < 0.5$ fall above the 'expected' lines for complete complexation. This is explained by the sequential formation of 1:1, 1:2, and 1:3 quinoline:**1** complexes with increasing **1** and will be discussed in the following section. Continuous variations experiments in which one of the 'reagents' was taken to be the dimer, $\mathbf{1}_2$, were performed to rule out the possibility of a dominant species with 1:2 stoichiometry for this particular complex (**Figure 3-2**). The results confirmed the 1:3 complex as the predominant complex.

Table 3-1. Stoichiometry, formation constant, and free energy of formation for a series of pyridine-like bases with **1** in FC-72 determined by the method of continuous variations, titrations, and Specfit global fitting.

Substrate	K_a[a]	Stoichiometry Base:**1**	K_f (M^{-1})	Complex $\Delta G°_f$ (kJ/mol)	$\Delta G_f°$ SEM[b] (kJ/mol)	N[c]
Pyrazine	0.7	1:1	$(1.5 \pm 0.2) \times 10^4$	-24	0.3	7
Pyrimidine	0.2	1:1	$(1.6 \pm 0.2) \times 10^3$	-23	0.3	6
Quinazoline	0.4	1:1	$(8.8 \pm 1.7) \times 10^4$	-22	0.3	4
Quinoline	0.9	1:3	$(2.4 \pm 0.3) \times 10^{13}$	-73	0.8	8
Pyridine	0.2	1:3	$(3.6 \pm 0.5) \times 10^{11}$	-65	0.8	6
Isoquinoline	0.4	1:3	$(2.8 \pm 0.5) \times 10^8$	-47	0.7	4

[a]Aqueous pK_a values for the conjugate acid

[b]$DG_f°$ standard errors of the mean (SEM) were determined from a $DG_f°$ pooled relative standard deviation for the method of 3.2%

[c]Number of determinations

Table 3-1 shows data for the six bases listed in the order (low to high) of the aqueous pK_a of their conjugate acids. Formation constants determined several ways from multiple experiments agree reasonably well. To verify the accuracy of the formation constants and validate the normalized continuous variations method, regression analysis (Specfit[78]) was applied to both continuous variations and titration data for each base. Formation constants are calculated for complexes of user-defined stoichiometries. Incorrect 'guesses' at what complexes are present are indicated by very large errors in the estimated binding constants. Formation constants determined from fitting the data to an assumed set of chemical equilibria were in good overall

agreement with those determined from the normalized continuous variations method. A straightforward 1:1 model was used for pyrazine, pyrimidine, and quinazoline complexes with **1** while a more complex model including 1:1, 1:2, and 1:3 (base:acid) complexes was employed for quinoline, pyridine, and isoquinoline. A simple model specifying the formation of a 1:3 complex alone was not sufficient to explain the data for any of these three bases. Formation constants (K_f) and free energies of formation (ΔG°_f) reported in **Table 3-1** are mean values from normalized continuous variations and regression analysis on titrations and continuous variations data. These do not depend monotonically on the pK_a values. It becomes clear that the stronger bases demonstrate a 1:3 (base:acid) stoichiometry while the weaker bases show a 1:1 stoichiometry.

3.3.2 Molecular vs. Ionic Complex Formation

3.3.2.1 Ultraviolet Spectra

Spectra and titration curves for constant-volume titrations of pyrazine, pyrimidine, quinazoline, quinoline, pyridine, and isoquinoline with **1** in FC-72 are shown below (**Figure 3-3** through **Figure 3-16**). Let us first discuss the 1:1 complexes of **1** with pyrimidine, pyrazine, and quinazoline. In FC-72, the spectrum of pyrimidine (**Figure 3-3**) has two systems of bands, $\pi\rightarrow\pi^*$ bands near 240 nm and $n\rightarrow\pi^*$ bands near 300 nm. In a titration of pyrimidine with **1** in FC-72 (**Figure 3-4**) the absorption maximum associated with the $n\rightarrow\pi^*$ transition (300 nm) persists but shifts to shorter wavelengths (273 nm) with increasing [**1**]. In neutral or basic aqueous solutions, the $n\rightarrow\pi^*$ bands are at 270 nm.[104] In acidic aqueous solutions where pyrimidine is protonated the $n\rightarrow\pi^*$ band is not observed.[104] Thus, electronic spectra are consistent with a 1:1 complex that is comprised of **1** hydrogen-bonded to pyrimidine with no proton transfer. Spectra of pyrazine

show similar behavior (**Figure 3-5**). In neutral and basic aqueous solutions[105] as well as in FC-72 solutions with **1**, the spectrum of pyrazine has a $\pi \rightarrow \pi^*$ band near 260 nm and an $n \rightarrow \pi^*$ band between 300-325 nm. The spectrum of protonated pyrazine in acidic aqueuous solutions shows no $n \rightarrow \pi^*$ band;[105] thus the observation of this band in FC-72 solutions with **1** is evidence for the molecular complex. The spectrum of quinazoline changes markedly upon protonation,[106] yet a titration of quinazoline with **1** (**Figure 3-7** and **Figure 3-8**) did not produce substantial changes. Only a small hypsochromic shift in the $\pi \rightarrow \pi^*$ transition band and a loss in vibronic structure of the $n \rightarrow \pi^*$ band were observed. This is evidence that the complex of quinazoline with **1** is hydrogen-bonded with no proton transfer.

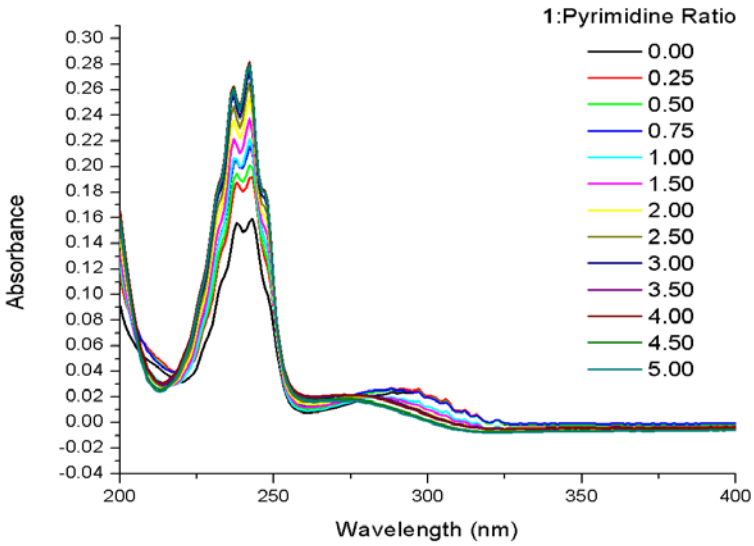

Figure 3-3. Representative UV spectra from a constant-volume titration of 1.0 mM pyrimidine with **1** (non-absorbing from 200-400 nm) in FC-72, path length = 0.1 cm. Arrows indicate increasing **1** concentration.

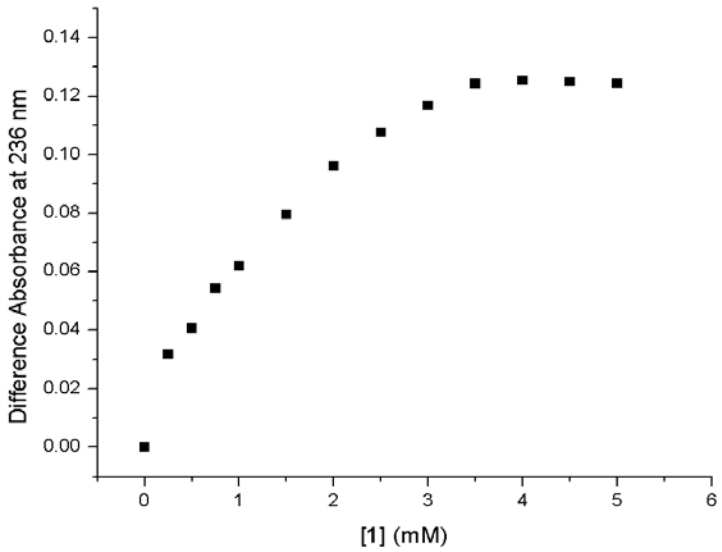

Figure 3-4. Difference absorbance at 236 nm from a representative constant-volume titration of 1.0 mM pyrimidine with **1** in FC-72.

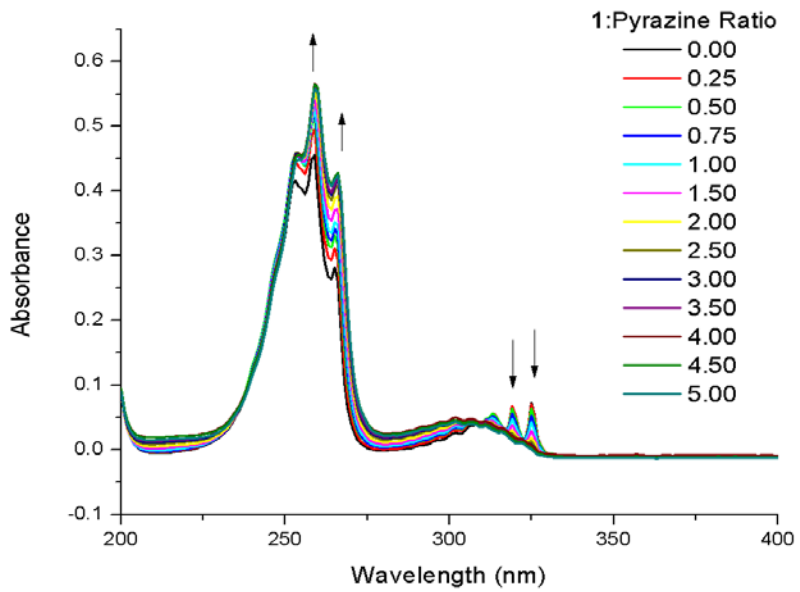

Figure 3-5. Representative UV spectra from a constant-volume titration of 1.0 mM pyrazine with **1** (non-absorbing from 200-400 nm) in FC-72, path length = 0.1 cm. Arrows indicate increasing [**1**].

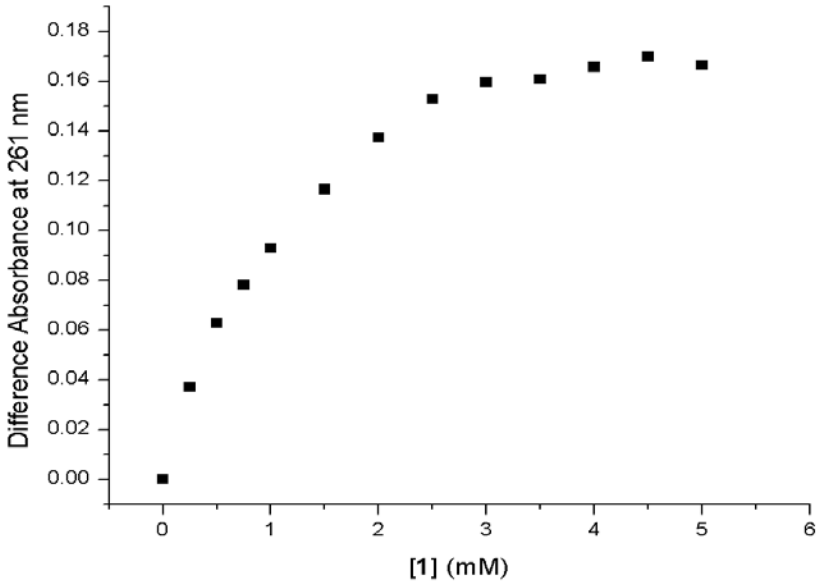

Figure 3-6. Difference absorbances at 261 nm for a representative constant-volume titration of 1.0 mM pyrazine with **1** in FC-72, demonstrating the formation of a 1:1 complex.

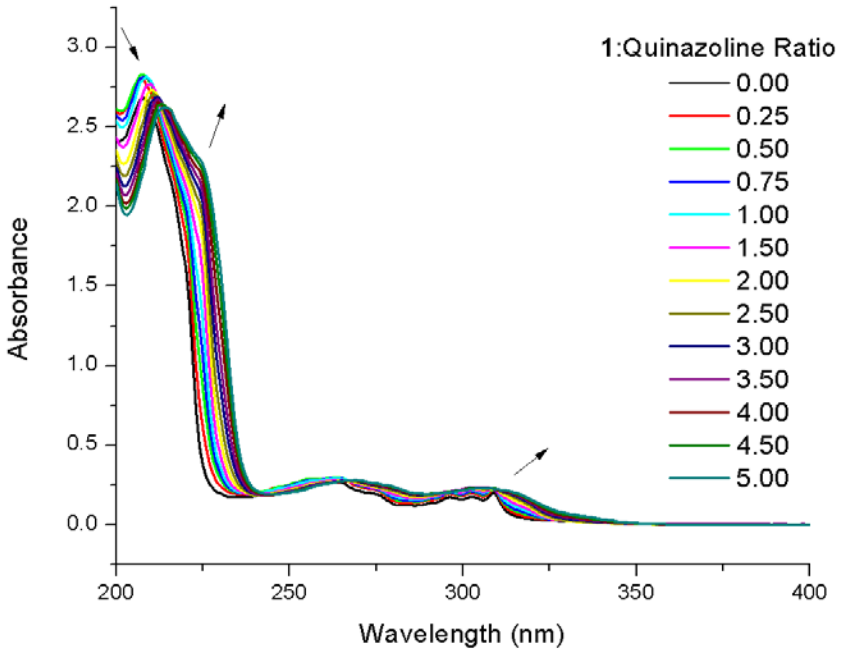

Figure 3-7. Representative UV spectra from a constant-volume titration of 1.0 mM quinazoline with **1** (non-absorbing from 200 -400 nm) in FC-72, path length = 0.1 cm. Arrows indicate increasing [**1**].

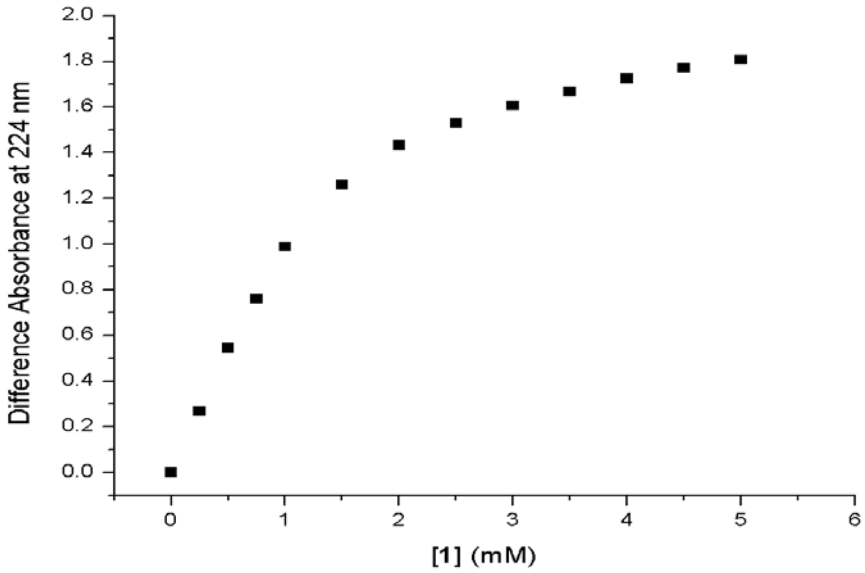

Figure 3-8. Difference absorbance at 224 nm from a representative constant-volume titration of 1.0 mM quinazoline with **1** in FC-72. The results demonstrate the formation of a 1:1 complex.

The 1:3 complexes formed by pyridine, isoquinoline, and quinoline with **1** in FC-72 show different behavior. The spectrum of pyridine in FC-72 (**Figure 3-9**) shows three distinguishable bands at 249, 255, and 261 nm, similar to the spectrum of pyridine in neutral or basic aqueous solutions that show maxima at 250, 256, and 261 nm.[107] After addition of **1** to a solution of pyridine in FC-72, the maximum remains at 255 nm while the other component bands become shoulders. The same behavior was observed with pyridine in acidic aqueous solutions,[107] indicating that proton transfer from **1** to pyridine occurs in FC-72. We have previously reported a detailed study on this complex.[20]

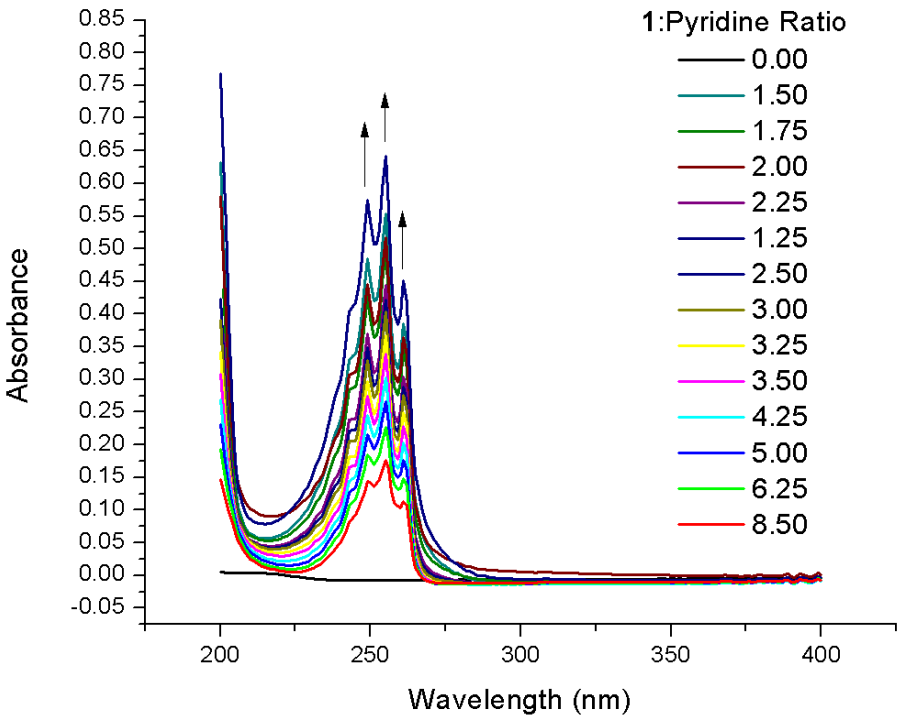

Figure 3-9. Representative spectra from a constant-volume titration of 1.0 mM pyridine with **1** (non-absorbing from 200-400 nm) in FC-72, path length = 0.1 cm. Arrows indicate increasing [**1**].

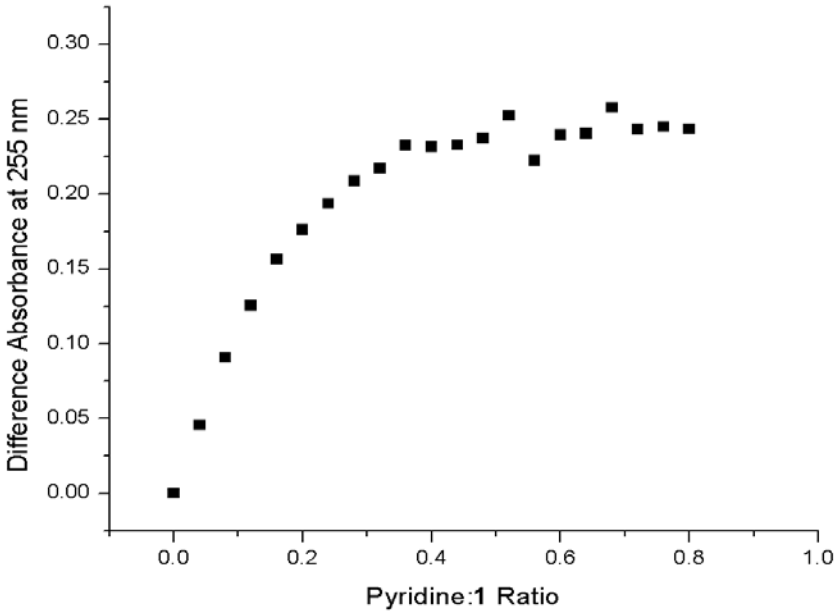

Figure 3-10. Difference absorbance at 255 nm from a representative constant-volume titration of 1.0 mM pyridine with **1** in FC-72.

The electronic absorption spectrum of isoquinoline in FC-72 (**Figure 3-11**) has a $\pi \rightarrow \pi^*$ band at 262 and an $n \rightarrow \pi^*$ band at 315 nm that is rich in vibronic structure. A constant-volume titration of isoquinoline with **1** in FC-72 (**Figure 3-11** and **Figure 3-12**) reveals two new $n \rightarrow \pi^*$ bands at 320 and 327 nm with addition of **1**. There is a complete loss of vibronic structure in the $n \rightarrow \pi^*$ band at 3:1 and greater excess of **1**. A similar loss of vibronic structure has been observed for a 1:2 isoquinoline:trifluoroacetic acid complex in acetonitrile in which the acid has transferred a proton to isoquinoline.[108] For 1:1 molecular isoquinoline-trifluoroacetic acid complexes with no proton transfer in octane and carbon tetrachloride, the vibronic structure is intact and no new peaks appear.[108] Titration curves in FC-72 (**Figure 3-12**) show the formation

of two different complexes with 1:2 and 1:3 (isoquinoline:**1**) stoichiometries. Meanwhile, the position of the $\pi \rightarrow \pi^*$ band gradually shifts from 262 to 271 nm as **1** is added, but remains at 271 nm at 3:1 excess of **1** and greater (**Figure 3-13**). Thus, the data indicate that proton transfer occurs in FC-72 as the excess of **1** to isoquinoline reaches 3 and beyond.

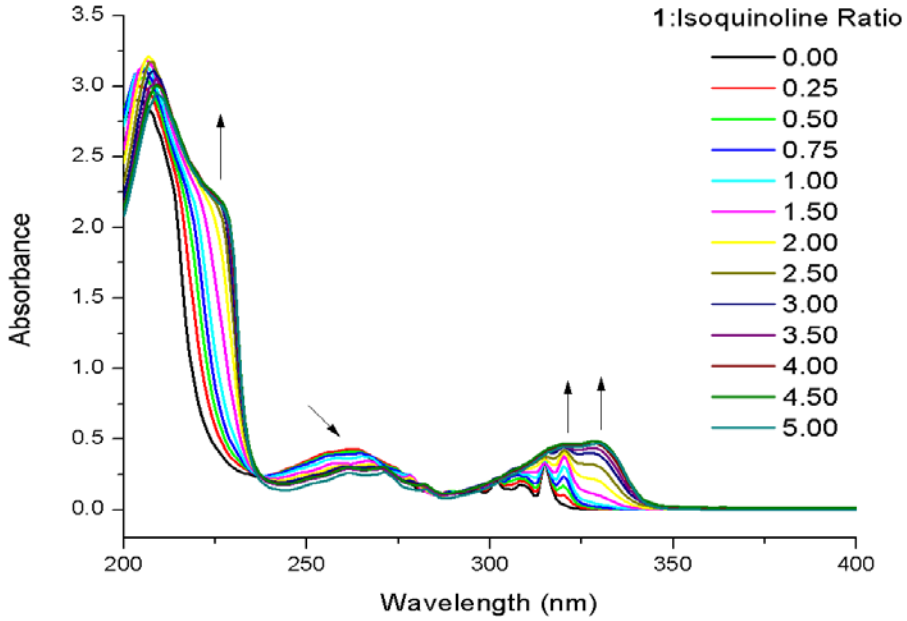

Figure 3-11. Representative spectra from a constant-volume titration of 1.0 mM isoquinoline with **1** (non-absorbing from 200-400 nm) in FC-72, path length = 0.1 cm. Arrows indicate increasing [**1**].

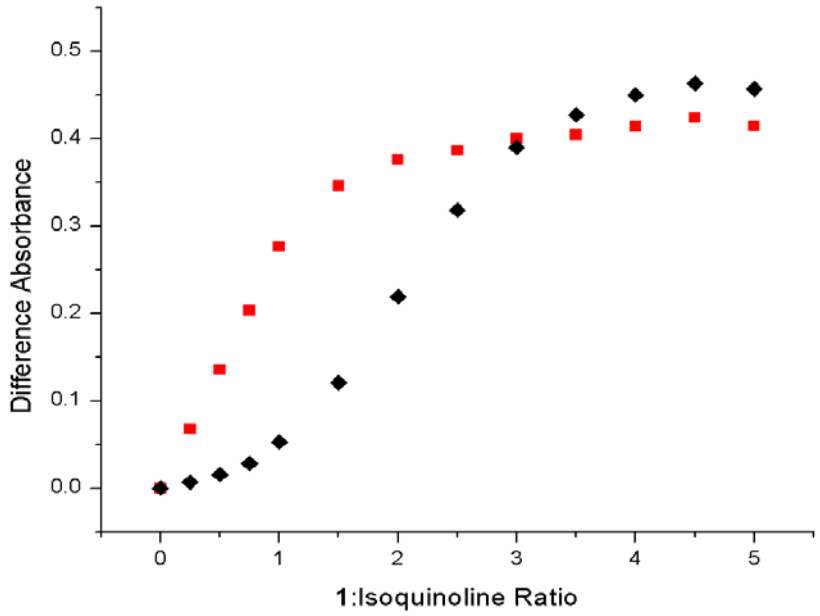

Figure 3-12. Difference absorbance at 320 (■) and 327 nm (◆) from a representative constant-volume titration of 1.0 mM isoquinoline with **1** in FC-72.

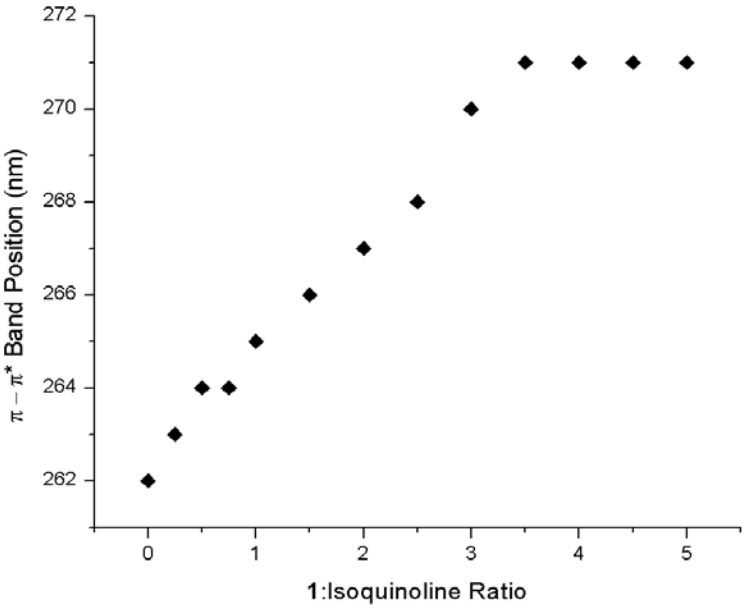

Figure 3-13. Position of the $\pi \rightarrow \pi^*$ electronic absorption band as a function of **1**:isoquinoline ratio in a constant-volume titration of isoquinoline with **1** in FC-72.

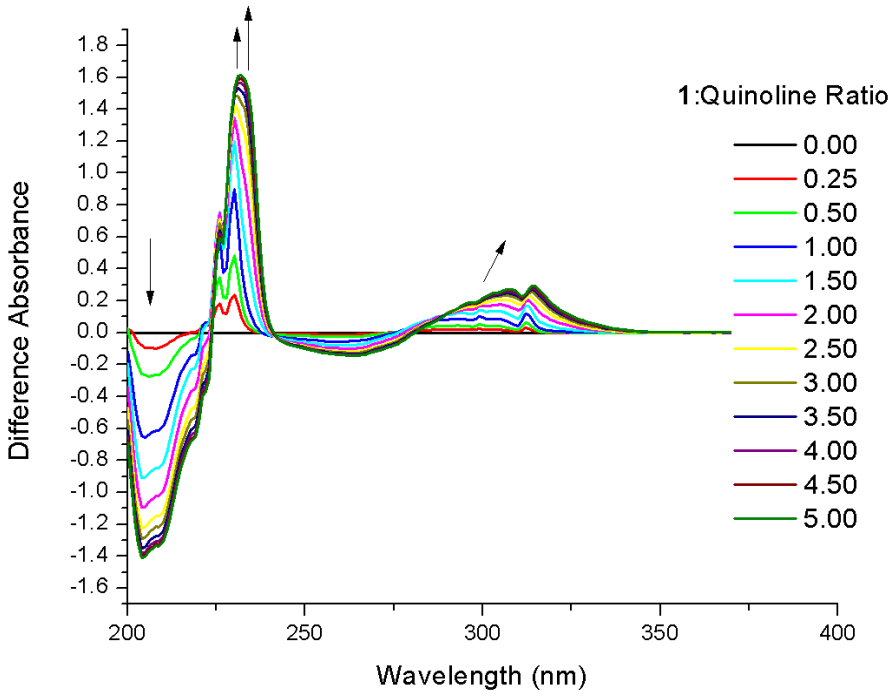

Figure 3-14. Difference absorbance spectra resulting from a constant-volume titration of 1.0 mM quinoline with **1** in FC-72. Arrows indicate increasing [**1**].

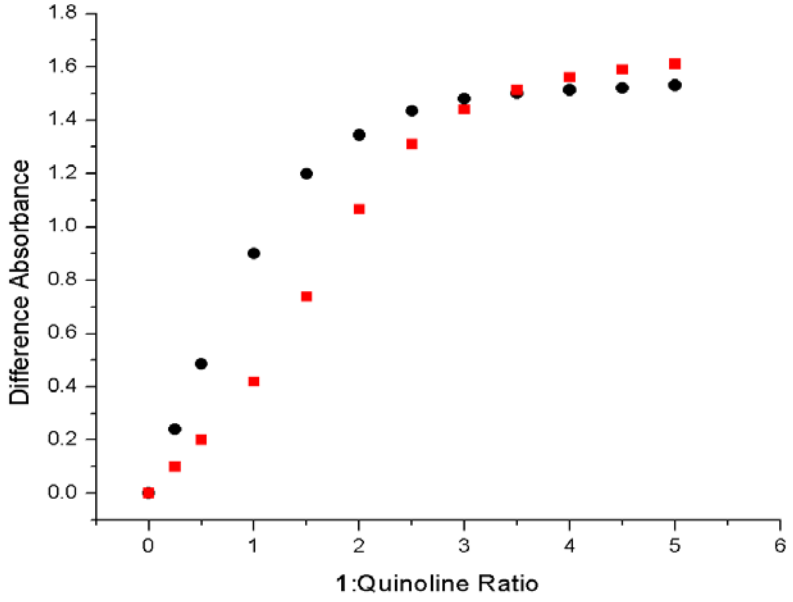

Figure 3-15. Titration curve at (●) 230 and (■) 232 nm of constant 1.0 mM quinoline with **1** in FC-72.

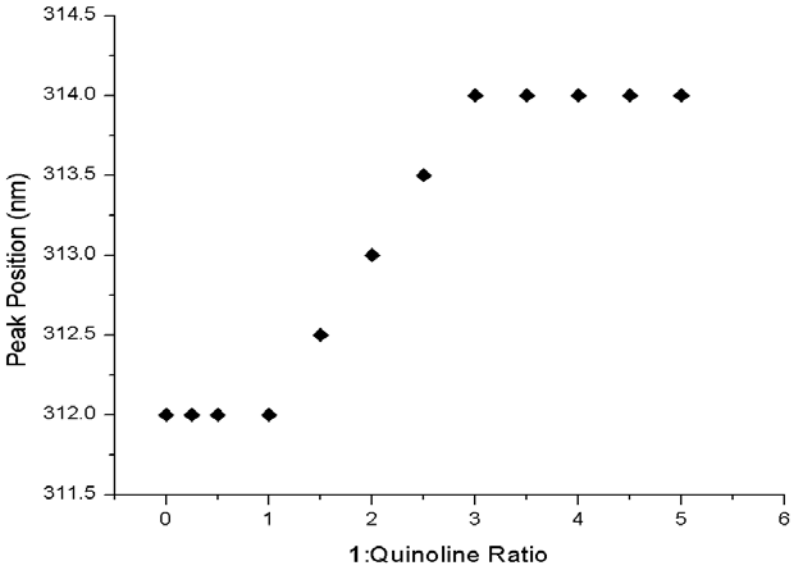

Figure 3-16. Peak position as a function of 1:quinoline mole ratio in the constant-volume titration of 1.0 mM quinoline with **1** in FC-72.

The electronic absorption difference spectra resulting from a constant-volume titration of quinoline with **1** in FC-72 are shown in **Figure 3-14**. Original absorbance spectra are shown in **Appendix B**. A close look at the difference absorbance from 220-240 nm shows a peak at 230 nm and a shoulder at 232 nm that appears at 1:2 (quinoline:**1**) mole ratios neither of which are present in the spectrum of free quinoline. **Figure 3-15** shows the intensity of these peaks as a function of mole ratio. The difference in the shape of the curves at the two wavelengths is further indication of the presence of more than one complex. From the titration curve at 230 nm (**Figure 3-15**), it is clear that there is a 1:2 hydrogen-bonded complex, while the titration curve at 232 nm suggests a 1:3 complex. A look at the remainder of the electronic spectrum reveals a sharp peak at 312 that exhibits a bathochromic shift with increasing [**1**]. Such a shift often indicates changes

in the polarity of the environment or a strengthening of the hydrogen bond.[109] The position of this peak as a function of mole ratio (**Figure 3-16**) shows that there is a transition between 1:1 and 1:3 (quinoline:1) mole ratios.

3.3.2.2 Factor Analysis

Factor analysis can be used to simplify the analysis of mixtures based on correlations among the spectra from solutions containing the same compounds but with various compositions. Singular value decomposition (SVD) produces linearly independent eigenvectors with all the spectroscopic information plus the noise contained in a data matrix (set of spectra). The number of significant (i.e., not due to noise) eigenvectors is equal to the number of chemical species contributing to the observed spectroscopic changes.[79] The program Specfit[78] carries out this sort of analysis, allowing for the determination of the number of chemical entities contributing to the observed spectra. The program can also be used to estimate how the contributions of the chemical entities change with conditions, e.g., as concentrations are changed. The latter estimation is called "model-free evolving factor analysis (EFA) applied following SVD". It is quite successful at determining the concentration profiles and component spectra from a series of spectra. The term "model-free" means that the user does not specify how many complexes are present, stoichiometries, etc. The user only provides a set of spectra and initial component concentrations. As described above, a regression analysis based on assumed complex stoichiometries can also be carried out. The two analyses should show the same result.

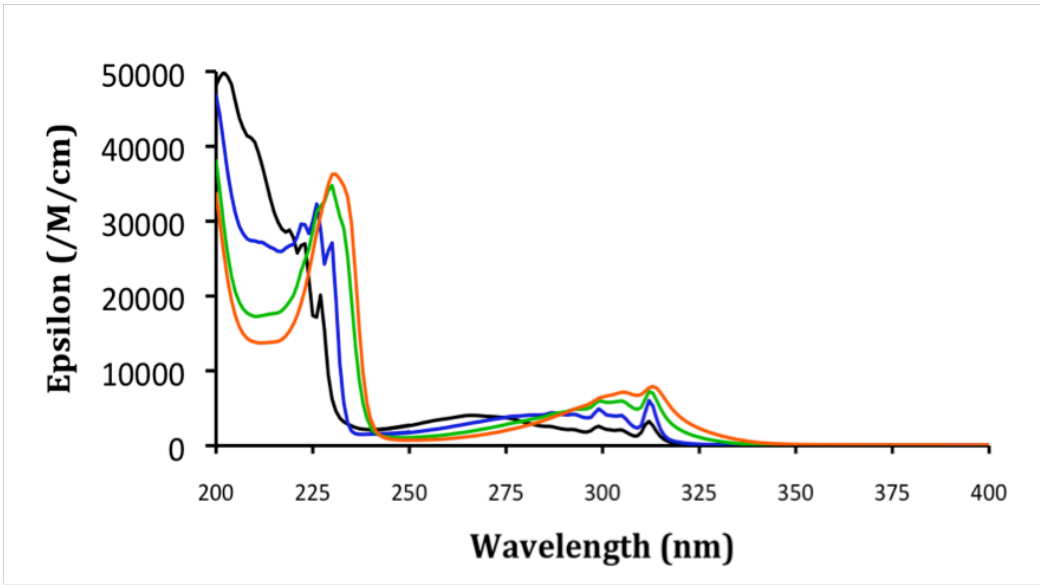

Figure 3-17. EFA predicted spectra of free quinoline (black), a 1:1 (blue), 1:2 (green), and 1:3 (orange) quinoline:**1** complex. The spectral regions 200-250 and 250-400 nm were calculated independently yet line up with excellent agreement.

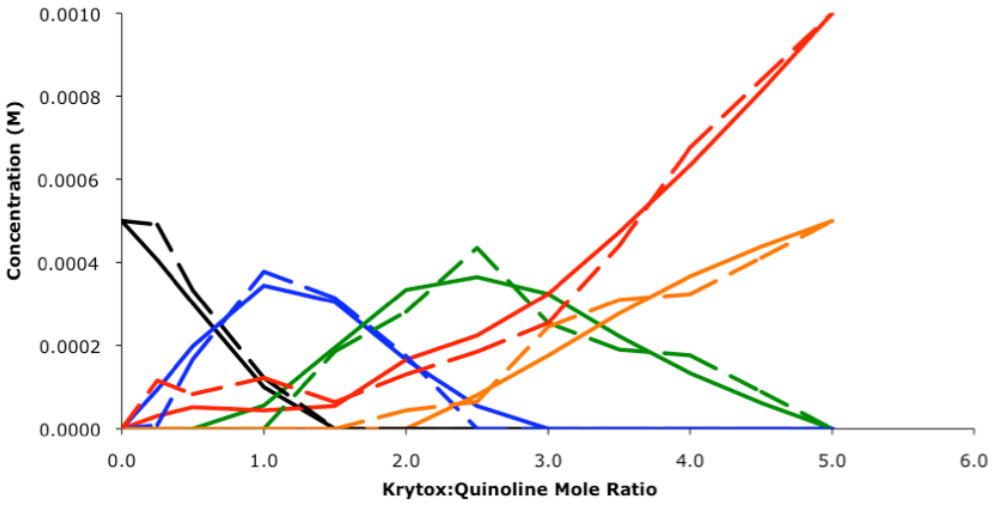

Figure 3-18. Overlay of concentration profiles from model-free EFA of two separate regions in the ultraviolet spectrum; (—) 200-250 nm and 250-400 nm (---) in the titration of quinoline with **1** in FC-72 for free quinoline (black), a 1:1 (blue), 1:2 (green), and 1:3 (orange) quinoline:**1** complex, and free **1** (red), respectfully.

We applied EFA to two regions of the spectrum independently, one below 250 nm and one above. In both spectroscopic regions, four factors (i.e., optically absorbing chemical species) were sufficient to explain the data. The predicted spectra corresponding to these chemical species are shown in **Figure 3-17**. These spectra account for > 99.9% of the variance in the data set. It is noteworthy that the spectra were analyzed in two sections (< 250 nm and ≥ 250 nm). The two sets of predicted spectra, one from < 250 nm and the other from ≥ 250 nm, fit together seamlessly in **Figure 3-17**. In order to perform a fit to the data, the complex stoichiometries have to be identified. From the factor analysis, we know that we must identify four chemical species. These are base, and complexes with stoichiometry 1:1, 1:2, and 1:3. The program does not give a spectrum for free acid because it is non-absorbing in the wavelength range studied. The program gives best-fit concentration profiles and equilibrium constants for each reaction. Concentration profiles from the regression analysis are in good agreement with concentration profiles resulting from the model-free EFA approach as seen in **Figure 3-18**. The fit shows that the concentration of a 1:1 hydrogen-bonded (quinoline:**1**) complex increases as the amount of free quinoline decreases until all free quinoline has been consumed. A 1:2 (quinoline:**1**) hydrogen-bonded complex begins to appear and reaches a maximum while the concentration of the 1:1 complex decreases as it is converted to 1:2. A 1:3 complex is dominant beyond a 3:1 excess of **1** and co-exists with excess **1**-dimer (non-absorbing from 200-400 nm). The concentration profiles determined independently from the two spectroscopic regions are in good agreement. The EFA predicted spectra for each absorbing species, free quinoline, 1:1 and 1:2 (quinoline:**1**) molecular complexes, and a 1:3 ionic complex, are shown in **Figure 3-17** and correspond to the sequential complex formation shown in the concentration profiles.

Table 3-2. Formation constant and free energy of formation for a 1:1 base:1 complexes in FC-72 determined by regression analysis of continuous variations and titrations data.

Substrate	K_a	K_f (M^{-1})	1:1 Complex $\Delta G°_f$ (kJ/mol)	N
Quinoline	0.9	1.8×10^8	-34	4
Pyridine	0.2	7.8×10^3	-22	3
Isoquinoline	0.4	5.7×10^2	-16	2

Table 3-2 lists the formation constants and free energies for 1:1 complexes of quinoline, pyridine, and isoquinoline with **1** in FC-72 determined through the regression analysis. Of the bases listed, quinoline forms the most stable 1:1 complex. It was mentioned above that the left-hand portion of **Figure 3-1 d** shows experimental difference absorbances greater than expected for complete 1:3 complex formation. The large formation constant for the 1:1 complex explains this. For comparison, concentration profiles resulting from a regression as well as those from the EFA approach for an isoquinoline-**1** complex in FC-72 are shown in **Appendix B**. Regression analysis and model-free EFA also confirms the sequential formation of 1:1, 1:2, and 1:3 complexes between isoquinoline and **1**.

3.3.2.3 Infrared Spectra

IR titrations of **1** with each base were performed. Representative spectra of the 1:1 complexes with **1**, pyrazine, pyrimidine, and quinazoline, as well as those of 1:3 complexes, quinoline, pyridine, and isoquinoline, are shown in **Figure 3-19 (a-c)** and **(d-f)**, respectively. Protonation of the heterocyclic nitrogen changes the vibrational spectrum of the complex. The C=O group of

free and hydrogen-bonded carboxylic acids produces a strong band in the 1800-1700 cm^{-1} region whereas the COO^- group of an ionized carboxylate salt exhibits a strong band between 1700-1550 cm^{-1}.[109] For each of the bases that formed 1:1 complexes with **1**, pyrazine, pyrimidine, and quinazoline, the carbonyl band broadened upon complex formation (**Figure 3-19, (a-c)**) as expected for hydrogen-bond formation. On the other hand, the IR spectra of the bases that formed 1:3 complexes with **1**, quinoline, pyridine, and isoquinoline, revealed a new band centered around 1650 cm^{-1} (**Figure 3-19, (d-f)**) that can be attributed to a carboxylate vibration. This is in agreement with the postulation from the electronic spectra, that the 1:1 complexes with **1** in FC-72 are molecular while the 1:3 complexes are ionic.

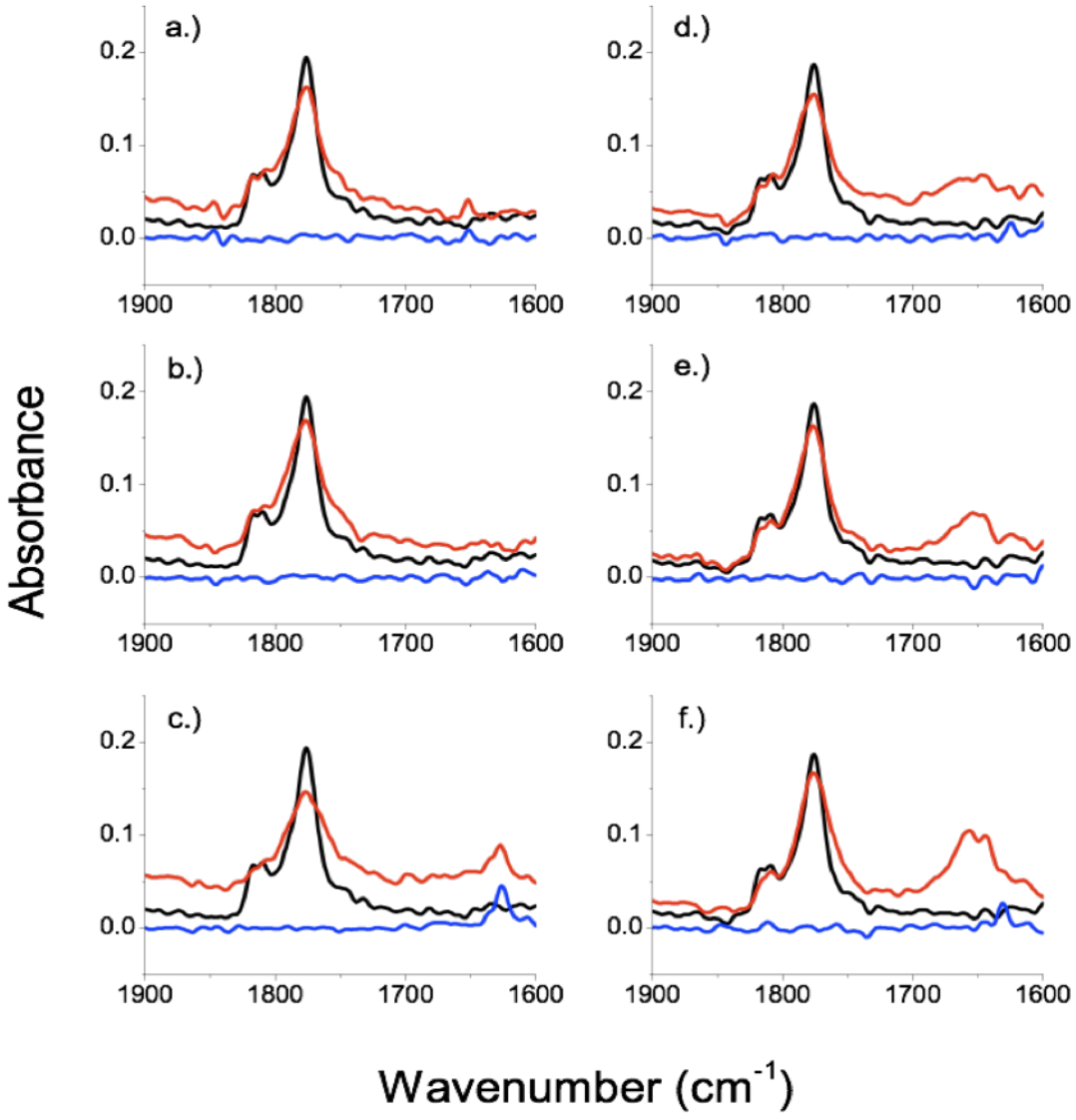

Figure 3-19. The carbonyl region of representative IR spectra from titration experiments. The colored lines represent **1** (black), base (blue), and the base-**1** complex (red) for a.) pyrazine, b.) pyrimidine, c.) quinazoline, d.) quinoline, e.) pyridine, and f.) isoquinoline, respectively. The spectra on the left (a-c) form 1:1 molecular complexes whereas the spectra on the right (d-f) form 1:3 (base:acid) ionic complexes.

To gain a better understanding of proton transfer interactions in such a non-polar environment, the remainder of this section will be focused on the IR spectra of 1:3 complexes of quinoline, isoquinoline, and pyridine with **1**. In addition, a few comments on the experiments and display of data are in order. We have learned that the information derived from IR spectra of solvent-free mixtures of **1** with pyridine is very similar to that in IR spectra of solutions in FC-72.[20] The advantage of the solvent-free mixtures is that the concentrations are higher thus the absorbances are higher than are achievable in solution. Doan has noted that perfluoropolyethers, such as **1**, are in themselves a fluorous anhydrous fluid medium,[32] therefore pair-wise functional group interactions can be studied in a 'solvent-free' environment to obtain spectra with higher signal-to-noise ratios. In principle, absorbances can be increased by increasing the pathlength, however the solvent background is significant. We have found that 1.0 mm is the longest pathlength that we can use and still derive information in the carboxylate region of the spectrum. Another difficulty in interpreting the spectra arises with quinoline and isoquinoline. Complexes from a titration of quinoline with **1** give IR spectra with overlapping carboxylic acid carboxylate bands and quinolinium bands. Thus, we have used second derivative spectroscopy to accentuate band profiles for sharp peaks and reveal small shoulders, allowing overlapped peaks to be identified.[73]

The results of a solvent-free titration of neat quinoline with **1** are shown in **Figure 3-20**; spectra not required for understanding the system have been removed for graphical clarity while the entire data set can be found in **Appendix B**. A similar titration of **1** with quinoline in FC-72 was performed to ensure that the solvent-free fluorous environment is representative of a fluorous solvent. The resulting spectra are shown in the **Appendix B**. The solvent background in the region below 1675 cm^{-1} gives rise to significant noise in this region of the spectra. The

quinoline ring region of the second-order derivative spectra is shown in **Figure 3-21**. The peak positions and assignments are summarized in **Table 3-3**.

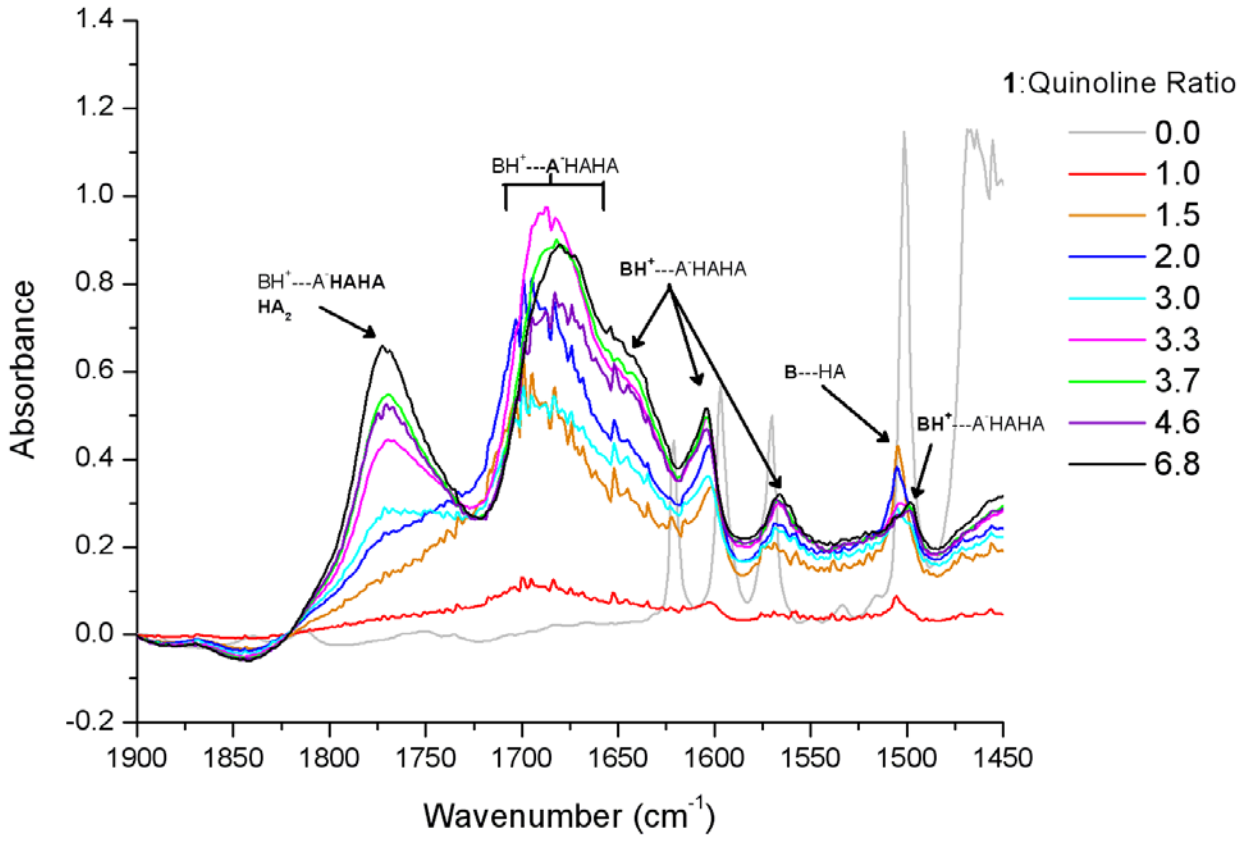

Figure 3-20. Representative spectra from a solvent-free FTIR titration of constant quinoline with 1. B, quinoline; HA, 1; B---HA; quinoline-1 molecular complex; BH^+---A^-HAHA, quinolinium-1-carboxylate ionic complex. The portion of the complex shown in bold is responsible for the vibration.

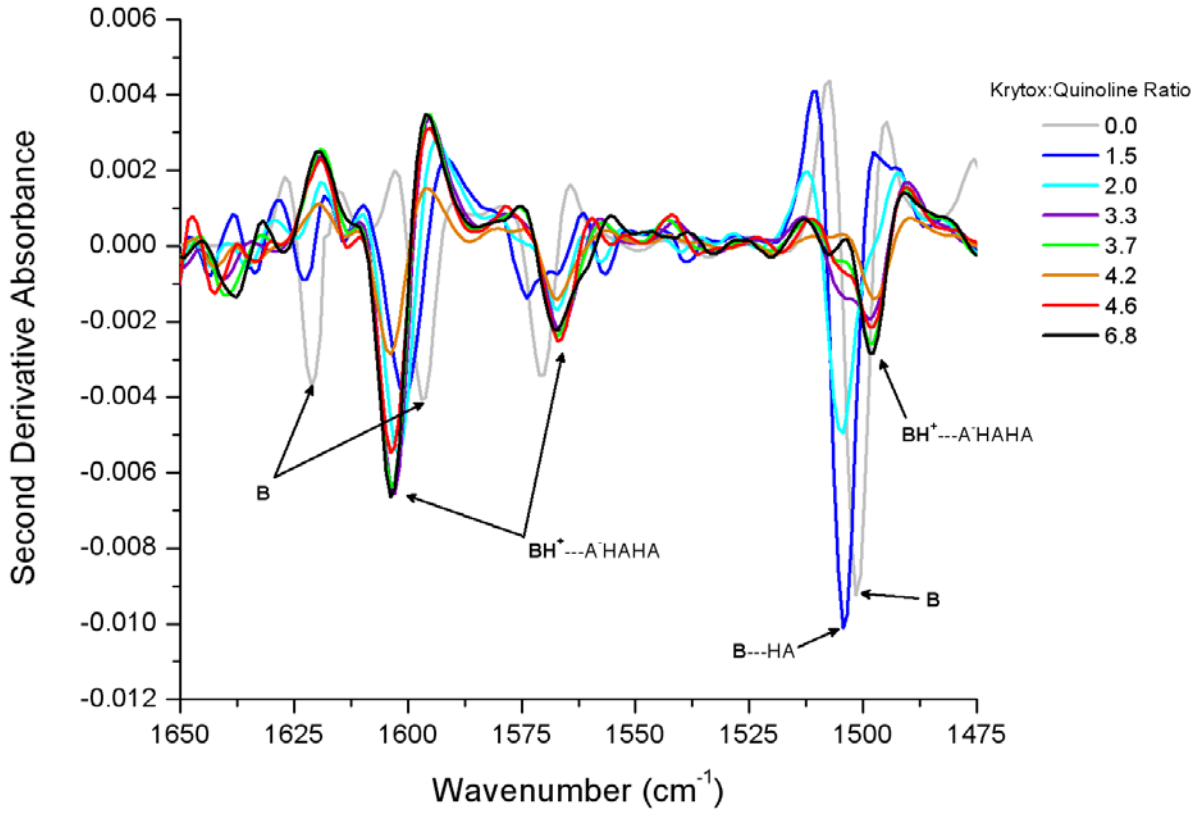

Figure 3-21. The quinoline-ring region from representative second-derivative IR spectra resulting from a solvent–free titration of neat quinoline with **1**. B, quinoline; HA, **1**; B---HA; quinoline-**1** molecular complex; BH^+---A^-HAHA, quinolinium-**1**-carboxylate ionic complex. The portion of the complex shown in bold is responsible for the vibration.

Table 3-3. Observed frequencies of the second derivative IR bands in the carbonyl and quinoline ring vibrational regions resulting from a solvent-free titration of quinoline with 1 along with the peak assignments.

Compound	Band (cm^{-1})	Assignment	Description
1(HA)	1817	C=O	monomer
	1808	C=O	polymer
	1775	C=O	dimer
Quinoline (B)	1621	ring	free
	1597	ring	free
	1571	ring	free
	1501	ring	free
	1468	ring	free
(1:1) B:HA	1601	ring	**B**•HA
	1503	ring	**B**•HA
(1:1) B:HA	1638	ring	$\mathbf{BH^+}$•A^-
	1604	ring	$\mathbf{BH^+}$•A^-
	1567	ring	$\mathbf{BH^+}$•A^-
	1490	ring	$\mathbf{BH^+}$•A^-
(1:2) B:HA	1680	COO^-	BH^+•$\mathbf{A^-}$•HA
	1670	COO^-	BH^+•$\mathbf{A^-}$•HA
(1:3) B:HA	1777	C=O	BH^+•A^-•**HA**•HA; $\mathbf{HA_2}$
	1767	C=O	BH^+•A^-•HA•**HA**
	1697	COO^-	BH^+•$\mathbf{A^-}$•HA•HA

B, qui noline; B H^+, qui nolinium; H A, 1-acid; A $^-$, 1-carboxylate; T he portion of the complex shown in bold is responsible for the vibration.

Let us first discuss the quinoline ring region of the spectra (~1650-1400 cm^{-1}). We observe four strong bands at 1621, 1597, 1571, and 1501 cm^{-1} for quinoline. These observations are consistent with the observations of Dines.[110] In the titration of quinoline (B) with **1** (HA) (**Figure 3-20** and **Figure 3-21**), molar ratios below 1:2 exhibit bands at 1503 and 1602 cm^{-1} that can be attributed to ring vibrations of hydrogen-bonded quinoline (B•HA) in accordance with Dines *et al.*[110] **Figure 3-21** shows that, as additional **1** is added, these bands are replaced with bands at 1638, 1604, 1567, and 1490 cm^{-1} that can be assigned to quinolinium (BH^+) vibrations. The band at 1638 cm^{-1} is broad[110] and thus does not appear strong in the second derivative spectrum (**Figure 3-21**) but it is easily seen as a shoulder in **Figure 3-20**. In support of the assignments for the quinolinium ion, Dines[110] observed bands at 1638, 1597, 1559, and 1489 cm^{-1} for quinolinium adsorbed on silica. Those bands were assigned to quinolinium based on calculations (bands predicted at 1634, 1594, 1583, 1551, and 1467 cm^{-1}).

Moving to the carbonyl region of the spectra, **1** exhibits a vibration centered at 1775 cm^{-1} characteristic of the carboxylic acid carbonyl stretch of the cyclic **1**-dimer (HA_2).[32] In **Figure 3-20**, the broad band near 1697 cm^{-1} is assigned to the ionic complex. Additional **1** causes a shift in this band from 1697 cm^{-1} to lower energy. These bands can be assigned to the carboxylate stretch (A^-) of the ionic complex. The wavenumber shift that is observed is caused by the 'solvation' of the ionic complex by additional acids. It is proposed that these 'solvating' acid molecules are necessary to stabilize the hydrogen bond to facilitate the sequential formation of a 1:3 quinoline:**1** ionic complex from a 1:1 molecular complex in a non-polarizable, poorly-solvating fluorous environment. The carbonyl (HA) bands (near 1775 cm^{-1}) of acids that are associated with quinoline but not directly hydrogen-bonded to the heterocyclic nitrogen (i.e., 'solvating' acids) become significant above ratios of 1:2 (quinoline:**1**). With excess acid, the

result is a single broadened band spanning 1725-1625 cm^{-1} that is clearly two overlapping peaks one from the carboxylate carbonyl and one from quinolinium. Crystalline perfluorodecanoic acid-quinoline also produced an IR spectrum (**Appendix B**) containing a convoluted carboxylate/quinolinium band spanning 1800-1600 cm^{-1} with sharp quinolinium (BH^+) ring vibrations (1638 cm^{-1}) and hydrogen-bonded quinoline bands (1602 cm^{-1}).

3.3.3 Solvent Effects

Figure 3-22 displays data from the literature on complexes between N-heterocyclic bases and carboxylic acids in a range of solvents. Results from the current work are included. The axes correspond to the Kamlet-Taft dipolarity/polarizability parameter (π^*)[111] of the solvent and the difference between the proton donating power of the conjugate acid of the base in water (pK_{aBH+}) and that of the acid (pK_{aHA}) also in water.

$$\Delta pK_a = pK_{aBH+} - pK_{aHA}$$

Equation 3-2

Each data point represents a hydrogen-bonded complex between an acid, HA, and a base, B. Squares represent molecular complexes (B---HA) while circles represent ionic complexes (BH^+---A^-). Large symbols are data reported here, while the smaller symbols represent data in the literature (see **Appendix B** for the citations). Note that the current work is mainly focused on the lower right side of the graph where there was a paucity of data. The stoichiometry of each

complex, if known, is indicated by the color of the point (see legend). This graphical view is necessarily approximate. The temperature and concentrations used vary among the reported data, the use of pK_a values measured in water for process occurring in other solvents must be to some degree inaccurate, and π^* by itself is insufficient to explain the effect of a solvent on acid, base, or complex free energy. With these caveats in mind, though, there is still information to be gained from **Figure 3-22**.

We note that there are two areas where circles (ionic complexes) are found, in polar solvents (top) and when ΔpK_a is large (right). Pyridinium (aqueous $pK_a = 5.2$) is observed with acids as weak as 4-fluorophenol if the solvent is sufficiently polar as well as in highly non-polar fluorous solvents if the acid has a sufficiently low pK_a. Pyridinium-carboxylate complexes in more polar solvents such as dichloromethane and tetrachloroethylene[100] are 1:1 whereas ionic complexes observed in lower polarity solvents, including fluorous solvents, often have more complex stoichiometries.

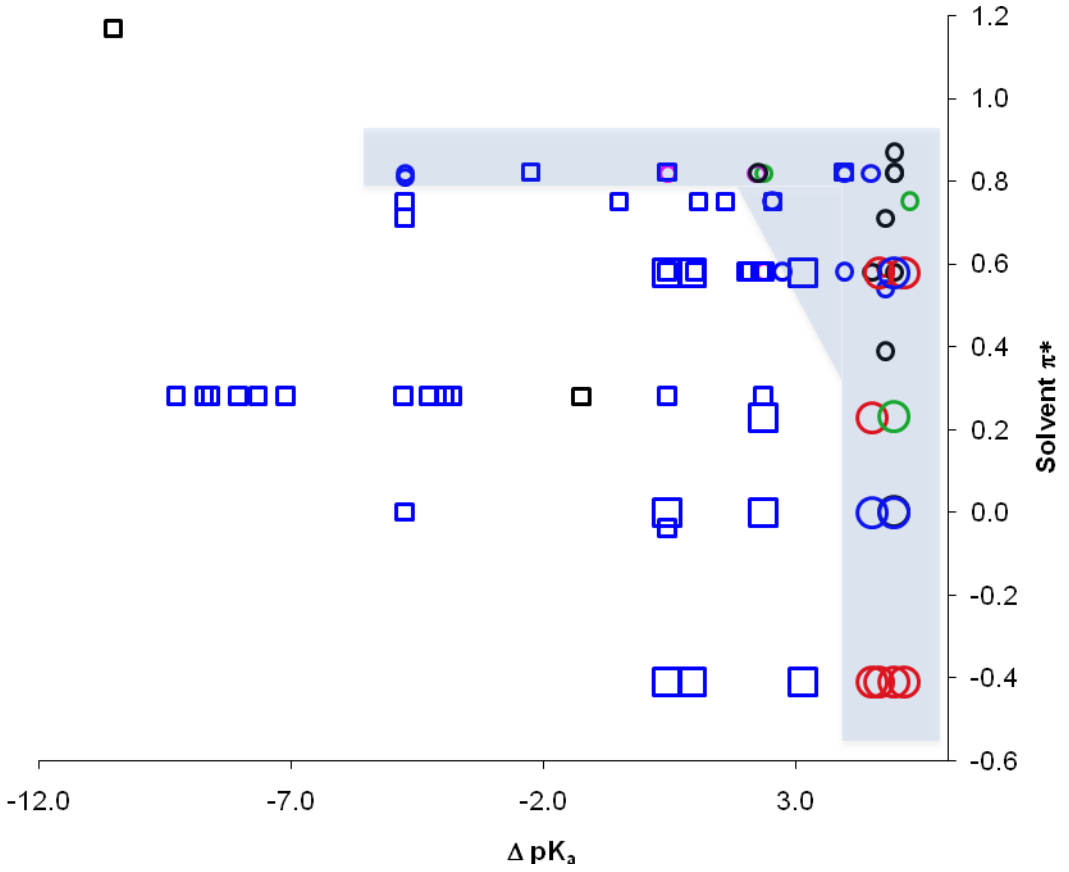

Figure 3-22. A survey of complexation between N-heterocyclic bases with carboxylic acids in a variety of solvents. Squares and circles represent molecular and ionic complexes, respectively; small symbols (○,□) are literature data and large symbols (○, □) are data reported here. 1:1 complexes are shown in blue, 1:2 (base:acid) in green, and 1:3 in red. Complexes with unknown stoichiometry are shown in black. The shaded zone is where proton transfer has been observed. See Supporting Information for data table. $\Delta pK_a = pK_{aBH+} - pK_{aAH}$; π* = Kamlet-Taft dipolarity/polarizability parameter.

Isoquinoline-trifluoroacetic acid complexes in a range of solvents (hexane, octane, carbon tetrachloride, toluene, butyl chloride, chloroform, acetonitrile,[108] and FC-72) are included in **Figure 3-22** and summarized in **Table 3-4**. The data show that the 1:1 complex changes from molecular to ionic with increasing solvent polarity.[108] It was reported that the electronic spectra of the ionic 1:2 complexes were not sensitive to the solvent. Through continuous variations experiments and IR spectroscopy (**Figure 3-1** and **Figure 3-19**) we have observed a 1:3 isoquinoline:**1** ionic complex in FC-72, confirming that more complex stoichiometry is required for proton transfer in *fluorous* solvents.

Table 3-4. Occurance of proton transfer in the complexation between trifluoroacetic acid (organic solvents) or **1** (FC-72) and isoquinoline in increasingly polar solvents.

Solvent	π^*	Stoichiometry (B:HA)	Type
acetonitrile[108]	0.75	1:1	$BH^+ \bullet A$
chlorobenzene[108]	0.71	1:1	$BH^+ \bullet A$
benzene[108]	0.59	1:1	$B \bullet HA/BH^+ \bullet A$
chloroform[a,108,112]	0.58	1:1/1:2 mixture	$B \bullet HA/BH^+ \bullet A \bullet HA$
toluene[108]	0.54	1:1/1:2 mixture	$B \bullet HA/BH^+ \bullet A \bullet HA$
butyl chloride[108]	0.39	1:1/1:2 mixture	$B \bullet HA/BH^+ \bullet A \bullet HA$
carbon tetrachloride[108]	0.28	1:1/1:2 mixture	$B \bullet HA/BH^+ \bullet A \bullet HA$
FC-72	-0.41	1:3	$BH^+ \bullet A \bullet HA \bullet HA$

[a]1:2 ionic form is dominant under conditions of excess acid

It is clear from the data that excess acid is generally required for proton transfer to occur in non-polar environments. Fluorous solvents require a larger excess of acid to base, 3:1, compared to the 2:1 excess observed in non-polar organic solvents. Reversible proton transfer along the N---H---O hydrogen bridge in a fluorous environment can be schematically represented in **Scheme 3-1**, where B is a pyridine-like base and HA is a fluorous-soluble acid. The hydrogen bonds of the carboxylic acid dimer must (a) first be broken, followed by (b) formation of a base-acid hydrogen-bonded complex. In non-polarizable environments such as fluorous liquids, (c) solvation by additional acids is necessary to facilitate proton transfer. Of the bases listed in **Table 3-1** only those that formed 1:3 (base:acid) complexes with **1** in FC-72 (quinoline, pyridine, and isoquinoline), show evidence of proton transfer (large red circles in **Figure 3-22**). The complexes of pyrazine, pyrimidine, and quinazoline are molecular and 1:1 (large blue squares in **Figure 3-22**). Proton transfer and the concurrent rearrangement of acid molecules, or rearrangement of the solvent in polar environments, are accompanied by a significant decrease in entropy. Therefore, for proton transfer to be energetically favorable, the free energy of formation of the complex must compensate for the entropic costs of forming a higher-order complex.

$$(HA)_2 \rightleftharpoons 2HA \qquad \text{(a)}$$

$$B + HA \rightleftharpoons B{\bullet}HA \qquad \text{(b)}$$

$$(B{\bullet}HA) + nHA \rightleftharpoons (BH^+{\bullet}A^-)(HA)_n \qquad \text{(c)}$$

Scheme 3-1

3.4 CONCLUSIONS

We have shown that proton transfer and stabilization of the cationic BH^+ occurs in strongly polar solvents and occurs in non-polar fluorous solvents, but only with excess acid. While a two-fold excess of acid is sufficient to promote proton transfer in non-polar organic solvents, a three-fold excess is necessary in fluorous solvents. 1:3 ionic hydrogen bonds ($BH^+ \bullet A^-HAHA$) are observed in complexes of quinoline, isoquinoline, and pyridine with **1** in FC-72. Proton transfer is possible in such a non-polar environment because the additional acids 'solvate' the ionic bond and shield it from the environment. The stoichiometry and formation of ionic complexes have been demonstrated using continuous variations methods and IR spectroscopy. 1:1 molecular complexes (B•HA) were observed between pyrazine, pyrimidine, and quinazoline and **1** in FC-72. We suggested that the free energy of complex formation between these bases and **1** is not enough to compensate for the free energy cost of the acid dimer dissociation and ordering required to solvate the ionic bond. Forcing the higher-order complexes by employing such a non-polar solvent could also prove useful in supramolecular chemistry applications.

3.5 ACKNOWLEDGEMENTS

This research was funded by the National Science Foundation (NSF) through grants CHE 0315188 and CHE0615952.

3.6 SUPPORTING INFORMATION

Supporting information for chapter 3.0 'Molecular and Ionic Hydrogen Bond Formation in Fluorous Solvents' can be found in **Appendix B**. This includes a derivation of the normalized method of continuous variations as well as Figures showing: (**Figure B-1**) UV spectra from a constant-volume titration of quinoline with **1** in FC-72, (**Figure B-2**) titration curve at 314 nm resulting from a titration of quinoline with **1** in FC-72, (**Figure B-3**) Overlay of predicted concentration profiles from model-free EFA and regression analysis of the UV spectra resulting from a constant-volume titration of isoquinoline with **1** in FC-72, (**Figure B-4**) IR spectra showing carbonyl and quinoline ring vibrational regions from a solvent –free titration of neat quinoline with **1**, (**Figure B-5**) IR spectra showing carbonyl and quinoline ring vibrational regions from a titration of constant 2.5 mM **1** with quinoline in FC-72, (**Figure B-6**) IR spectrum of a perfluorodecanoic acid-quinoline crystal/KBr pellet, (**Table B-1**) a listing of literature and experimental data corresponding to molecular complexes shown in **Figure 3-22**, and (**Table B-2**) a listing of literature and experimental data corresponding to ionic complexes shown in **Figure 3-22**.

4.0 EXTRACTION AND METALATION OF PORPHYRINS IN FLUOROUS LIQUIDS WITH CARBOXYLIC ACIDS AND METAL SALTS

Abstract:

Porphyrins have found application in a remarkable variety of areas such as sensors, ion selective electrodes, photodynamic therapy, and energy transfer systems. Here, we demonstrate the extraction of 5,10,15,20-tetraphenylporphyrin (TPhP) and 5,10,15,20-tetra(4-pyridyl)porphyrin (TPyP) into a mixture of perfluorohexanes (FC-72) through noncovalent interactions with Krytox (**1**), a carboxylic acid terminated perfluoropolyether. We found that **1** transfers two protons to the TPhP tetrapyrrole ring to create the porphyrin dication (H_2TPhP^{2+}) in FC-72 while up to six protons are transferred to the TPyP pyridyl and tetrapyrrole nitrogens to create a hexavalent cation macrocycle in the fluorous phase. The total charge on TPyP is controlled by adjusting the concentration of **1** in the fluorous phase. In addition, we observed extraction of ZnTPyP from $CDCl_3$ with **1**/FC-72, while ZnTPhP is not extracted by **1**/FC-72. We prepared the Zn salt of **1** and found that it extracts (from $CDCl_3$) and metalates TPyP but not TPhP. Competitive binding between the porphyrins and an ethanol co-solvent hinders the extraction of both TPhP and TPyP and inhibits the formation of the TPyP dication in FC-72. By controlling the concentration of porphyrin, **1**, and ethanol, it is possible to reversibly solubilize TPyP in the

fluorous phase through non-covalent interactions between the pyridyl moieties and **1** while leaving the tetrapyrrole ring available to interact with metals or other substrates. In addition, both porphyrins and ZnTPyP are easily recovered from the flurous phase using commercially available fluorous solid phase extraction cartridges. Understanding noncovalent interactions in fluorous matrices should lead to development of more robust devices for sensing and energy transfer.

4.1 INTRODUCTION

Porphyrins have interesting optical and electrical properties resulting from their highly conjugated π-electron system that is sensitive to changes to the conjugation pathway. This makes porphyrins and their derivatives particularly useful in optical sensor development.[113-130] In addition, there has been great interest in synthetic functionalized metalloporphyrins as photosensitizers in photodynamic therapy, molecular[131-133] and ion-pair[134] receptors, electrodes in molecular photovoltaic devices,[135,136] and building blocks in supramolecular chemistry.[137,138] Porphyrins and metalloporphryins have been exploited as ionophores in the development of ion selective electrodes[139-144] and as chemically modified electrodes[145] in amperometric and voltammetric sensors.

In general, chemical sensors involve some sensing material embedded in a matrix. It is well known that sensor performance, although highly dependent on the properties of the sensing material, is often limited by this supporting matrix.[146] A poorly-solvating matrix provides a more selective environment for chemical sensing by reducing the concentration of interfering species in the matrix. Fluorous liquids are the ultimate non-competitive solvent.[86] However,

solubilization of large organic molecules, such as porphyrins, in extremely non-polar fluorous liquids at room temperature is challenging. There are only a handful of reports on covalently modified fluorous-tagged porphyrins that are soluble in fluorous liquids[147-151] and even fewer on non-fluorous tagged porphyrins in a fluorous matrix.[56,152] In fact there are only a few reports exploiting noncovalent interactions in perfluorocarbons[20,32,51,86,88,153,154] and the fundamental science is not fully understood. El Bakkari *et al*.[56] have demonstrated near-complete reversible extraction of 5,10,15,20-tetra(4-pyridyl)porphyrin (TPyP) from chloroform into a perfluorodecalin solution using a neat excess of a 'heavy fluorous' (i.e. containing eight perfluorooctyl fragments) $Cu(II)_2$-tetracarboxylate complex (**2**). The resulting perfluorosoluble **2**-TPyP supramolecular assembly showed no evidence of TPyP metalation by copper(II) ions under the conditions used.[155] With an equimolar ratio of **2** to TPyP, a red precipitate formed and was postulated to be a polymeric supramolecular assembly with limited solubility in perfluorocarbons.[56] Because **2** was not able to extract 5,10,15,20-tetraphenylporphyrin (TPhP), it was concluded that the interaction between **2** and TPyP occurs only through the pyridyl nitrogens.

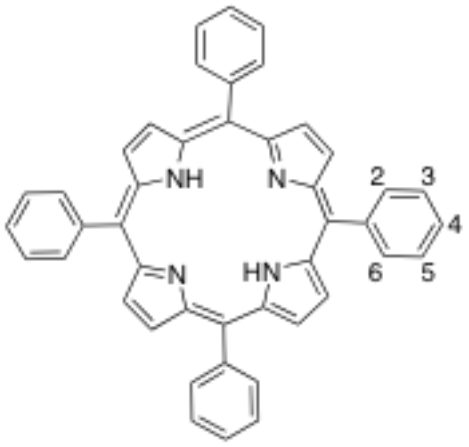

TPhP

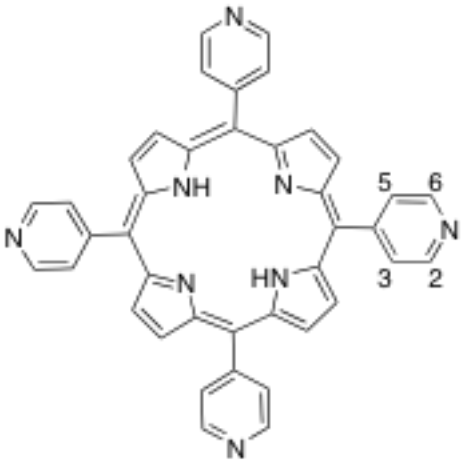

TPyP

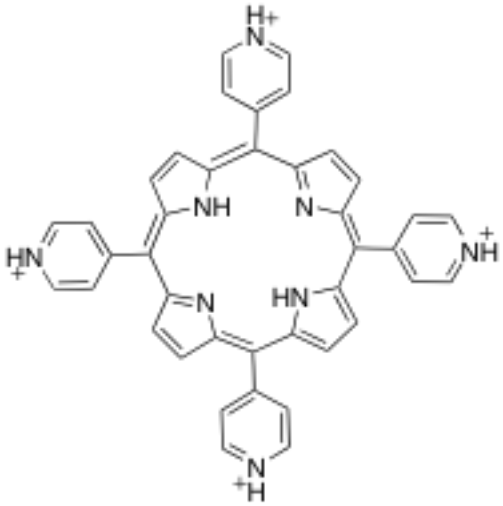

N, 'neutral' TPyP

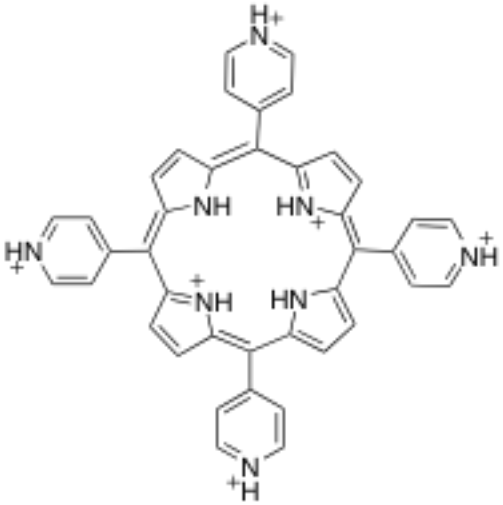

P, 'protonated' TPyP

We have observed[20] that Krytox (**1**), a carboxylic acid terminated poly-hexafluoropropylene oxide, significantly enhances the extraction of pyridine (100-fold with excess **1** as compared to **1**-free) and substituted pyridines from chloroform into a mixture of

perfluorohexanes (FC-72) while having little effect on the non-heterocyclic counterparts (i.e. phenol or aniline).

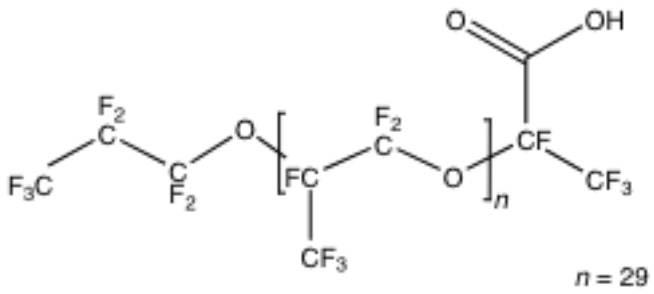

1

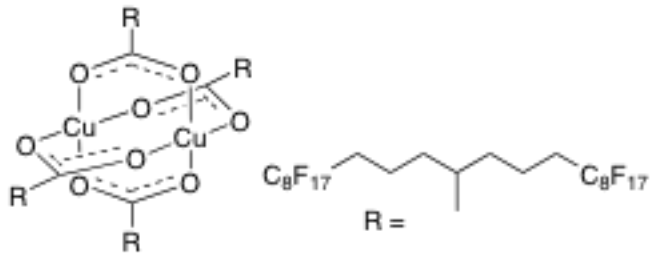

2

Knowing this, we wondered if the much simpler **1** (compared to **2**)[56,155,156] would effectively extract TPyP. Here we demonstrate reversible extraction of both TPhP and TPyP from $CHCl_3$ with **1** in FC-72. Two protons are transferred from **1** to the macrocyclic tetrapyrrole (tetrapyrrole hereafter) of TPhP. In addition to the two protons transferred to the tetrapyrrole, four protons can be transferred from **1** to the TPyP pyridyl nitrogens for a total of six protons. The overall charge on TPyP is controlled through adjusting the relative concentrations of **1** and TPyP. Interestingly, we observed that Zn$\mathbf{1}_2$ salts effectively extract and rapidly metalate TPyP in

the fluorous phase under ambient conditions while we saw no interaction with TPhP. The copper complex (**2**) previously employed to extract TPyP into the fluorous phase did not metalate TPyP under similar conditions.[155,156] However, Zn$\mathbf{1}_2$ is able to metalate TPyP. Easy recovery of both the porphyrin (metalated and free base) and **1** is achieved using commercially available fluorous solid phase extraction (F-SPE) cartridges. The purpose of this work is to gain a fundamental understanding of the nature of the interactions of porphyrins with **1** in a highly fluorinated matrix leading to the development of more robust and selective porphyrin-based sensors and devices for energy transfer, optical communication, and data storage in fluorous media.

4.2 EXPERIMENTAL

4.2.1 Chemicals and Solutions

Chloroform (Fisher Scientific, Fair Lawn, NJ) and deuterated chloroform (Cambridge Isotope Laboratories, Inc., Andover, MA) were dried over activated molecular sieves, and treated with potassium carbonate (EM Science, Cherry Hill, NJ) to neutralize any HCl that had formed as a result of exposure to light.[157,158] Commercially available $CHCl_3$ contains ~1% (v/v) ethanol as a stabilizer to prevent the formation of HCl and phosgene[157,158] while deuterated chloroform does not. Methanol, ethanol, and dimethylformamide (DMF) were purchased from J.T. Baker (Phillipsburg, NJ) and dried over molecular sieves. Meso-tetraphenylporphyrin (TPhP), 5,10,15,20-tetra(4-pyridyl)porphyrin (TPyP), and 2,2,2-trifluoroethanol were purchased from Sigma-Aldrich and used as received. FC-72 Fluorinert Electronic Liquid (a mixture of perfluorohexanes) was purchased from 3M (St. Paul, MN) and Krytox 157FSH (**1**) from Miller-

Stephenson Chemical Co., Inc. (Danbury, CT). ^{19}F-NMR analysis of **1** resulted in a number-averaged molecular weight of 5150 g mol^{-1} with an average of 29 polymer repeat units. We have previously reported a molecular weight of 5840 g mol^{-1} with 33 repeat units[20] from a different lot.

As mentioned above, all $CHCl_3$ solutions within this work contain ethanol. Solutions made from $CDCl_3$ contain 0.00, 1.00, or 2.00 % (v/v) added ethanol as specified. Separate stock solutions of 1.0 mM TPhP and TPyP were made in $CHCl_3$, and $CDCl_3$ with 0.00, 1.00, and 2.00 % (v/v) ethanol as the solvent. All containers of stock solutions were placed in a Cole-Parmer (Chicago, IL) ultrasonicator bath for 10-30 minutes to ensure dissolution of the materials in their respective solvents.

4.2.2 Preparation of Zinc Salt and Metalloporphryins

The following procedure was adapted from Doan, *et al.*[32] for the preparation of the zinc salt of **1** (Zn**1**$_2$). Equal weights (2.0 g each) of **1** and a 1.0 M $ZnCO_3$ aqueous slurry were mixed in a separatory funnel and shaken vigorously until an emulsion formed. To break the emulsion, 2.0 mL each of methanol and trifluoroethanol were added to the separatory funnel. The resulting mixture was extracted with 2.0 mL of FC-72 several times. The FC-72 solution was then stirred over activated molecular sieves overnight, and passed through a 0.22 μm pore-size nylon syringe filter (Acrodisc) before allowing the solvent to evaporate. The resulting Zn**1**$_2$ oil was then dried overnight at 180 °C. FTIR spectra confirmed the formation of the salt with the disappearance of the **1**-carboxylic acid dimer band and the appearance of a carboxylate band (**Figure 4-1**). ^{1}H NMR spectra taken before and after formation of Zn**1**$_2$ (**Figure 4-2**) show that the **1** proton signal disappears upon salt formation. The zinc metalloporphyrins, ZnTPhP and ZnTPyP, were

synthesized according to Adler[159] and formation of the metalloporphyrin was verified using UV/vis and ^{1}H NMR.

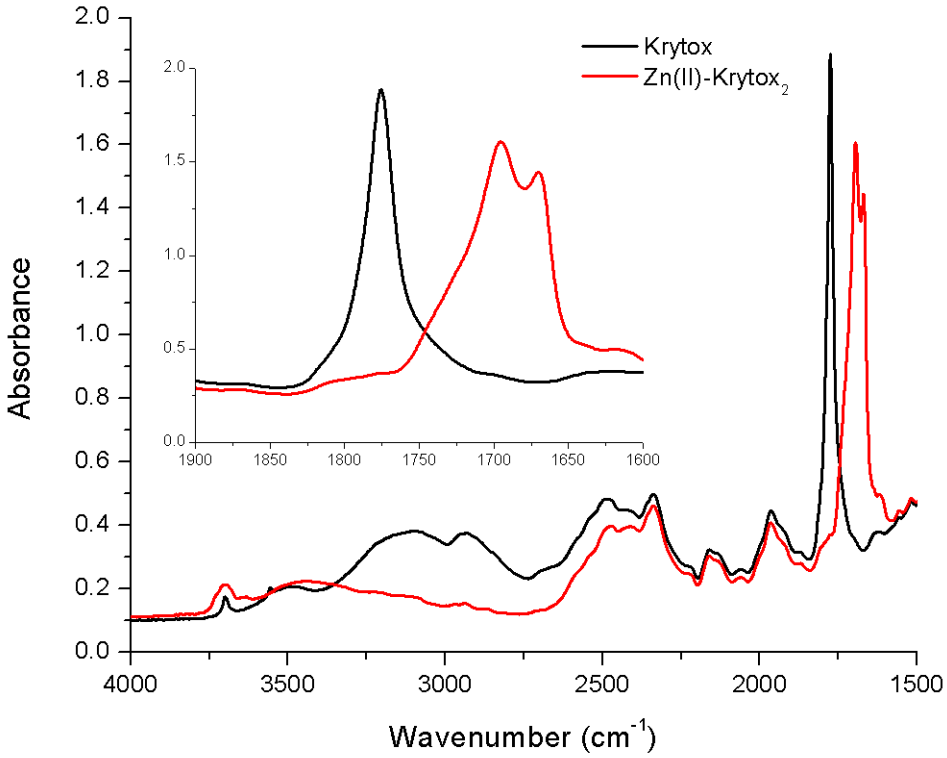

Figure 4-1. FTIR spectrum of **1** carboxylic acid (black line) and the Zn(II)-**1**$_2$ metal-salt (red line). The inset shows a closer view of the carbonyl region of the spectrum. The splitting of the carboxylate band (~1700 cm^{-1}) is caused by restriction of the C_α-C_β bond in the cyclic –COO^- - Zn^{2+} - COO^- bond by the bulky CF_3 group on **1**.[32]

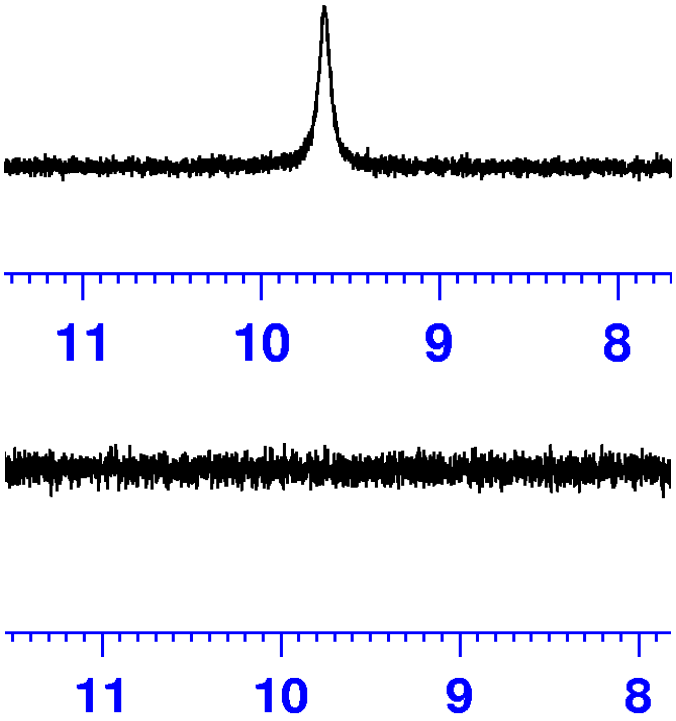

Figure 4-2. ^{1}H-NMR spectra of 8.0 mM **1** (top) and 5.0 mM Zn-$\mathbf{1}_2$ in FC-72 (bottom).

4.2.3 Fluorous Biphasic Extractions

A series of liquid-liquid fluorous biphasic extractions was carried out by placing aliquots of each porphyrin solution and 0.0 – 20.0 mM **1**/FC-72 (phase ratio, $\Phi = 1.0$ for all extractions) in GC autosampler vials and shaking for 10 minutes on a mechanical shaker (in-house construction) to ensure homogeneity. The samples were allowed to rest for 10 minutes before measurements were taken. Samples of each porphyrin solution were extracted with **1**-free FC-72 as controls. The layers were physically separated using a syringe and all baseline-corrected absorbance values

were measured under ambient conditions (22.0 ± 1 °C). ^{1}H NMR measurements of the stock solutions and FC-72 receiving phase were carried out.

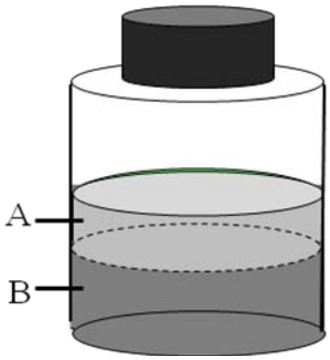

Figure 4-3. Diagram of biphasic extraction experiments. Phase A (source phase) contains TPhP or TPyP dissolved in either $CHCl_3$ with ~1% (v/v) ethanol, $CDCl_3$, $CDCl_3$ with 1.00% (v/v) ethanol, or $CDCl_3$ with 2.00% (v/v) ethanol while phase B contains **1** (concentration varies by sample) in FC-72 (phase ratio, Φ = 1.0).

Extractions of TPhP and TPyP were carried out similar to those discussed above but with Zn**1**$_2$ in place of **1** in the FC-72 receiving phase. Extractions of ZnTPhP and ZnTPyP from $CHCl_3$ were also carried out as discussed above.

Extractions were carried out to determine the distribution of ethanol between $CDCl_3$ and FC-72 with and without **1** in FC-72. 1.0 mL $CDCl_3$ with 1.00% (v/v) ethanol was shaken separately with 1.0 mL FC-72 and a 10.0 mM solution of **1**/FC-72. A 0.3 mL aliquot of each resulting FC-72 solution was transferred to a NMR tube and 10.0 μL trifluoroethanol was added as an internal standard. ^{1}H NMR measurements were taken at 25 °C using a melting-point capillary filled with deuterated acetone as the locking solvent. Using the same procedure,

extractions with $CHCl_3$ ~1% (v/v) ethanol in place of $CDCl_3$ were carried out to determine the concentration of $CHCl_3$ in FC-72.

4.2.4 Recovery of Porphyrins using Fluorous Solid Phase Extraction

Both T PhP and T PyP were recovered using fluorous solid phase extraction (F-SPE). A commercially available 5 g FluoroFlash F-SPE cartridge (Fluorous Technologies Incorporated, Pittsburgh, PA) was emptied and 0.25 g of the fluorous silica sorbent material was placed into a 1 g capacity tube (Sigma Aldrich, St. Louis, MO) and topped with a frit. The cartridge was then conditioned by first loading 0.5 mL of DMF onto the cardridge using a vacuum and then passing 2.0 mL of a hydrophilic eluant (80:20 methanol:H_2O) through the cartridge. After each fluorous biphasic extraction (described above) the resulting fluorous receiving phase contains the **1**-porphyrin complex. The fluorous phase was separated with a syringe and 0.3 mL was loaded onto the cartridge under a vacuum. The porphyrin was then desorbed by passing two 0.5 mL aliquots of a fluorophobic eluent (50:50 $CHCl_3$:ethanol) through the cartridge. **1** was then recovered separately with two separate washes of 0.3 mL FC-72 eluent under vacuum.

4.2.5 Instrumentation

A Hewlett-Packard 8452A UV-visible diode array spectrophotometer was used for all UV absorbance measurements. All samples were measured in a 0.1 cm path length sample cell (Fisher Scientific, Pittsburgh, PA). A Varian Excalibur FT-IR spectrophotometer was used for IR measurements and all samples were measured in a 0.1 mm path length cell against a blank background at resolution = 2 cm^{-1} with 50 scans averaged. All IR spectra were smoothed using a

5-point boxcar and baseline corrected. ^{1}H and ^{19}F NMR spectra were collected with a Bruker 300 MHz spectrometer. For FC-72 samples, a melting point capillary was filled with $CDCl_3$ and inserted into the NMR tube so that the fluorous solvent remained unaffected by the locking solvent.

4.3 RESULTS AND DISCUSSION

4.3.1 Receptor-based extractions of TPhP and TPyP into FC-72

A series of liquid-liquid fluorous biphasic extractions was carried out with 0.1 mM TPhP/$CHCl_3$ in the source phase and from 0.0 – 10.0 mM **1**/FC-72 in the receiving phase. Absorbance spectra of the FC-72 receiving phase resulting from these extractions along with a plot of the absorbance as a function of [**1**] are shown in **Figure 4-4**.

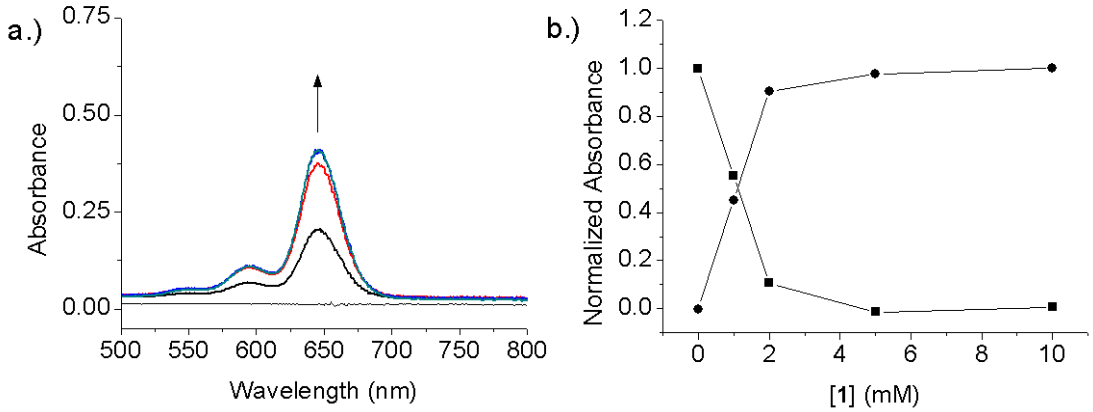

Figure 4-4. From a series of fluorous biphasic extractions of 0.1 mM TPhP/$CHCl_3$ with increasing **1**/FC-72 (0.0-10.0 mM) in FC-72 (see **Figure 4-1**): a.) the *Q*-band region of the absorbance spectra from the FC-72 receiving phase following extraction, the arrow indicates direction of change with samples containing higher [**1**]; and, b.) the normalized absorbance of the $CHCl_3$ source phase at 516 nm (squares) and of the FC-72 receiving phase at 645 nm (circles) as a function of [**1**]. **1** is non-absorbing above 205 nm.

Figure 4-5. Photograph of samples from the extraction of 1.0 mM TPhP in $CHCl_3$ (top phase) with 0.0 - 20.0 mM **1** in FC-72 (bottom phase).

A solution of TPhP/$CHCl_3$ is deep red in color (top phase, **Figure 4-5**) and the *Q*-band region of the spectrum is the typical four-banded spectrum of the free base (grey line, **Figure 4-8**a) Upon extraction into FC-72, the solution turns bright green (botton phase, **Figure 4-5**) and the spectrum changes to the two-banded form indicative of the dication[160] (**Figure 4-4**a). This two-banded spectrum is the only type observed in the FC-72 phase. The absorbance intensity, but not the shape of the spectrum, changes with increasing with [**1**]. The two hydrogen-bond accepting tetrapyrrole nitrogens of TPhP are the only available binding sites for **1**. Thus, the macrocycle is 'pulled' into the fluorous phase through interactions between **1** carboxylic acid groups and the TPhP tetrapyrrole nitrogens. **Figure 4-4**b shows that > 90% of 0.1 mM TPhP is extracted with an equal volume of 2.0 mM **1**.

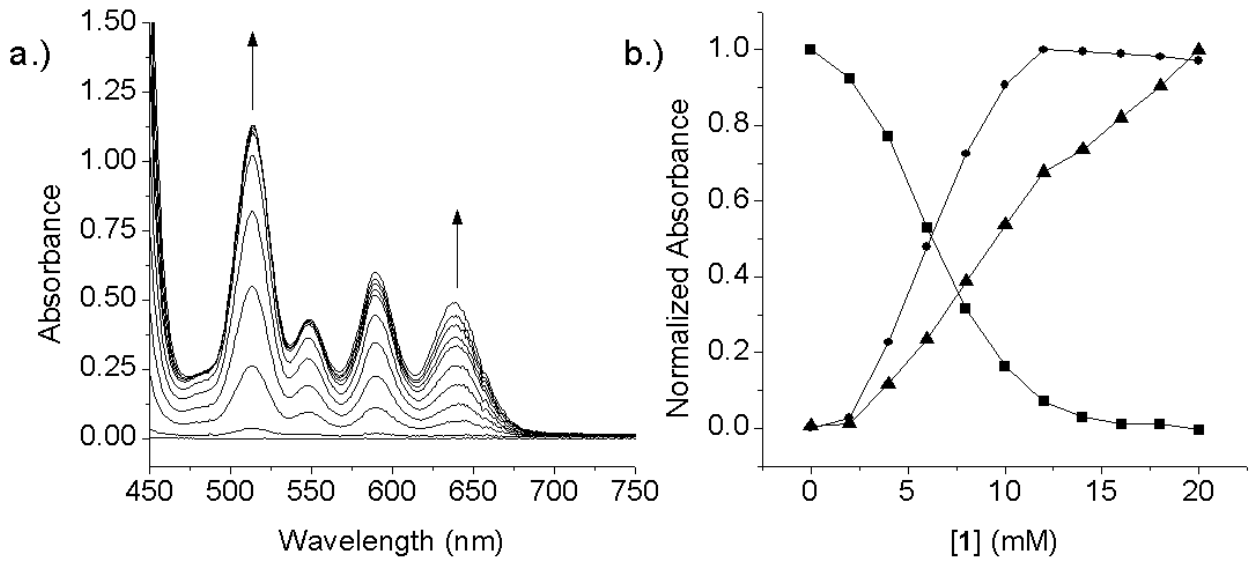

Figure 4-6. From a series of fluorous biphasic extractions of 1.0 mM TPyP/$CHCl_3$ with increasing **1**/FC-72 (0.0-20.0 mM): a.) the *Q*-band region of the absorbance spectra from the FC-72 receiving phase following extraction, the arrows indicate direction of change for samples with increasing [**1**]; and, b.) the normalized absorbance of the $CHCl_3$ source phase at 514 nm (squares) and of the FC-72 receiving phase at 516 nm (circles) and 638 nm (triangles). **1** is non-absorbing above 205 nm.

Figure 4-7. Photograph of the extraction of 1.0 mM TPyP in $CHCl_3$ ~ 1% ethanol (top phase) with 0-20 mM Krytox in FC-72 (bottom phase).

The extraction of TPyP (**Figure 4-6**) is not as straightforward as that of TPhP (**Figure 4-4**). A solution of TPyP/$CHCl_3$ is deep red in color (top phase, **Figure 4-7**) and the *Q*-band region of the spectrum is the four-banded spectrum of the free base. Upon extraction into FC-72 the solution does not turn bright green (bottom phase, **Figure 4-7**) typical of the fully protonated tetrapyrrole[160] (P) as we observed for TPhP. Instead, the spectrum of a solution of **1**-TPyP/FC-72 remains the four-banded type as seen with the free base, although the relative intensities of the *Q* bands have changed. **Figure 4-6**b shows that with increasing [**1**], the absorbance of the highest energy *Q* band (516 nm) reaches a maximum around 12 mM **1**. On the other hand, the absorbance of the lowest energy *Q* band continues to increase even though the concentration of TPyP in the receiving phase remains relatively constant beyond solutions of 12.0 mM **1**. As El Bakkari[156] observed in the extraction of TPyP with receptor **2**, it is expected that the receptor-TPyP interaction occurs through the pyridyl nitrogens. However, we have shown in **Figure 4-4** that receptor **1** extracts TPhP by protonating the tetrapyrrole nitrogens whereas **2** showed no interaction with TPhP.[87] Consequently, it is possible that **1** has some interaction with TPyP tetrapyrrole nitrogens. Fleisher[161] reported that the TPyP tetrapyrrole nitrogen atoms are considerably less basic than the pyridyl nitrogens. Thus, we expect the interaction with **1** to be more favorable with the pyridyl over the tetrapyrrole nitrogens on TPyP.

Both TPhP and TPyP can be easily recovered from the fluorous phase using commercially available F-SPE cartridges. **Figure 4-8** shows the absorbance spectra of the **1**-porphyrin complex before loading onto the F-SPE cartridge (black lines) and of an organic eluent containing the porphyrin (grey lines). F-SPE cartridges contain a silica-based perfluoroalkyl bonded phase that retains compounds based on fluorine content. The spectra of the samples following extraction (black lines, **Figure 4-8**) match that of the respective **1**-TPhP and **1**-TPyP

complexes (compare to **Figure 4-4**a and **Figure 4-6**a). When this solution was loaded onto the column under vacuum, the **1**-porphyrin complex was retained on the F-SPE column through interactions with **1**. The porphyrin was then eluted with an organic eluent (50:50 $CHCl_3$:ethanol). The *Q*-band spectra of the eluted porphyrin in the organic eluent correspond to the four-banded spectra of the free base. In other words, the porphyrin is eluted by the organic eluent while **1** is retained through fluorophilic interactions with the fluorous silica. **1** was then eluted from the cartridge with FC-72.

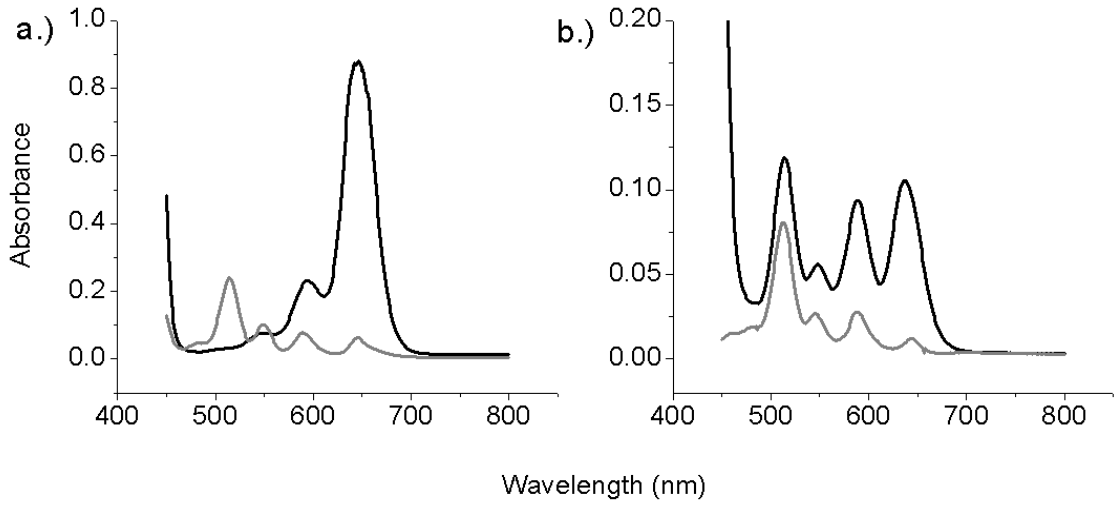

Figure 4-8. The *Q*-band region of the absorbance spectrum of flurous phase (black) resulting from the extraction of a.) 1.0 mM TPhP and b.) 1.0 mM TPyP in $CDCl_3$ before loading onto a F-SPE cardridge and of a 50:50 $CHCl_3$:ethanol wash of the loaded cartridge (grey).

To investigate further the nature of **1**-TPyP interactions, TPyP was first extracted from $CHCl_3$ with a solution of **1** in FC-72, then separated from the source phase and titrated with additional **1** in FC-72. The resulting spectra are shown in **Figure 4-9**. Addition of **1** causes the absorbance of the high energy *Q* band in the TPyP spectrum to decrease while the low energy band increases. This is consistent with protonation of the tetrapyrrole ring.

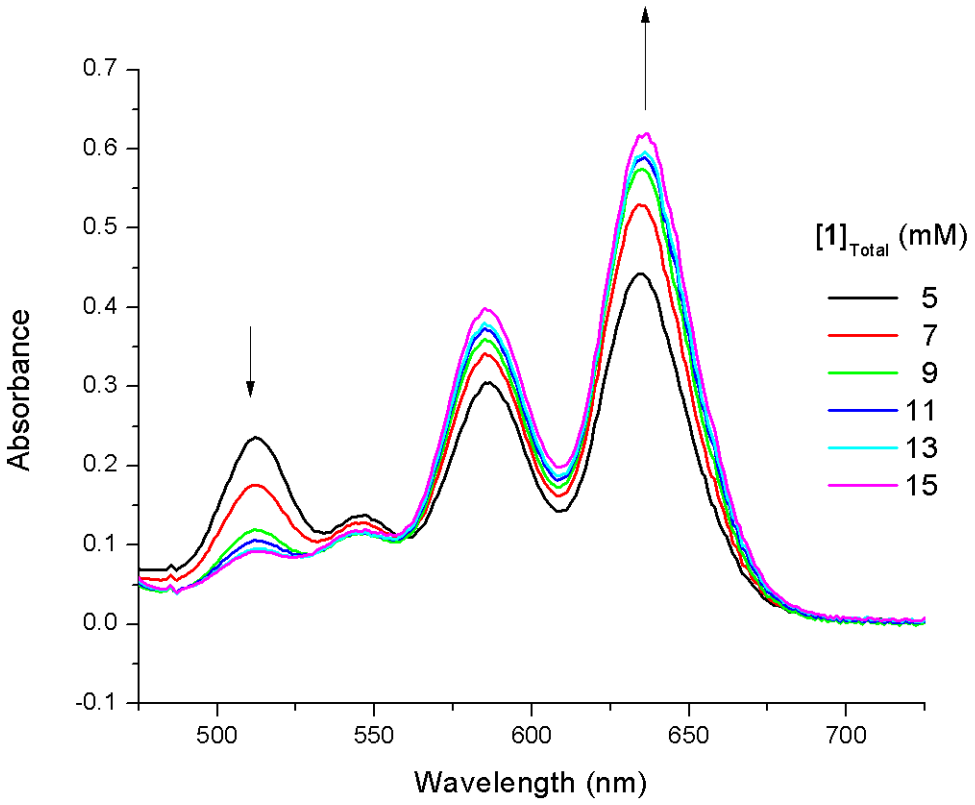

Figure 4-9. *Q*-band region of the spectra resulting from a constant-volume titration of a **1**-TPyP solution in FC-72 with additional **1**. Each sample contains 0.36 mM TPyP. Spectra are labeled according to total [**1**] and arrows indicate direction of change with increasing [**1**] (non-absorbing in visible range).

Absorbance spectroscopy is impractical for studying the nature of the **1**-TPyP pyridyl interactions because protons on the pyridine nitrogens do not interact significantly with the porphyrin tetrapyrrole conjugation pathway.[161,162] Therefore, ^{1}H-NMR was employed to verify that **1** transfers a proton to the pyridyl moieties on TPyP in FC-72. The effects of increasing [**1**] on the ^{1}H-NMR spectra of a series of **1**-TPyP and **1**-TPhP solutions in FC-72 are shown in **Figure 4-10**. Here, an extraction of TPyP was carried out with $CDCl_3$ as the source phase in place of $CHCl_3$ so that the small amount of source phase dissolved in the receiving phase did not interfere with the resulting spectrum.

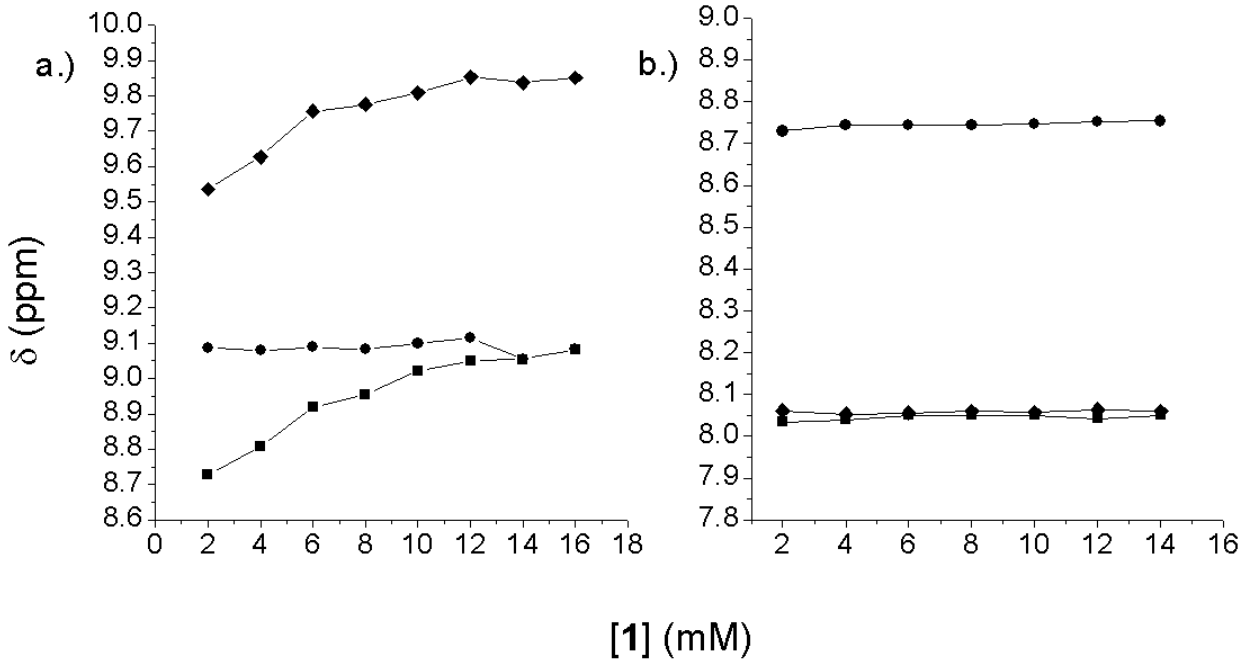

Figure 4-10. ^{1}H-NMR position of peaks due to a.) TPyP pyridyl H_3, H_5 (square), tetrapyrrole (circle), and pyridyl H_2, H_6 (diamond) protons and b.) TPhP phenyl H_3, H_5 (square), tetrapyrrole (circle), and phenyl H_2, H_4, H_6 (diamond) protons as a function of [**1**] in FC-72 resulting from extraction of 1.0 mM porphyrin in $CDCl_3$ with FC-72 containing **1** (Φ = 1).

The signals of the $H_{2,6}$ and $H_{3,5}$ protons (see structures) of the peripheral aromatic rings of TPyP shift downfield with increasing [**1**] while the difference in chemical shifts ($\Delta\delta$) between these two types of protons as well as the chemical shift of the tetrapyrrole protons all remain fairly constant. Meanwhile, **1** protons are becoming more shielded as the peaks shift upfield (**Figure 4-11**). A similar experiment was performed with TPhP as a control because the TPhP phenyl moieties are not proton acceptors. The chemical shifts of the protons associated with the TPhP phenyl groups (**Figure 4-10**b) remain constant with addition of **1**. Therefore, the downfield shift of the pyridyl protons and concurrent upfield shift of **1** protons can be attributed to the formation of pyridinium ions, as we have previously seen between **1** and pyridine-like bases in fluorous solvents.[20,153]

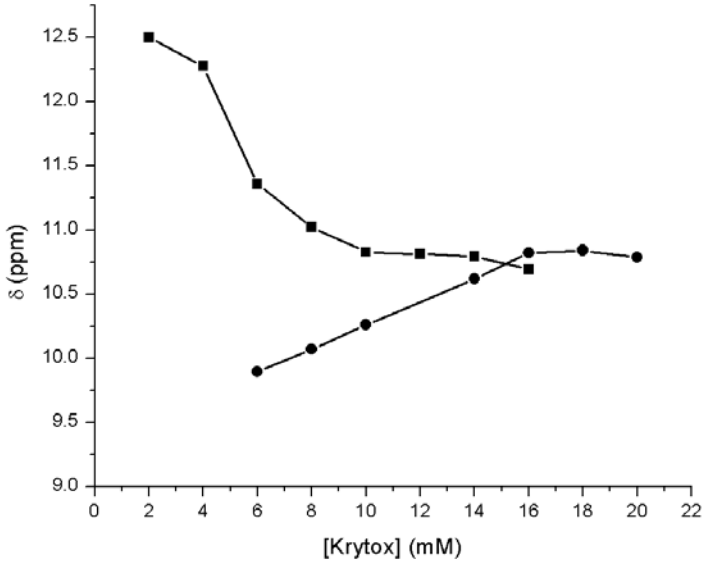

Figure 4-11. The ^{1}H-NMR position of **1** proton peaks as a function of [**1**] in FC-72. The squares are from the receiving phase of an extraction of 1.0 mM TPyP in $CDCl_3$ with FC-72 containing **1** (Φ = 1) and circles are control **1** samples.

We draw the conclusion that the interaction between **1** and TPhP is through protonation of the porphyrin ring while the interaction between **1** and TPyP depends on the ratio of **1** to TPyP. At low **1**:TPyP ratios, the interaction is primarily through protonation of the more basic pyridyl moieties while protonation of the porphyrin tetrapyrrole ring occurs only under a greater excess of **1**.

The *Q*-band spectrum of TPyP is sensitive to whether the tetrapyrrole is neutral (N) or fully protonated (P) (refer to structures) and it is independent of the state of protonation of the pyridine moieties.[161] Despite the presence of charge on the pyridinium moieties, we will use N and P to refer to the molecule as a whole. The molar absorptivity (ε) of P at the wavelength of the high energy *Q* band (513 nm) is equal to zero (**Equation 4-1**).

$$\varepsilon_{513}^{P} = 0$$

Equation 4-1

The absorbance (A) at 513 nm is then a function of the concentration of TPyP with a neutral pyrrolene ring (N) according to the Beer-Lambert Law, where b is path length and C is concentration.

$$A_{513} = \varepsilon_{513}^{N} b C_N$$

Equation 4-2

Substituting $x_{513} = 1/\varepsilon_{513} b$ and rearranging gives the concentration of N.

$$C_N = x_{513} A_{513}$$

Equation 4-3

Both the N and P contribute to the absorbance at the wavelength of the low energy *Q*-band (638 nm), which can be described by **Equation 4-4**.

$$A_{638} = \varepsilon_{638}^{P} b C_P + \varepsilon_{638}^{N} b C_N$$

Equation 4-4

Thus, we can define the concentration of the fully protonated species (C_P) with a function of the absorbance at 638 nm minus a correction factor for the contribution of the neutral species (N).

$$C_P = x_{638} A_{638} - y_{513} A_{513}$$

Equation 4-5

Here, $x_{638} = 1/\varepsilon_{638} b$ and $y_{513} = 1/\varepsilon_{513} b$. Because of the nature of the system, it is not possible to obtain the spectrum of pure N or P TPyP in FC-72. Thus, we cannot determine the molar absorptivity for either species. Nonetheless, for a single species in a given solvent, the ratio of absorptivites at 638 and 513 nm should be fairly constant. For N in $CDCl_3$, $\left(\frac{\varepsilon_{638}^{N}}{\varepsilon_{513}^{N}}\right) = 0.10$.

The total concentration of porphyrin in the fluorous phase (C_T) is then the sum of C_N and C_P.

$$C_T = x_{638}A_{638} - y_{513}A_{513} + x_{513}A_{513}$$

Equation 4-6

For constant C_T, a plot of A_{638} vs. $-A_{513}$ should yield a straight line defined by **Equation 4-7**.

$$A_{638} = -A_{513}\left(\frac{x_{513} - y_{513}}{x_{638}}\right) + \frac{C_T}{x_{638}}$$

Equation 4-7

Figure 4-12 shows the results of such an analysis on the receiving phase spectra resulting from an extraction of 1.0 mM TPyP in $CDCl_3$ with increasing **1** in FC-72 ($\Phi = 1.0$). Recalling that $x = 1/\varepsilon b$, we are able to obtain the molar absorptivity of P at 638 nm (ε_{638}^P) and N at 513 nm (ε_{513}^N) from the regression.

$$\varepsilon_{638}^P = 10300\ \mathrm{M}^{-1}$$

Equation 4-8

$$\varepsilon_{513}^N = 7800\ \mathrm{M}^{-1}$$

Equation 4-9

Introducing these values into **Equation 4-3**, **Equation 4-5**, and **Equation 4-6** gives the absolute values for C_N, C_P, and C_T, respectively, that can be obtained from the spectrum of a mixture containing both species using only the absorbance (A) at 513 and 638 nm.

$$C_N = 1.28A_{513}$$

Equation 4-10

$$C_P = 0.97A_{638} - 0.097A_{513}$$

Equation 4-11

In addition, C_T can be determined independently from the fluorous phase spectra through mass balance from the source phase ($C_T = C_N^i - C_N^f$), where C_N^i and C_N^f represent the initial and final concentration of neutral porphyrin in the source phase, respectively. C_T from mass balance agrees quite well with the sum of C_N and C_P in the fluorous phase (see **Figure 4-13**).

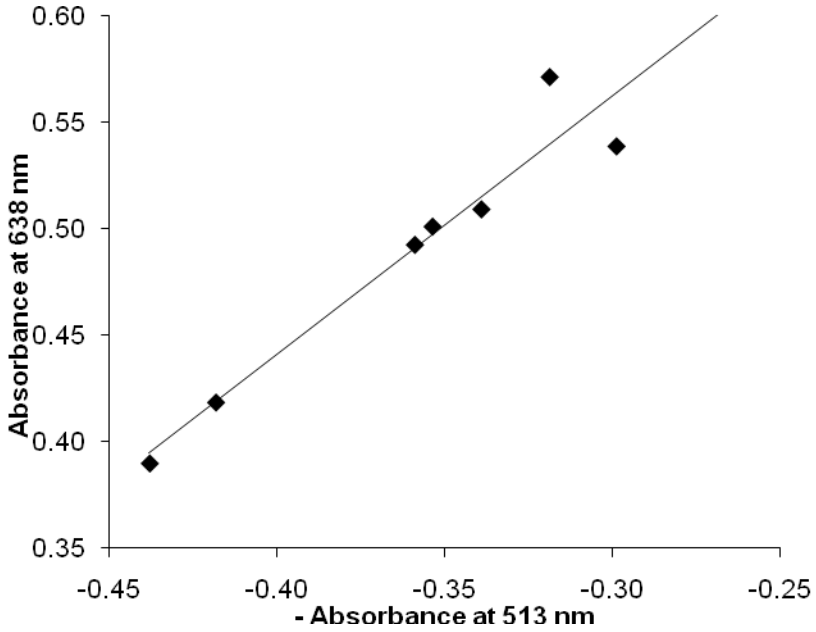

Figure 4-12. Absorbance at 638 nm vs. –absorbance at 513 nm (b = 0.1 cm) from the receiving phase of an extraction of TPyP from $CDCl_3$ with **1** in FC-72, (Φ = 1.0). The total porphyrin concentration for all data used in the regression is constant, $C_T \sim 0.9$ mM. Multiple linear regression yields the equation: y = 1.22x + 0.93, R^2 = 0.93.

Protonation of the tetrapyrrole nitrogens follows protonation of the TPyP pyridyl nitrogens with greater excess **1** (**Figure 4-13**). Thus, it is no surprise that C_P increases with

increasing [**1**]. It is interesting that **1** not only extracts the non-fluorous macrocycle into the fluorous phase through noncovalent interactions, but that the nonpolar fluorous environment can support such a highly charged species (i.e. a total charge of 6^+ for the four pyridyl ligands and two tetrapyrrole nitrogens).

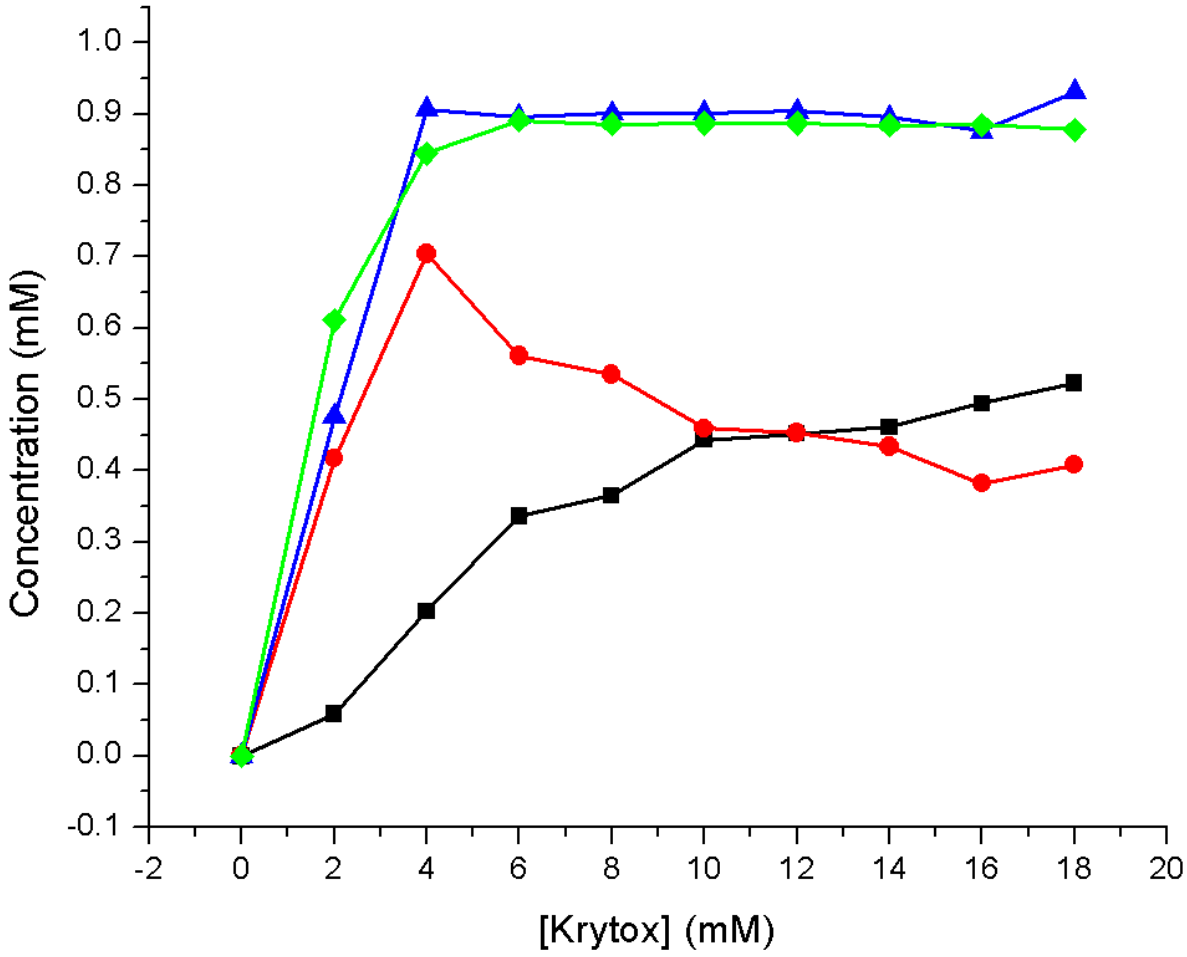

Figure 4-13. The concentrations of P (■) and N (●) forms of TPyP in the receiving phase resulting from an extraction of TPyP from 1.0 mM TPyP solution in $CDCl_3$ source phase with a **1**-containing FC-72 receiving phase (Φ = 1.0), shown as a function of [**1**]. C_T in the fluorous

phase determined by the sum of C_N and C_P (▲) as well as mass balance from $CDCl_3$ phase measurements (◆) are also shown.

We have previously performed a detailed study on the interaction between **1** and pyridine, showing that proton transfer can occur even in extremely nonpolar fluorous environments (see Chapter 2.0, page 15).[20] A further study on complexation between N-heterocyclic bases and carboxylic acids in a range of solvents showed that proton transfer occurs in fluorous environments when both the acid:base ratio and the difference in pK_a between the acid and conjugate acid of the base (ΔpK_a) are sufficiently high (see Chapter 3.0, page 43).[153] Specifically, we have observed proton transfer with 3:1 **1**:base ratios and ΔpK_a in the range from 4.0 - 6.0, where the pK_a of **1** is approximately 0.26.[153] Based on previous observations, protonation of the TPhP tetrapyrrole (pK_a = 4.0)[163] with excess **1** (ΔpK_a = 3.7) is not unexpected. On the other hand, TPyP has a significantly less basic tetrapyrrole (pK_a = 1.8)[163] as a result of the four charged pyridine moieties. It seems surprising that such a highly charged hexacationic macrocycle (P) would exist in the fluorous phase because ΔpK_a = 1.5 deviates significantly from the range in which we have previously observed proton transfer in FC-72. However, TPyP differs from the small bases studied in that the less basic tetrapyrrole ring is surrounded by four contact ion pairs. Although the macromolecule is electronically neutral, the local dipolarity is increased. Thus, the solvation environment perceived by the tetrapyrrole is substantially more polar than a solution of **1**/FC-72 and we observe proton transfer as a result.

4.3.2 Metalloporphyrins

It has been shown that Cu^{2+} can be incorporated into porphyrins with an excess of copper(II)-acetate in organic solvents, where the basic acetate anions act to deprotonate the pyrrole rings.[155,164] El Bakkari, *et al.*[155] have demonstrated complete metalation of 5,10,15-tripyridyl-20-phenylporphyrin after 5 hours and of 5,15-dipyridyl-10,20-diphenylporphyrin in less than 10 minutes in perfluorodecalin with **2**. However, **2** did not metalate TPyP even after several hours of stirring. Based on kinetics experiments and space-filling models, the authors postulate that steric rather than electronic effects explain the differences in metalation behavior by the bulky **2**.

The absorbance spectra of the fluorous phase resulting from an extraction of TPyP from $CHCl_3$ with zinc-carboxylate salt of **1** ($Zn\mathbf{1}_2$) in FC-72 are shown in **Figure 4-14**. The absorbance spectrum of separately synthesized ZnTPyP in $CHCl_3$ is shown for comparison in the inset of **Figure 4-14**. It is clear that TPyP is metalated in the fluorous phase. The absorbance increases with increasing concentration of **1**, but the shape of the spectrum does not change, demonstrating that there is only one form of TPyP in the fluorous phase. The products of the reaction between TPyP and $Zn\mathbf{1}_2$ are ZnTPyP and **1**. The interactions between **1** and the pyridyl groups of ZnTPyP stabilize the complex in the fluorous phase. An extraction of 0.2 mM ZnTPyP in $CHCl_3$ with **1** in FC-72 resulted in similar spectra, owing to the formation of the same product in the fluorous phase, a **1**-ZnTPyP supramolecular complex. In both cases, ^{1}H NMR shows disappearance of the pyrrolic N-H proton signal, indicative of metalation. We conclude that the $Zn\mathbf{1}_2$ salt reacts with TPyP yielding the metalated porphyrin and **1** in the time it takes to shake the solutions. In addition, the metalloporphyrin is recovered when the resulting **1**-ZnTPyP complex is subjected to F-SPE. As discussed above with TPhP and TPyP, the porphyrin is eluted in the organic fluorophobic eluant while **1** elutes with the fluorous solvent.

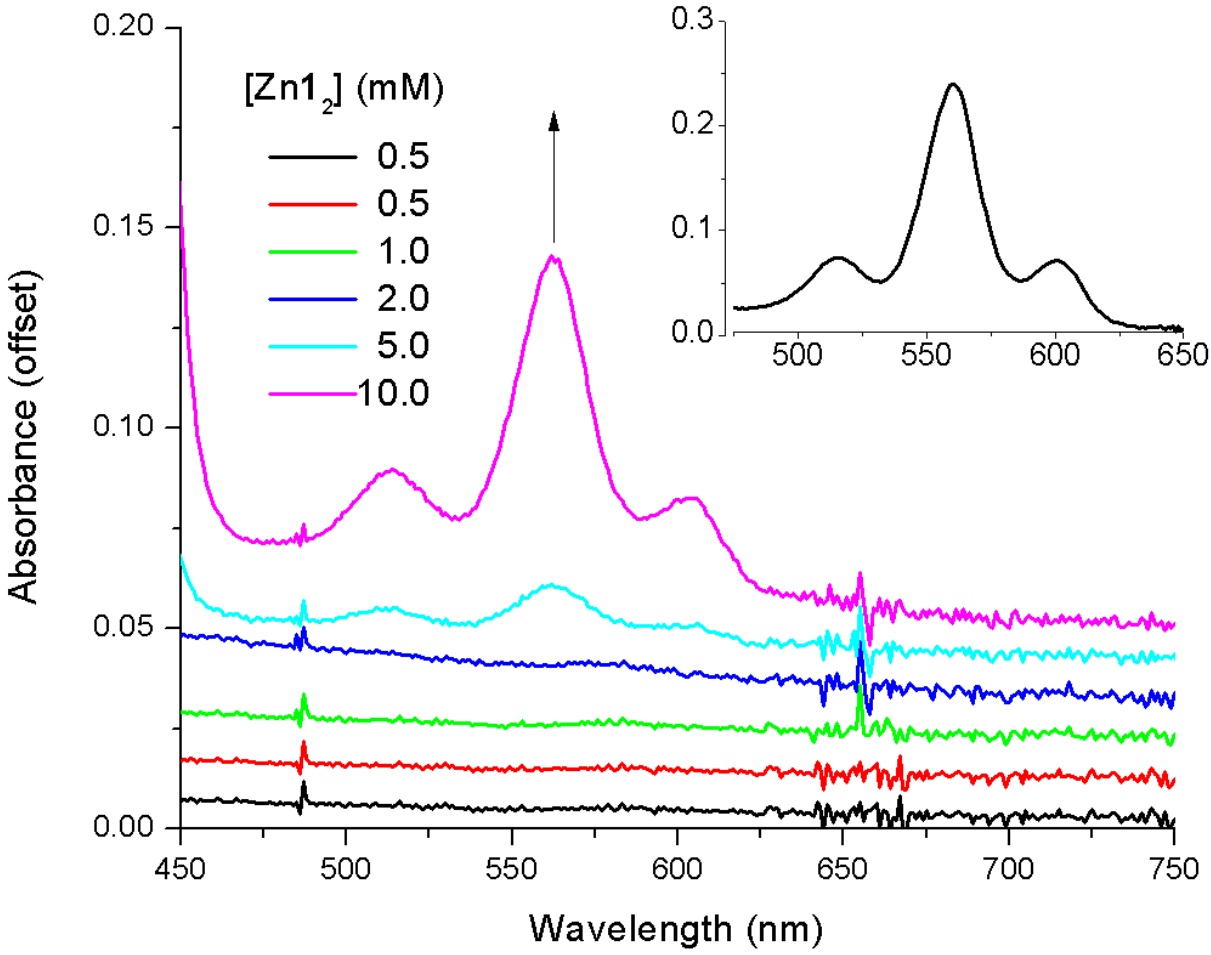

Figure 4-14. UV/Vis absorbance *Q* bands from the fluorous phase resulting from an extraction of 0.1 m M TPyP in $CHCl_3$ with $Zn\mathbf{1}_2$ in FC-72, arrow indicates increasing [$Zn\mathbf{1}_2$] from 0.0 - 10.0 mM. Inset: absorbance spectrum of ZnTPyP in $CHCl_3$.

Similar extractions with TPhP were carried out to confirm the significance of the **1**-pyridyl interaction in solubilizing the complex. There was no partitioning of 0.1 mM TPhP into the fluorous phase observed with up to 10.0 mM Zn**1**$_2$. Correspondingly, there was no detectable partitioning of ZnTPhP from $CHCl_3$ to an FC-72 phase containing up to 20.0 mM **1**. Thus, ZnTPhP showed no interaction with **1**. With Zn^{2+} occupying the TPhP tetrapyrrole ring, the only possible binding site for **1** would be through axial metal-ligand coordination. The lack of interaction confirms that axial coordination of a Lewis acid (ZnTPhP) and carboxylic acid (**1**) is unfavorable. Thus, we conclude that it must be the interaction between **1** and the pyridyl moieties that immobilizes ZnTPyP in FC-72.

4.3.3 Competitive Equilibria

Chloroform was chosen as the source phase for this study because it is relatively unreactive, miscible with most organic solvents, and is minimally soluble in fluorous solvents at room temperature.[22,165] We found that the solubility of $CHCl_3$ in FC-72 is 0.28 M by ^{1}H-NMR measurements. Although common knowledge, it is often overlooked that commercial chloroform contains approximately 1% (v/v) ethanol stabilizer to prevent the formation of HCl and phosgene during storage.[157,158] Quantitative ^{1}H-NMR measurements of the FC-72 phase after being shaken with with $CDCl_3$ containing 1.00% (v/v) ethanol show that the ethanol fluorous/organic distribution coefficient ($D_{c,F/O}$) is 0.09. This doubles to $D_{c,F/O} = 0.18$ with 10.0 mM **1** dissolved in FC-72.

The fractions of TPhP and TPyP extracted from $CHCl_3$ containing ~1% (v/v) ethanol, and $CDCl_3$ containing 0.00, 1.00, and 2.00% (v/v) ethanol with **1** in FC-72 are shown in **Figure 4-15** and **Figure 4-17**, respectively. Photographs of each extraction experiment are shown below

in **Figure 4-16** and **Figure 4-18**, respectively. It is evident that the addition of ethanol significantly hinders the extraction of both TPhP and TPyP into **1**-containing FC-72. For a given [**1**], the fraction extracted from $CHCl_3$ ~1% (v/v) ethanol and $CDCl_3$ 1.00% (v/v) ethanol differ. This is because the addition of ethanol to $CHCl_3$ is from the factory and not quantitatively accurate, especially after a particular bottle is opened, whereas the $CDCl_3$ 1.00% (v/v) ethanol solution was made fresh before the experiment. In addition to reducing the effectiveness of the receptor in the receiving phase, ethanol acts as a hydrogen bond donor in the source phase, therefore reducing the porphyrin chemical potential and the thermodynamic driving force for extraction. Thus, to clarify the role of ethanol in the fluorous phase more completely, we attempted to determine the state of protonation of TPyP in **1**/FC-72 with ethanol.

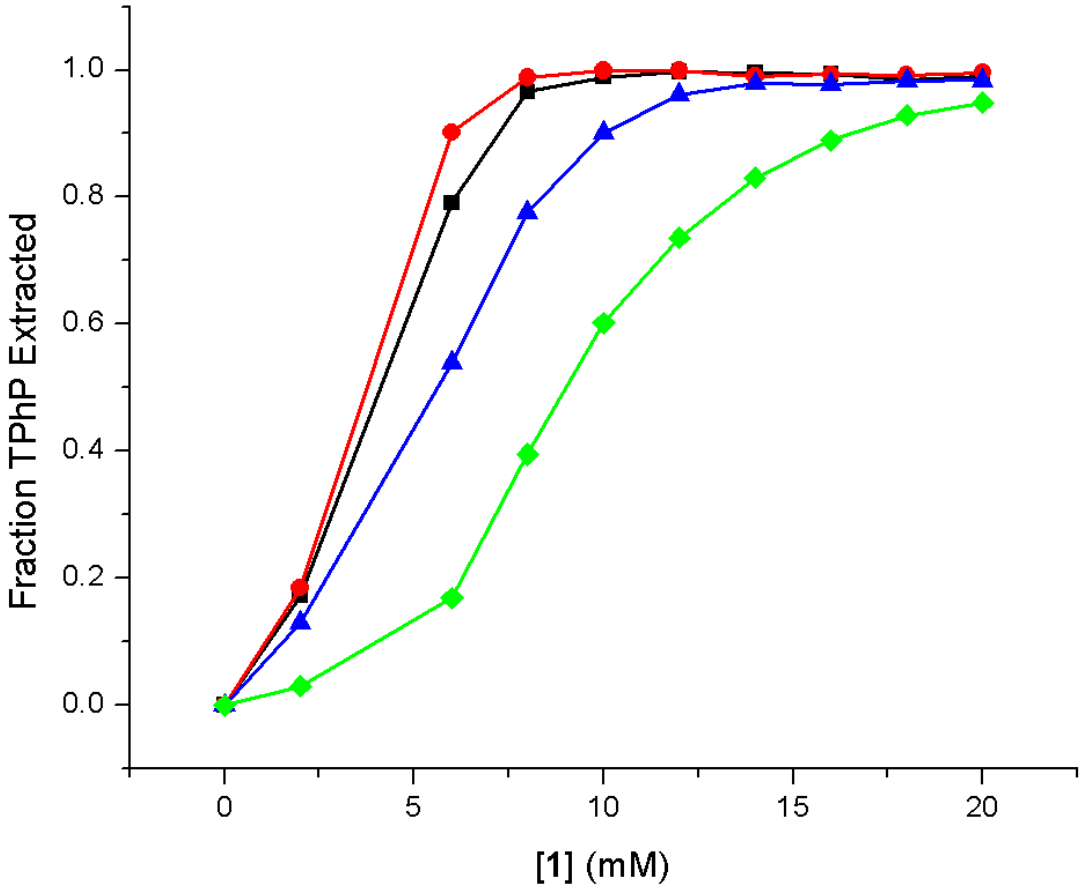

Figure 4-15. The fraction of TPhP extracted from 1.0 mM solution in $CHCl_3$ (■), $CDCl_3$ (●), $CDCl_3$ 1% ethanol (▲), and $CDCl_3$ 2% ethanol (◆) source phase with a **1**-containing FC-72 receiving phase ($\Phi = 1.0$) shown as a function of [**1**].

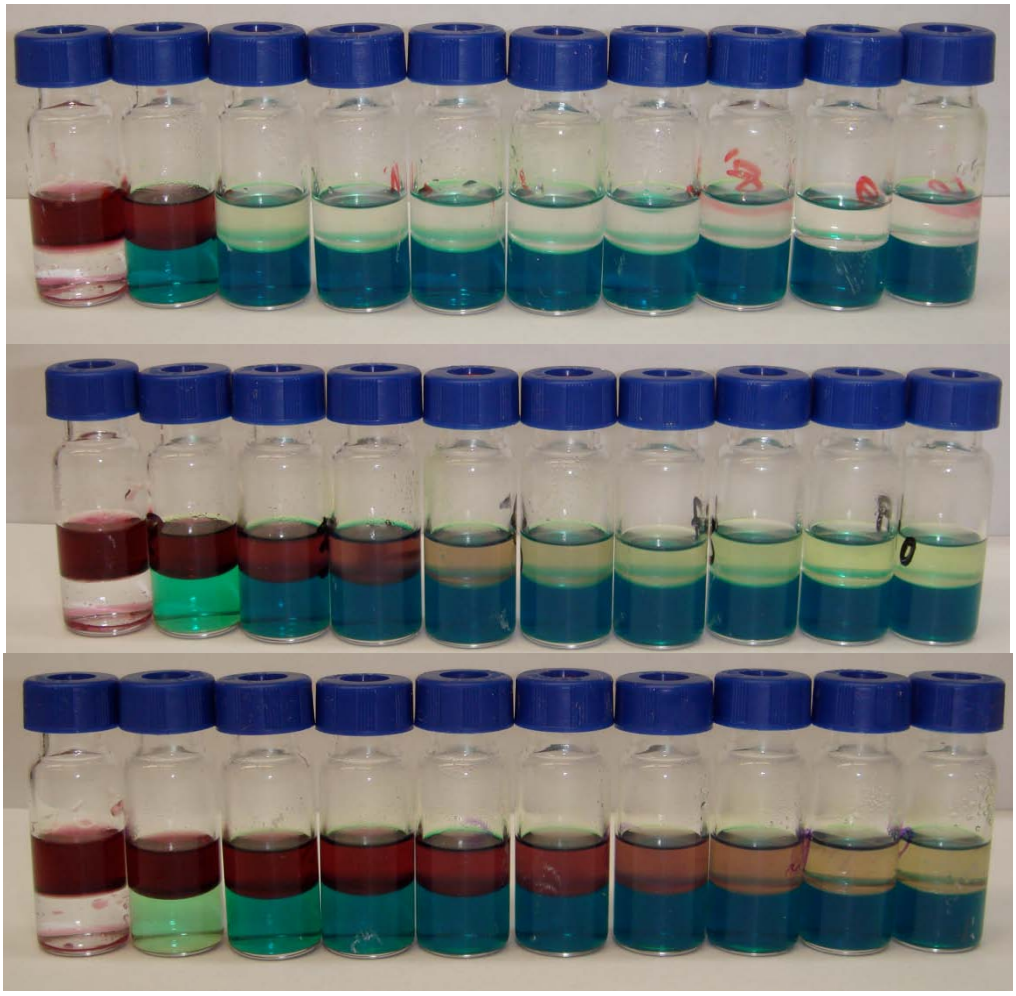

Figure 4-16. Top to bottom, photographs of samples from extractions of 1.0 mM TPhP in $CDCl_3$ with (a) 0.00, (b) 1.00, and (c) 2.00% ethanol (top phase) with 0.0-20.0 mM **1** in FC-72 (bottom phase).

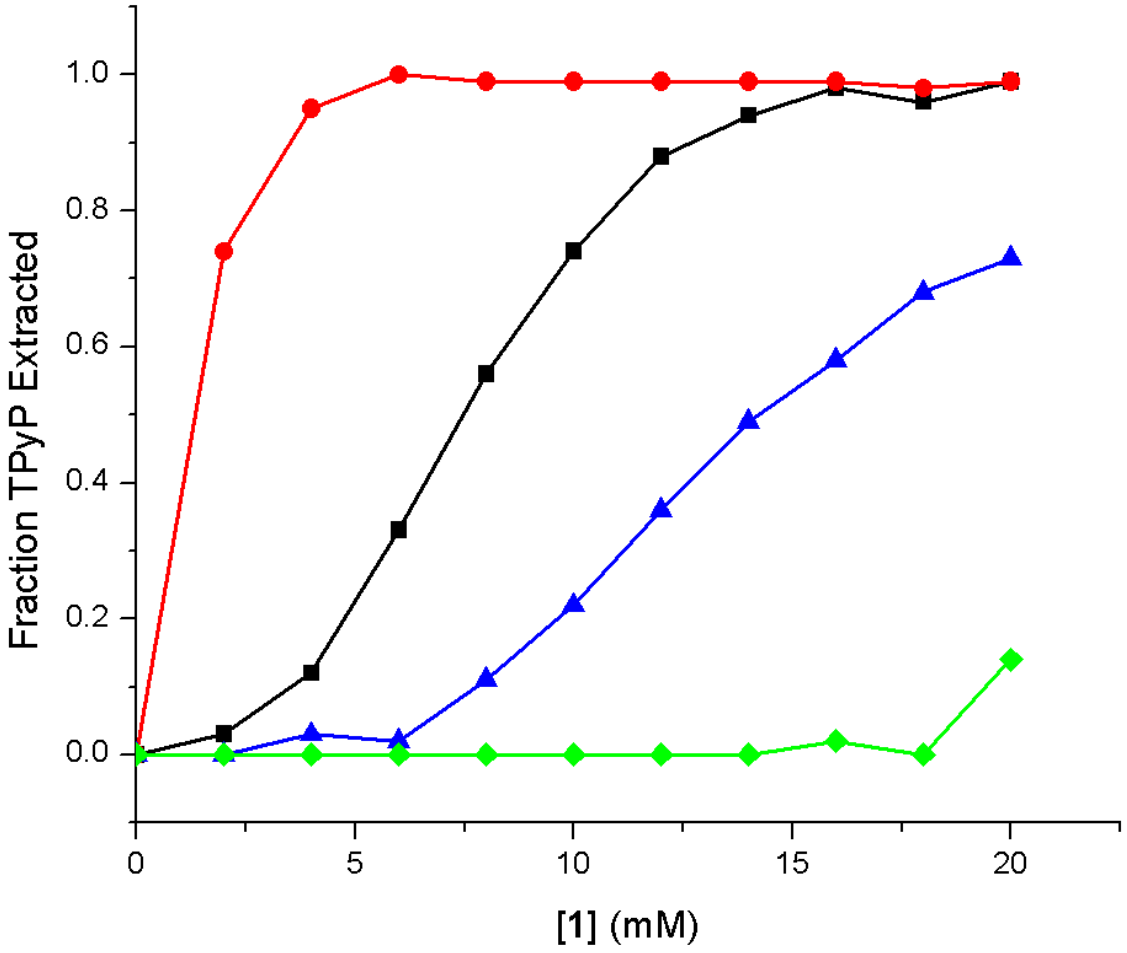

Figure 4-17. The fraction of TPhP extracted from 1.0 mM solution in $CHCl_3$ (■), $CDCl_3$ (●), $CDCl_3$ 1% ethanol (▲), and $CDCl_3$ 2% ethanol (◆) source phase with a **1**-containing FC-72 receiving phase ($\Phi = 1.0$) shown as a function of [**1**].

Figure 4-18. Top to bottom, photographs of samples from extractions of 1.0 mM TPyP in $CDCl_3$ with (a) 0.00, (b) 1.00, and (c) 2.00% ethanol (top phase) with 0.0-20.0 mM **1** in FC-72 (bottom phase).

We have described above a method for determining the absolute concentrations of TPyP in both the protonated (P) and unprotonated (N) form in the fluorous phase. Recall that all four pyridyl groups are protonated in both species (see Supporting Information). Unfortunately, the presence of ethanol in FC-72 significantly changes the solvent environment and thus the molar absorptivities at both 513 and 638 nm. As a result of the multiple equilibria between ethanol, **1**,

and TPyP, the previously described method is no longer applicable. Nonetheless, because the molar absorptivity of N at 638 nm is much smaller than that of P at 638 nm, the ratio of the absorbances at 638 and 513 nm (A_{638}/A_{513}) is approximately related to the ratio of P to N in the fluorous phase. **Figure 4-19** shows A_{638}/A_{513} in the fluorous phase plotted against [**1**] from extractions of TPyP from $CHCl_3$ containing ~ 1% ethanol (v/v), and $CDCl_3$ containing 0.00, 1.00, and 2.00% (v/v) ethanol with **1** in FC-72. Although necessarily approximate, **Figure 4-19** demonstrates that ethanol decreases the acidity in the fluorous phase, inhibiting the formation of the dication (P). Ethanol, then, modulates the solution environment in **1**/FC-72.

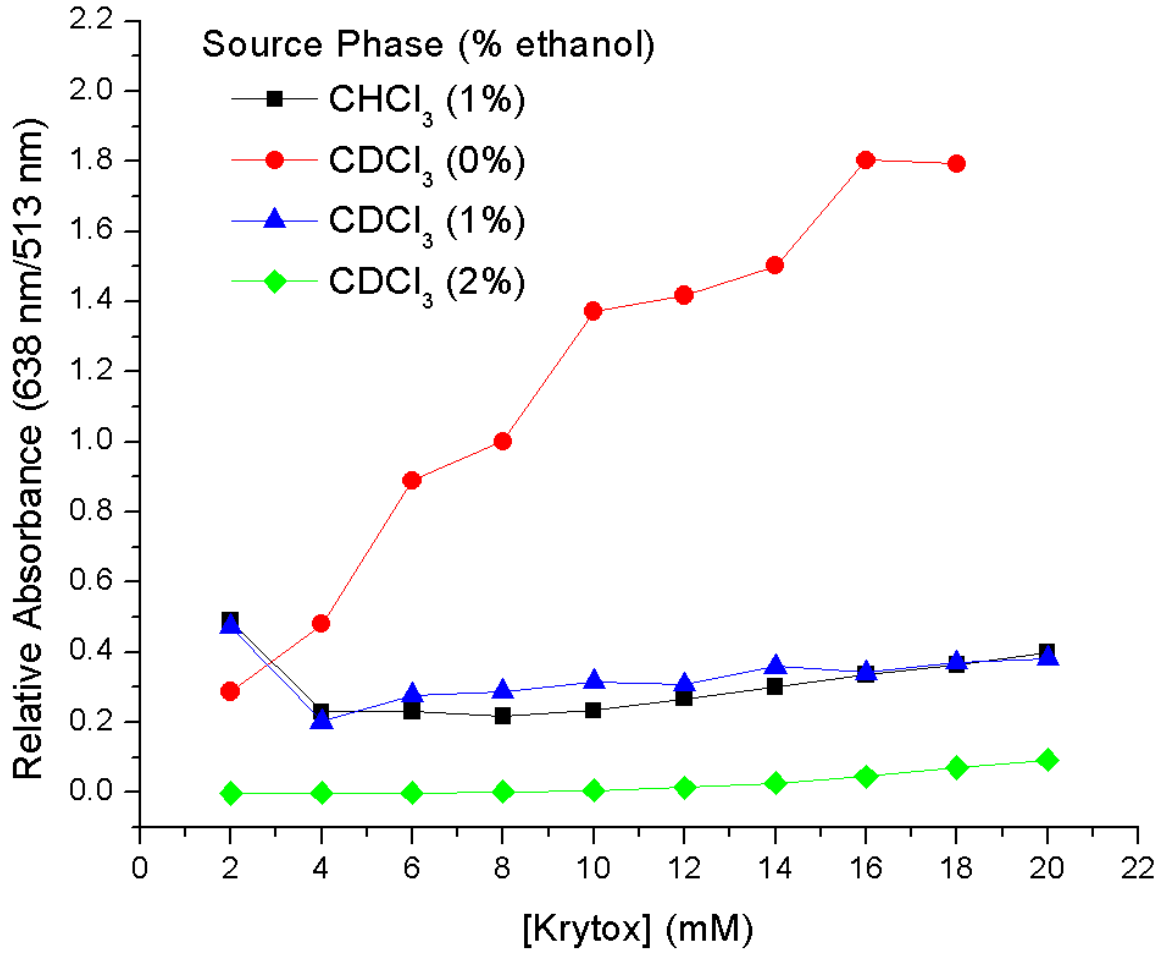

Figure 4-19. The relative total absorbance (638 nm/513nm) of the receiving phase resulting from an extraction of TPyP from 1.0 mM TPyP solution in $CHCl_3$ (■), $CDCl_3$ (●), $CDCl_3$ 1% ethanol (▲), and $CDCl_3$ 2% ethanol (◆) source phase with a **1**-containing FC-72 receiving phase (Φ = 1.0) shown as a function of [**1**].

Interestingly, the inhibitory effect of ethanol on the formation of the dication is reversible. As ethanol evaporates from FC-72, the absorbance at 628 nm of an FC-72 solution containing 10.0 mM 1 and TPyP extracted from a 1.0 mM solution of and CHCl3 (1% ethanol) increases to match that of the same solution extracted from $CDCl_3$ (ethanol-free). **Figure 4-20** shows the absorbance an FC-72 solution containing 10.0 mM **1** and TPyP extracted from a 1.0 mM solution in $CDCl_3$ and $CHCl_3$ as ethanol evaporates from FC-72 over time.

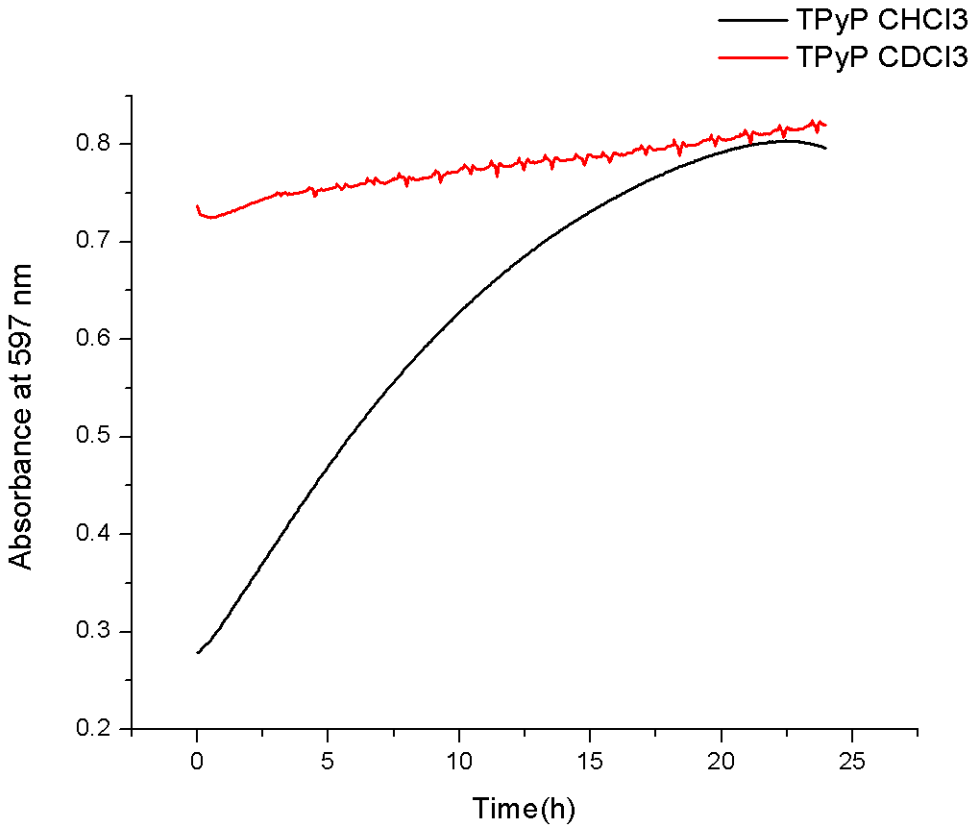

Figure 4-20. The absorbance at 597 nm of a FC-72 solution containing 10.0 mM **1** and TPyP extracted from a 1.0 mM solution in $CDCl_3$ (red) and $CHCl_3$ (black) containing 1% ethanol stabilizer as a function of time as ethanol evaporates.

4.4 CONCLUSIONS

We have shown that **1** is an effective fluorous receptor for extracting both TPhP and TPyP from $CHCl_3$ into FC-72. While **1** transfers two protons to the to the tetrapyrrole ring of TPhP to create the porphyrin dication (H_2TPhP^{2+}), the interaction between **1** and TPyP occurs through protonation of both the pyridyl and tetrapyrrole nitrogens. It is interesting that a hexacation is formed in the fluorous environment. Protonation of the TPyP tetrapyrrole can be attributed to the surrounding contact ion pairs increasing the polarity of the immediate solvation environment. In other words, the 'solvent' perceived by the tetrapyrrole is substantially more polar than a solution of **1**/FC-72. Thus, the overall charge on TPyP can be 'tuned' by adjusting the relative concentrations of **1** and TPyP. In addition, the charge on the macromolecular complex can be manipulated using a competitive cosolvent. A smaller fraction of the extracted TPyP is in the fully protonated (P) state under the influence of presence of ethanol in the fluorous phase; likely because ethanol lowers the acidity in **1**/FC-72. Adjusting the relative concentration of ethanol then makes it possible to reversibly solubilize TPyP in the fluorous phase through non-covalent interactions while leaving the tetrapyrrole ring available to interact with metals or other substrates.

We have also observed near-complete extraction of ZnTPyP from $CDCl_3$ with **1** in FC-72 and extraction and metalation of TPyP with Zn**1**$_2$. However, there was no interaction between ZnTPhP and **1** or between Zn**1**$_2$ and TPhP. This is because Zn**1**$_2$ metalates TPyP yielding ZnTPyP and **1**. The liberated **1** maintains the solubility of the complex in FC-72 through interactions with the TPyP pyridyl groups. Once metalated, ZnTPhP has no binding sites for **1**. This is the first report demonstrating metalation of TPyP in a fluorous environment. This fundamental understanding of the interactions of porphyrins and metalloporphyrins with **1** in the

fluorous phase should lead to the development of more robust and selective porphyrin-based sensors and application to other devices.

4.5 ACKNOWLEDGMENTS

This research was funded by the National Science Foundation (NSF) through grants CHE0315188 and CHE0615952.

5.0 PARTITIONING IN RECEPTOR-DOPED TEFLON AF2400 FILMS FOR MOLECULAR RECOGNITION BASED FLUOROUS SOLID PHASE MICROEXTRACTION (F-SPME)

5.1 INTRODUCTION

A growing concern for protecting the environment has lead to an increased emphasis on green analytical methods and stricter regulations on waste production. According to the principles of green chemistry,[166] solvent-free systems are ideal for preventing hazards to the environment and human health and they often save time and energy while having increased analytical performance. Not surprisingly, there have been great efforts towards the development of solvent-free methods, with an emphasis on the development of solvent-free sample preparations.

Solid phase micro extraction (SPME) is a widely accepted sorbent technique that was first developed by the Pawliszyn group in the early 1990's. It involves the removal of chemical constituents from a sample matrix via retention on a sorbent with subsequent desorption of target analytes.[7,8] Coating the sorbent material on a fine rod allows rapid mass transfer during extraction and desorption, resulting in fast, simple separations in a solvent-free system. The process of SPME involves two main steps, (1) partitioning of the target analyte between the sample matrix and sorbent membrane, and (2) desorption of the concentrated analyte from the membrane to an instrument for analysis.[8,167] Because it is a 'micro' process, SPME is particularly

sensitive to matrix effects. Because of this, the selection of sorbent material is crucial to the success of the separation, it is the most important step governing the selectivity of the extraction.[167] There is no universal sorbent,[11] even though silica is the most widely applicable and most commonly applied solid phase. Retention behavior of a target analyte can vary dramatically between sorbent materials. Thus, it is necessary to continue to explore new materials for separations and design sorbents for specific analyte/matrix systems.

Molecular receptors embedded in the receiving phase have been known to enhance the selectivity of an extraction by reducing the free energy of the target analyte in the desired phase.[14,18,42,167] Valenta *et al.*[18] observed a 40-fold increase in extraction efficiency when they incorporated an artificial molecular receptor into a chloroform receiving phase in the extraction of phenobarbital from human control serum as compared with receptor-free chloroform. This work was later extended to the development of a reusable, plasticized-poly(vinyl chloride) (PVC) extraction medium.[13] Li and coworkers[14] have been the only group to report SPME coupled with molecular recognition. They incorporated a phenobarbital receptor into a plasticized PVC film coated on a primed steel rod and followed the sampling with micro back-extraction for capillary electrophoresis-based determination.

It is well known that the free energy for receptor-substrate complex formation depends strongly on the solvent in which the complexation occurs.[23,168-170] Solvent properties (π^*, α, β)[111] have been shown to affect the distribution, receptor association, and solubility equilibria in molecular recognition-based extractions of phenobarbiatal.[13,168,169] The selectivity of an extraction based on a molecular receptor is then limited by the solvating power of the matrix.

Fluorous solvents are the least polar and least polarizable solvents known.[22] The highly electronegative fluorine atom makes the C-F bond strongly resistant to induced dipoles. This

makes fluorous materials highly nonpolarizable with very little attractive intermolecular forces. As a result, fluorous liquids are practically immiscible with both aqueous and organic phases.[22] Molecular recognition has been combined with fluorous matrices to improve extraction selectivity by reducing the interfering species extracted. In addition, the strength of substrate-receptor interactions is increased by effectively eliminating solute-solvent competition.[22,23,86] Boswell *et al.*[57,58,88] have used fluorous liquids to provide a medium for more stable ion-ionophore complexes, creating exceptionally selective sensor membranes. We have recently reported on a carboxylic acid terminated poly-hexafluoropropylene oxide, Krytox 157FSH (**1**), that significantly enhances the extraction of pyridine (100-fold with excess **1** as compared to **1**-free) and substituted pyridines from chloroform into a mixture of perfluorohexanes (FC-72).[20]

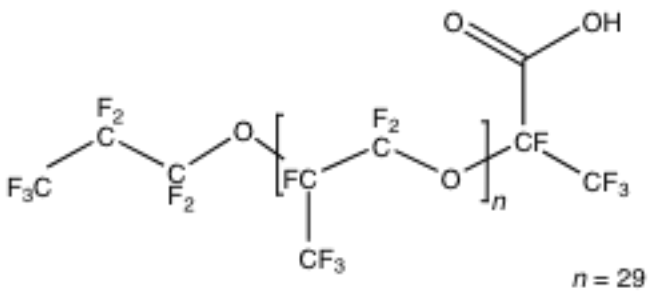

1

Teflon AF2400 (**2**) is a chemically inert and thermally stable amorphous fluorinated polymer. It is a copolymer of tetrafluoroethylene (13%) and 2,2-bistrifluoromethyl-4,5-difluoro-1,3 dioxole (87%). Thin films are easily prepared through solvent casting and are transparent through a wide UV-Vis and IR range, making them ideal for studying intermolecular interactions in films. Sorption and permeation studies of light gases,[35,36] C_1-C_{12} hydrocarbons,[36,37] C_1-C_7 perfluorocarbons,[36] chlorinated hydrocarbons,[37] and small alcohols,[37] in Teflon AF films have

revealed high permeabilites and large fractional free volumes (FFVs). Transport studies of organic substrates from a chloroform source phase through **2** films to a chloroform receiving phase have shown that the substrate permeability is proportional to the size of the substrate.[39] In addition, the films demonstrated selectivity for fluorinated substrates in comparison to the hydrogen-containing control. **1** can easily be incorporated into **2** and plasticizes the films. For 50% **1** (w/w), T_g = -40 °C compared to intitial T_g = 240 °C.[39,40] However, it was also found that **1**-plasticized thin films reduce the permeability of organic substrates by decreasing their diffusivity in the films.[39] The opposite effect is expected in **1**-doped **2** films for substrates that exhibit a favorable interaction with the –COOH functional group of **1**.

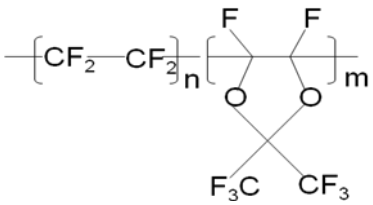

Teflon AF2400

2

We are interested in using receptor-doped fluorous films for solvent-free extractions. The hydrophobic and lipophobic nature of the film will reduce the partitioning of all substrates but the receptor should increase the partitioning of substrates that have complimentary functional groups, making the extraction more effective. To investigate the potential of **2** films for receptor-based extractions, we start with a simple carboxylic acid receptor, **1**. This work focuses on the equilibrium distribution of pyridine-like substrates between buffered aqueous solutions into **1**-

doped **2** thin films. We found that the addition of **1** to the film increased the film/aqueous distribution coefficient for most pyridine-like bases. Unfortunately, the receptor-free films were not as discriminating towards non-fluorous substrates as we has expected. To create a fluorous molecular recognition-based SPME device for aqueous extractions followed with direct GC thermal desorption, primed optical fibers were dip-coated with receptor-doped films. When compared to commercially available polydimethylsiloxane (PDMS) SPME fibers, **1**-doped Teflon AF showed a preference for pyridine-like bases over their non-heterocyclic counterparts. To our knowledge, this is the first report coupling receptor-doped fluorous membrane extraction with SPME.

5.2 EXPERIMENTAL

5.2.1 Chemicals and Solutions

All of the 2-, 3-, and 4-hydroxy- (2HP, 3HP, and 4HP) and 2-, 3-, and 4-amino- (2AP, 3AP, 4AP) substituted pyridines, as well as aniline, 2-ethylnapthalene, phenanthridine, acridine, pyrazine, pyrimidine, quinazoline, quinoline, isoquinoline, quinine, isopropanol, citric acid, disodium phosphate, and tris(hydroxymethyl)aminomethane hydrochloride buffer substance (tris buffer hereafter) were obtained from Aldrich (Milwaukee, WI). Sigmacote®, a chlorinated organopolysiloxane solution in heptane, was also purchased from Aldrich. Pyridine and concentrated hydrochloric acid were purchased from J.T. Baker (Phillipsburg, NJ) and phenol and nitric acid from EM Science (Cherry Hill, NJ). Chloroform (Fisher Scientific, Fair Lawn, NJ) was dried over activated molecular sieves, and treated with potassium carbonate (EM

Science, Cherry Hill, NJ) to neutralize any HCl that had formed as a result of exposure to light.[157,158] Krytox 157F SH (**1**) was purchased from Miller-Stephenson Chemical Co., Inc. (Danbury, CT). ^{19}F-NMR provided a number averaged molecular weight of 5150 g mol^{-1} with an average of 29 polymer repeat units. Teflon® AF 2400 (**2**) was purchased from Dupont (Wilmington, DE). A linear perfluoropolyether (**3**, M_n = 4500 g mol^{-1}) was purchased from Alpha Aesar (Ward Hill, MA). FC-72 Fluorinert Electronic Liquid (a mixture of perfluorohexanes) was purchased from 3M (St. Paul, MN) and used as received. Solutions of **2** in FC-72 (10 mg/mL) were prepared and the containers were placed in a Cole-Palmer (Chicago, IL) ultrasonicator bath until visible inspection showed complete dissolution. Aliquots (25 mL) of 10 mg/mL **2** in FC-72 were placed in separate vials and 62.5, 87.5, 125.0, and 212.5 mg of **1** was added to create 25.0, 35.0 , 50.0 and 85.0% (w/w) **1**-doped **2** solutions in FC-72. Separately, 62.5 and 125.0 mg of **3** was added to 10 mg/mL solutions of **2** to make 25.0 and 50.0% (w/w) **2**/**3** in FC-72. All solution vials were placed in an ultrasonicator bath to ensure dissolution.

Aqueous buffer solutions (10.0 mM, pH = 8.2) were prepared by dissolving tris buffer in purified water from a Millipore Synthesis A 10 system (Millipore, Billerica, MA). Separate substrate solutions (1.0 mM, aniline, 2AP, 3AP, 4AP, 2HP, 3HP, 4HP, imidazole, isoquinoline, quinazoline, quinoline, phenol, pyrazine, pyrazole, pyridine, and pyrimidine) were prepared in tris buffer and each container placed in an ultrasonicator bath until dissolved. Citric acid/disodium phosphate buffer solutions (10.0 mM, pH = 3.0) were prepared using 2.05 mM disodium phosphate and 7.95 mM citric acid in Millipore purified water. Solutions of acridine, quinine, and phenanthridine (1.0 mM) were prepared in the citric acid/disodium phosphate buffer.

5.2.2 Thin Film Preparation and Extractions

The general procedure for creating thin films in a 96-well microplate is outlined in **Figure 5-1**. Aliquots of 0.0, 35.0, or 85.0% (w/w) **1**/**2** solutions in FC-72 (200 μL) were deposited into the wells of a polypropylene microplate using a multichannel pipette. The plate was lightly covered and the FC-72 was allowed to evaporate overnight in the fume hood. The film thickness was measured using a micrometer (The L.S. Starrett Company, Athol, MA). A Varian Excalibur FT-IR spectrophotometer was used to verify that **1** had been incorporated into the films. After the films had set in the plate, 200 μL aliquots of the respective aqueous substrate solutions were deposited into the plate using a multichannel pipette, sealed, and equilibrated in a Deep Well Maximizer (Bioshaker MBR-022U, made by Taitec and distributed by Bionexux Inc., Oakland, CA) at 460 revolutions/min for 6 days at 23.0 °C. Following equilibration, 100 μL aliquots were taken from each well using a multichannel pipette, deposited into a UV-transparent microplate, and sealed using UV-transparent adhesive film. Absorbance measurements were taken every 2 nm from 200-400 nm in a SpectraMax M2 microplate reader (Molecular Devices, Sunnyvale, CA).

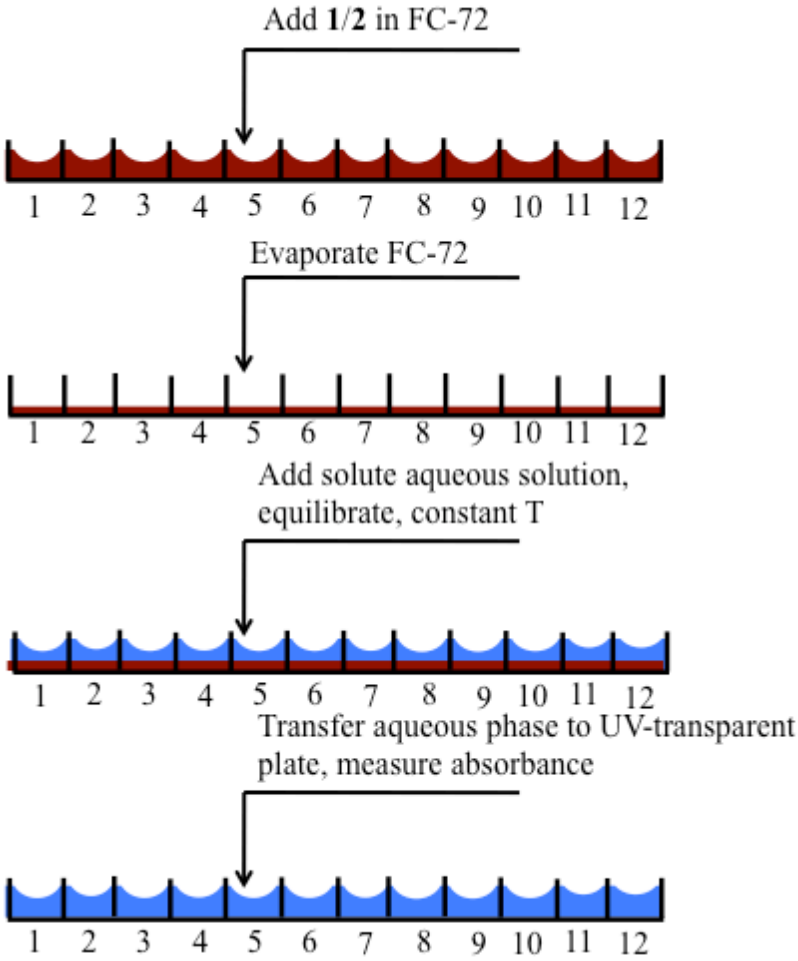

Figure 5-1. Adapted from Chen and Weber,[1] the general procedure for determining partition coefficients from the aqueous phase to thin films in a 96-well microplate. The fluorous phase (solution or thin film) is shown in red and the aqueous phase in blue. The black lines represent the walls of the 96-well microplate.

The microplates were divided into quadrants as shown in **Figure 5-2**. Quadrant I was used as a control to monitor evaporation and contained no film. Quadrant II contained 35.0% (w/w) **1/2** films, quadrant III contained 85.0% (w/w) **1/2** films, and quadrant IV contained 0.0% (w/w) **1/2** films. The fraction of substrate extracted was determined for each well relative to the average concentration of the same solution in the control wells (quadrant I, no film). Columns 1-6 contained six different substrate solutions, one column for each substrate, and the series was repeated for columns 7-12 as shown in **Figure 5-2** where each color represents a different substrate. For each series of solutions, two identical plates were made for a total of eight partition coefficient (K_P) measurements for each substrate in each film composition.

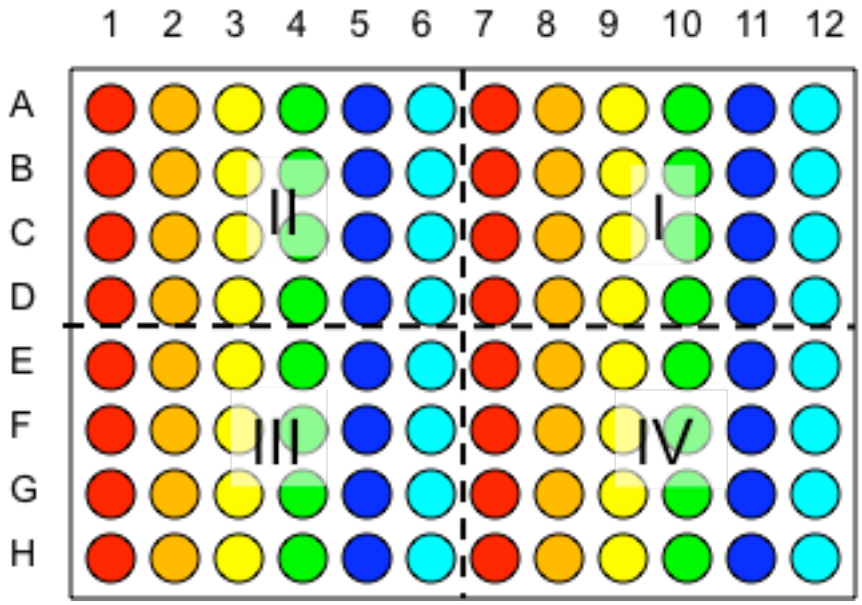

Figure 5-2. Experimental setup for thin film extractions. Each color represents a different aqueous substrate solution. Each quadrant of the 96-well microplate contains a different film composition: I) no film, II) 35.0% (w/w) **1/2**, III) 85.0%(w/w) **1/2**, and IV) 0.0%(w/w) **1/2**.

5.2.3 Fluorous Solid Phase Microextraction (F-SPME) Device: Preparation and Use

The process for fabricating F-SPME fibers is demonstrated graphically in **Figure 5-3**. Gold-coated optical fibers (AFS 105/125G, 125 μm diameter) were obtained from Fiberguide Industries (Stirling, NJ) and cut into 12-14 cm long strips. The gold coating was removed from a 2-3 cm section of the end of the fiber strip by soaking it in freshly prepared aqua regia (1:3 HNO_3:HCl by volume). The fibers were then rinsed with DI water, soaked in isopropanol for 30 min and dried at 100 °C for 3 hrs. The exposed optical fibers (105 μm diameter) were then dip-coated with Sigmacote® to deposit a neutral, hydrophobic, microscopically thin film of silicon on the glass. The siliconized optical fibers were rinsed with DI water to remove any HCl byproducts and dried at 100 °C for 30 min to create a more durable coating. The fibers were then dip-coated 15 times each with the respective **1**/**2** FC-72 solution (0.00, 25.0, 35.0, 50.0, 75.0 and 85.0% (w/w) **1**) or a **3**/**2** solution (25.0 and 50.0% (w/w)) and dried at 100 °C for 3 hrs. Before use, each fiber was threaded into a Hamilton (Reno, NV) 26 g auge needle and exposed in a Thermo Finnigan Focus GC inlet for conditioning at 250 °C for 0.5 hrs. The GC injection splitter was opened during the conditioning step to reduce the amount of impurities in the column. After conditioning, the oven temperature was ramped from 100 °C to 280 °C at 50 °C/min to remove any residual contaminants that may have entered the column.

For the F-SPME extraction, the fiber was exposed to a tris buffer solution (pH = 8.2) containing 1.0 mM quinoline and 0.05 mM 2-ethylnapthalene under medium stirring for 1.0 min or a solution of 0.5 mM quinoline and 0.25 mM napthalene for 10 min. The fibers were then rinsed with buffer solution, air dried, and exposed to the GC inlet to be separated under the following conditions: 280 °C inlet temperature, 100 °C initial temperature, hold 0.5 min, ramp

120 °C/min to 250 °C, hold 0.1 min, 60 mL/min split flow, split ratio = 20, in a 7 m, 0.32 mm ID Restek (Bellfonte, PA) Rxi-5ms column.

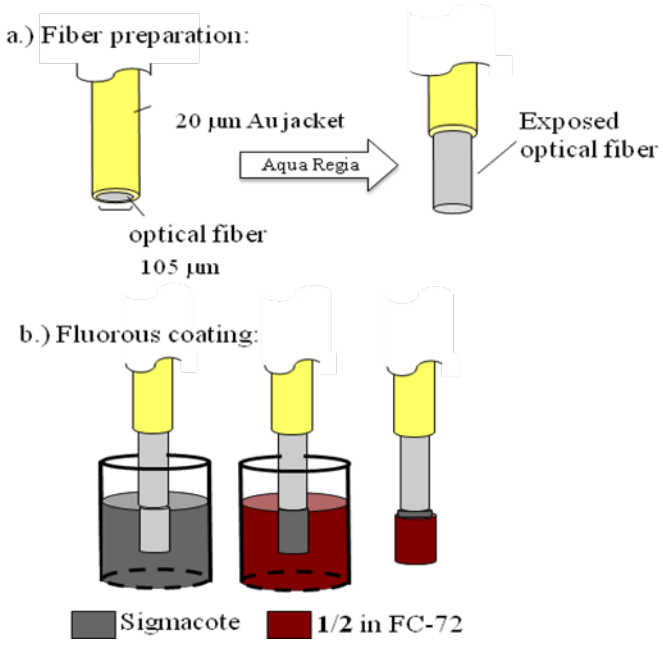

Figure 5-3. The general procedure for coating optical fibers with **1/2** thin films; a.) demonstrates the removal of the gold jacked using aqua regia, b.) shows silicanization of the exposed fiber with subsequent dip-coat application of the fluorous film.

A commercially available SPME fiber assembly (Supelco, Bellfonte, PA) with a 30 µm polydimethylsiloxane (PDMS) coating was assembled in a Supelco manual SPME holder. The fiber was conditioned in the GC injection port at 250 °C for 0.5 hrs before use. Between uses, the fibers were immersed in a 50/50 mixture of ethanol and water for 15-30 min for cleaning. The extraction procedure for the PDMS fibers was the same as described above for the **1/2** coated fibers.

5.3 RESULTS AND DISCUSSION

5.3.1 Thin film Validation and Extractions

FTIR spectroscopy was used to verify that **1** was incorporated into the films. The carbonyl region of the spectra are shown in **Figure 5-4**. The absorbance intensity of the **1**-carbonyl stretching band (1775 cm^{-1}) associated with the carboxylic acid dimer[32] increases with increasing **1** weight fraction. It was found that **1** is miscible with **2** in any proportion.

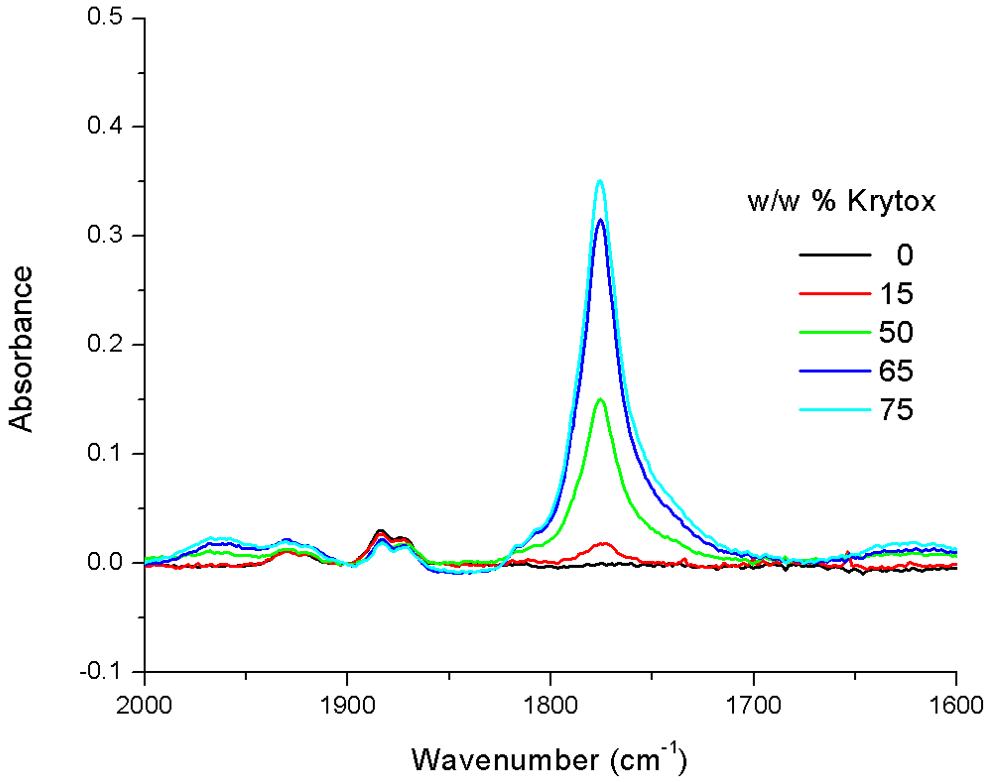

Figure 5-4. The carbonyl stretching region of the FTIR spectra from **1**/**2** thin films containing increasing fractions of **1** as indicated in the legend. The absorbance was corrected for the thickness of the film (path length) and baseline corrected.

Thin film extractions were carried out in 96-well microplates from buffered aqueous solution (pH = 8.2) into 0.0, 25.0, or 75.0% **1/2** films in the bottom of the well as described above. After six days of shaking, the concentration of substrate remaining in the aqueous phase was measured using UV/Vis spectroscopy relative to the concentration of substrate in the wells containing no film. The fraction of solute extracted (q) was determined using mass balance from the source phase (**Equation 5-1**), where C_{aq}^{i} and C_{aq}^{f} are the initial and final concentration of substrate in the aqueous phase, respectively.

$$q = \frac{C_{aq}^{i} - C_{aq}^{f}}{C_{aq}^{i}}$$

Equation 5-1

The partition coefficient (K_P), the ratio of concentrations of substrate in the aqueous phase and thin film, can be determined using **Equation 5-2**, where Φ is the phase ratio, the ratio of the volume of the film to the aqueous phase.

$$K_P = \frac{q}{(1-q)\Phi}$$

Equation 5-2

The volume of the film was determined by measuring the thickness of each film in the bottom of each well of a 96-well microplate. The thicknesses from each quadrant were averaged and this value was used to calculate the volume of the film according to the diagram in **Figure 5-5**. **Table 5-1** shows the resulting Φ for film compositions of 0.0, 35.0, and 85.0% (w/w) **1/2**. The pooled relative standard error of the mean for the film thickness measurements is rather large as a result of the increased softness and compressibility of the film with added **1**.

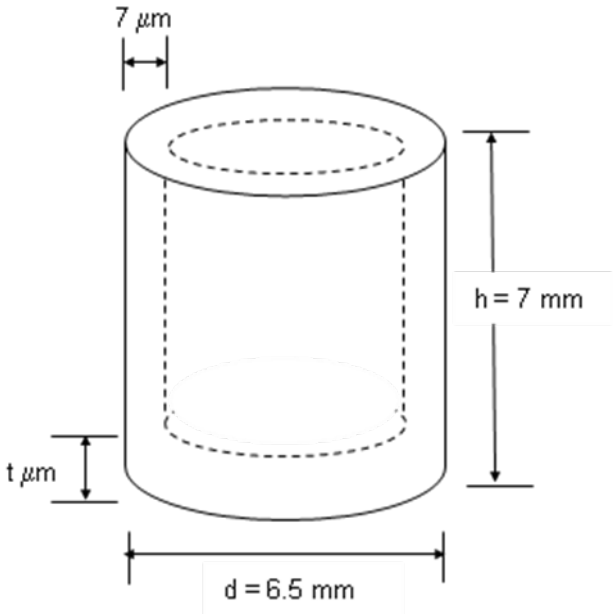

Figure 5-5. Diagram of a microplate well. The volume of the film was calculated by taking the difference in the volume ($V = \pi r^2 h$) of the outer and inner cylinder.

Table 5-1. The average thickness of **1/2** films in the 96-well microplate, volume of the film, and the phase ratio (Φ) for the film relative to 200 μL aqueous solution.

w/w % **1/2**	t[a] (μm)	Volume (mm^3)	Φ (film/aqueous)
0.00	18.3 +/- 4.3	1.60	7.98×10^{-3}
35.0	27.5 +/- 3.1	1.93	9.63×10^{-3}
85.0	35.8 +/- 8.3	2.19	11.0×10^{-3}

[a]N = 24, pooled relative standard error of the mean = 20.3%

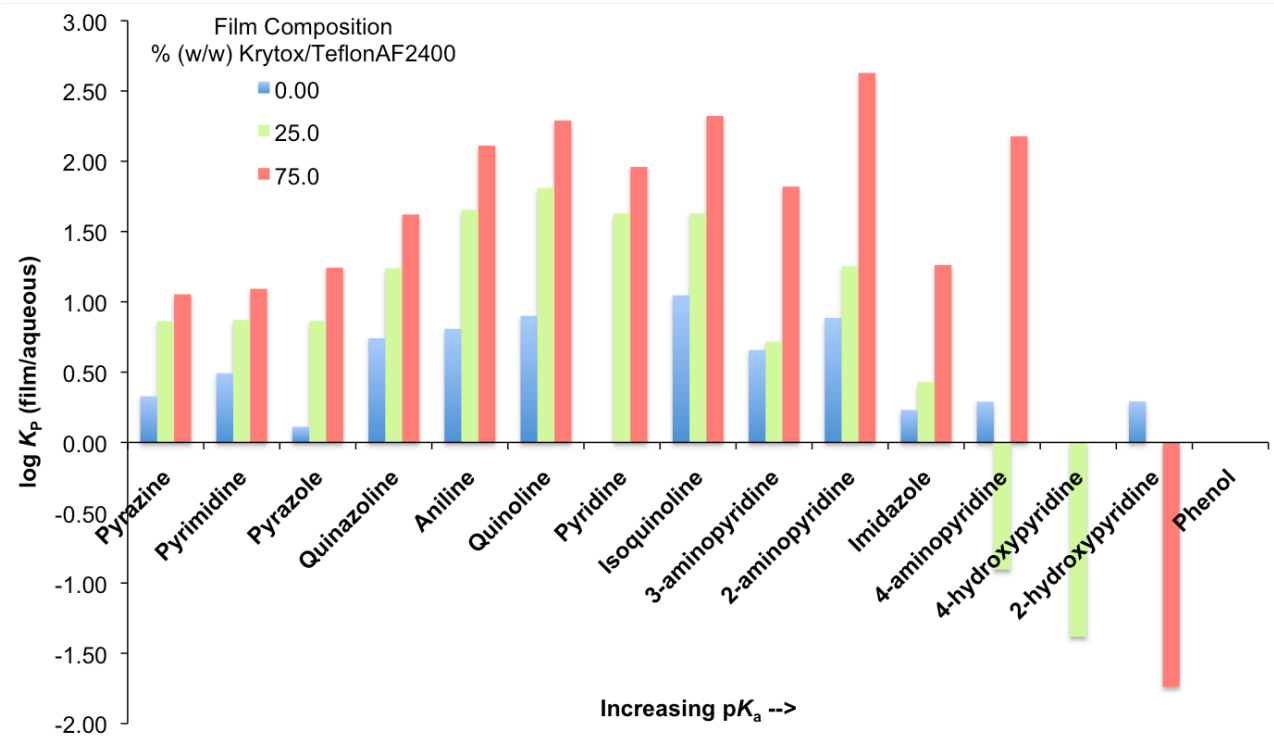

Figure 5-6. The $\log_{10}$ K_P between an aqueous phase (pH = 8.2) and 0.00, 25.0, and 75.0% (w/w) 1/2 films listed in order if increasing p K_a of the conjugate acid. Each reported distribution coefficient is the average of 8 absorbance measurements from extractions using independent films, resulting in a pooled relative standard error of the mean of 4.96%.

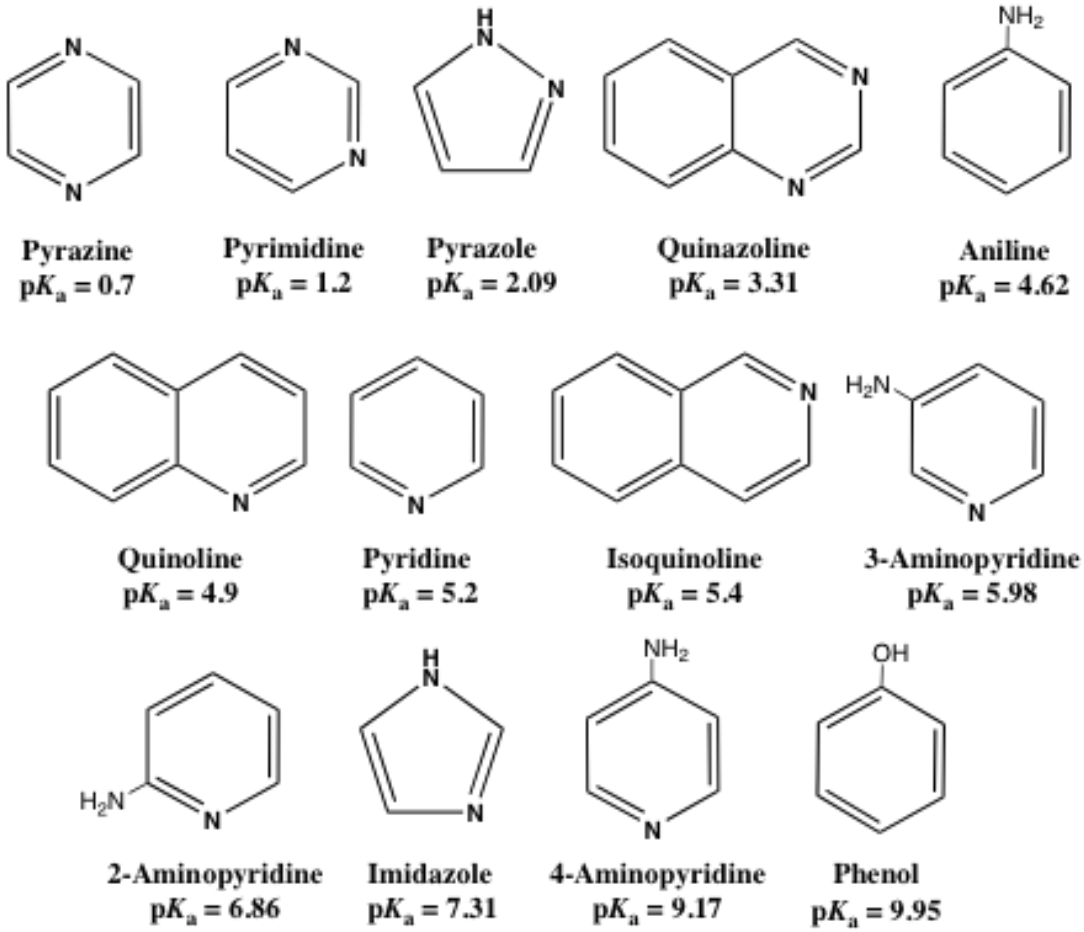

Scheme 5-1

The average log K_P (N = 8) for each substrate, listed in the order of increasing conjugate acid pK_a, is shown in

Figure 5-6 for each film composition. The pooled relative standard error of the mean was 4.96% for the absorbance values, demonstrating good precision for the method described above. The structure and pK_a of the conjugate acid for each substrate is shown in Scheme 5-1. In general, addition of 1 to the film increases the film/aqueous log K_P, i.e. more substrate partitions into the film in the presence of 1, more 1 leads to a higher K_P. To better understand the variance in

partitioning of between the substrates, we wanted to investigate how substrate properties (solute descriptors) affect log K_P for the set of pyridine-like substrates studied. We used the group contribution method described by Platts, *et. al.*[2,3] to calculate the hydrogen bond dipolarity/polarizability (π_2^H), basicity ($\beta_2°$), and acidity (a_2^H), as well as the molecular volume (V_X) of the substrates studied. Proton affinites (H^+_{aff}) were obtained from the Beilstein Crossfire database.

Because the log K_P increases with the addition of **1**, the formation of a receptor-substrate complex must play a role in the extraction. In addition to substrate properties, it would be interesting to study how the receptor-substrate interactions affect log K_P. Experimental challenges prevented measurement of the free energy of complex formation (ΔG_f) for the **1**-substrate complex for most of the substrates studied. Fortunately, complex formation thermodynamics for a limited subset of the substrates could be investigated. The formation constant (K_f), and thus ΔG_f ($\Delta G_f = \ln K_f$), for each of these **1**-substrate complexes was determined using the method of continuous variations,[61] which requires that separate solutions of the substrate and **1** be made. Thus, ΔG_f (in FC-72) could only be determined for those that showed solubility in FC-72 in the absence of **1**. Pyrazine, pyrimidine, quinazoline, quinoline, pyridine, and isoquinoline all demonstrated some solubility in FC-72 without **1**. The determination of ΔG_f for pyrazine, pyrimidine, quinazoline, quinoline, pyridine, and isoquinoline is discussed in detail in Chapter 3 and the results are reproduced in **Table 5-3** for convenience.

Table 5-2. Solute descriptors determined using the group contribution method;[2,3] π_2^H is the hydrogen bond dipolarity/polarizability, $\beta_2°$ and a_2^H are the hydrogen bond basicity and acidity, respectively, and V_X is the molecular volume.

Solute	$^H_2$	$^O_2$	$^H_2$	V_x (A^3/mol)
Acridine	.215	.916	.000	167.871
2AP	.907	.674	.247	91.176
3AP	.907	.674	.247	91.176
4AP	.907	.674	.247	91.176
Aniline	.734	.386	.247	96.332
2HP	.771	.659	.543	87.905
3HP	.771	.659	.543	87.905
4HP	.771	.659	.543	87.905

Imidazole	.644	.649	.321	6 4.873
Isoquinoline	.844	.638	.000	1 23.879
Napthalene	.042	.628	.000	1 72.027
Pheananthridine	.215	.916	.000	1 67.871
Phenol	.598	.371	.543	9 2.061
Pyrazine	.595	.575	.000	7 5.731
Pyrazole	.644	.649	.321	6 4.873
Pyridine	.473	.360	.000	7 9.887
Pyrimidine	.606	.535	.000	7 5.731
Quinazoline	.977	.813	.000	1 19.722
Quinoline	.844	.638	.000	1 23.879

Table 5-3. Reproduced from Chapter 3, Stoichiometry, formation constant, and free energy of formation for a series of pyridine-like bases with **1** in FC-72 determined by the method of continuous variations, titrations, and Specfit global fitting.

Substrate	pK_a[a]	Ratio Base:**1**	K_f	Complex $\Delta G°_f$(kJ/mol)	$\Delta G_f°$ SEM[b] (kJ/mol)
Pyrazine	0.7	1:1	$(1.5 \pm 0.2) \times 10^4$ M^{-1}	-24	0.3
Pyrimidine	1.2	1:1	$(1.6 \pm 0.2) \times 10^3$ M^{-1}	-23	0.3
Quinazoline	3.4	1:1	$(8.8 \pm 1.7) \times 10^4$ M^{-1}	-22	0.3
Quinoline	4.9	1:3	$(2.4 \pm 0.3) \times 10^{13}$ M^{-3}	-73	0.8
Pyridine	5.2	1:3	$(3.6 \pm 0.5) \times 10^{11}$ M^{-3}	-65	0.8
Isoquinoline	5.4	1:3	$(2.8 \pm 0.5) \times 10^8$ M^{-3}	-47	0.7

[a]Aqueous pK_a values for the conjugate acid

[b]$\Delta G_f°$ standard errors of the mean (SEM) were determined from a $\Delta G_f°$ pooled relative standard deviation for the method of 3.2%

[c]Number of determinations ranges from 4-8

Even though we were not able to measure ΔG_f for all of the substrates, we were able to perform a multiple linear regression (Intercooled STATA, Version 9.2[171]) using experimental ΔG_f values and group contribution solute descriptors for the limited subset of substrates (pyrazine, pyrimidine, quinazoline, quinoline, pyridine, and isoquinoline). The dependant variable was ΔG_f for the **1**-substrate complex in FC-72 (a mixture of perfluorohexanes), while the independent variables were hydrogen bond basicity (β_2^O) and proton affinity (H^+_{aff}), which were uncorrelated to one another (correlation coeffient, $\rho = 0.1869$). Although only six substrates

could be included in the regression, we were able to increase the number of data points by using each value determined, rather than the average. A good fit was obtained for ΔG_f based on $\beta_2°$ H^+_{aff} for the limited substrate subset. The results of the linear regression are listed below (

Table 5-4) and shown in **Equation 5-3**. This allowed us to generate data for the substrates for which ΔG_f could not be experimentally determined. The calculated ΔG_f values are shown in **Table 5-5**.

$$\Delta G_f = -59.38\ H^+_{aff} + 46.24\ \beta_2° + 471.88$$

Equation 5-3

Table 5-4. Multiple linear regression results (STATA) on experimentally determined ΔG_f values based on proton affinity (H^+_{aff}) and hydrogen bond basicity ($\beta_2°$).

	Coefficient	Standard Error	p value
H^+_{aff}	-59.38	4.72	0.000
$\beta_2°$	46.24	16.23	0.008
constant	471.88	42.62	0.000

Table 5-5. ΔG_f values for the formation of **1**-substrate complexes in FC-72 calculated using Equation 3. Note that not all substrates are listed because H^+_{aff} was not available.

Solute	ΔG_f (kJ mol^{-1}) calculated
2AP	-55.8
3AP	-56.2
Aniline	-51.9
Imidazole	-55.5
Isoquinoline	-56.0
Phenol	-48.1
Pyrazine	-51.6
Pyridine	-54.8
Pyrimidine	-52.1
Quinoline	-56.1

We then performed a multiple linear regression with log K_P (film/aqueous) as the dependant variable based on calculated ΔG_f and V_X. The results are tabulated below (**Table 5-6**). **Figure 5-7** shows the fitted values plotted against experimental values for films 85.0% (w/w) **1/2**. The fitted values agreed quite well with the experimental values for 85.0% (w/w) **1/2** films. Similar multiple linear regressions on 0.0 and 35.0% (w/w) **1/2** films showed no correlation. These regressions demonstrate that the ability of the receptor to form a complex with the

substrate is a significant factor in substrate partitioning from the aqueous phase into the highly nonpolar fluorous film.

Table 5-6. Multiple linear regression results (STATA) on experimentally determined log K_P values based on V_X calculated ΔG_f ($R^2 = 0.85$).

	Coefficient	Standard Error	p value
ΔG_f(calc.)	0.4667	0.0284	0.000
V_X	0.01001	0.00287	0.001
constant	-22.34	1.50	0.000

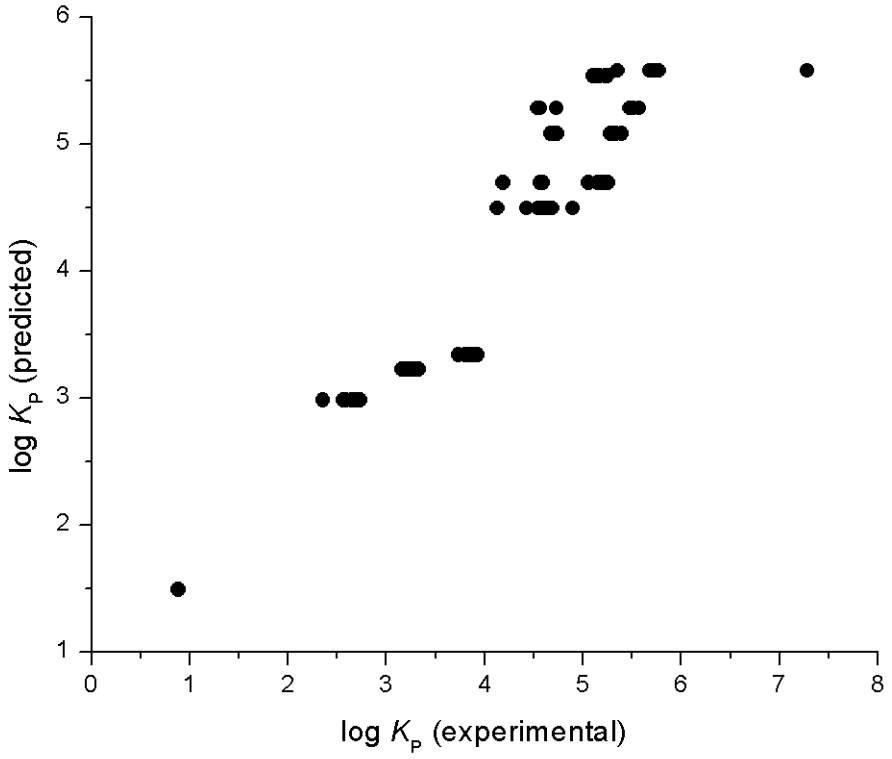

Figure 5-7. The predicted log K_P (film/aqueous) from a 1.0 mM aqueous phase (pH = 8.2) into a 85% (w/w) **1**/**2** thin film determined from multiple linear regression based on calculated ΔG_f and V_X plotted as a function of experimental values ($R^2 = 0.85$).

We have shown that the substrate has a higher K_P (film/aqueous) with a receptor-doped film resulting from the formation of a substrate-receptor complex. Yet it is not clear why there is partitioning of some substrates into 0.0% (w/w) **2**. We expected the distribution of non-fluorous pyridine-like substrates in receptor-free **2** films to be negligible. A recent study by Lai, *et. al*[172] showed that **2** contains carboxylic acid groups, as many as 1 per 854 monomer units, formed by

hydrolysis of the carboxylic acid fluoride groups that are initially present on **2**. In the highly nonpolar fluorous environment, this carboxylic acid was found to bind to Na^+, K^+, and Ca^{2+} with binding constants of $10^{3.5}$, $10^{1.8}$, and $10^{6.8}$, respectively. While it is possible that these carboxylic acid groups have a small effect on the partitioning of neutral bases from aqueous solution in the absence of **1**, it is more likely a result of the high FFV of **2**.

5.3.2 Fluorous Solid Phase Extraction (F-SPE): Preliminary Results

A F-SPE device was created as shown in **Figure 5-8**. The fiber coating process is described above. The coated fiber was exposed to an aqueous solution containing 1.0 mM quinoline and 0.05 mM 2-ethylnapthalene. The chromatogram of this stock solution is shown in **Figure 5-9**. The chromatograms resulting from exposure of 0.0, 35.0, 85.0% (w/w) **1**/**2** coated fibers as well as PDMS fibers to this solution are shown in **Figure 5-10** through **Figure 5-13**, respectively.

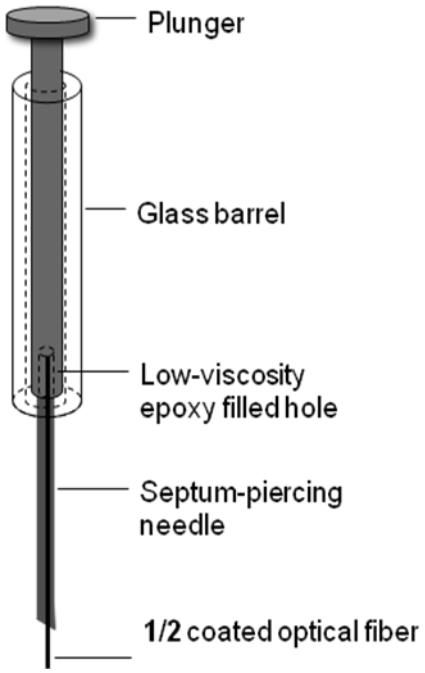

Figure 5-8. F-SPME device and parts.

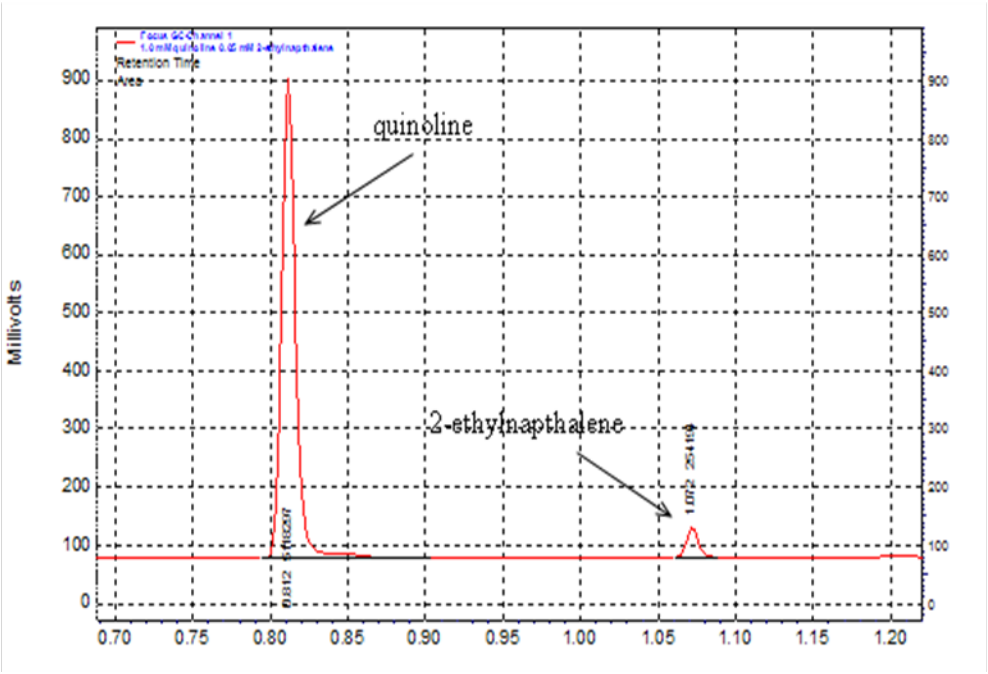

Figure 5-9. Gas chromatograph of a 1.0 µL injection of a 1.0 mM quinoline and 0.05 m M 2-ethylnapthalene aqueous solution (pH = 8.2).

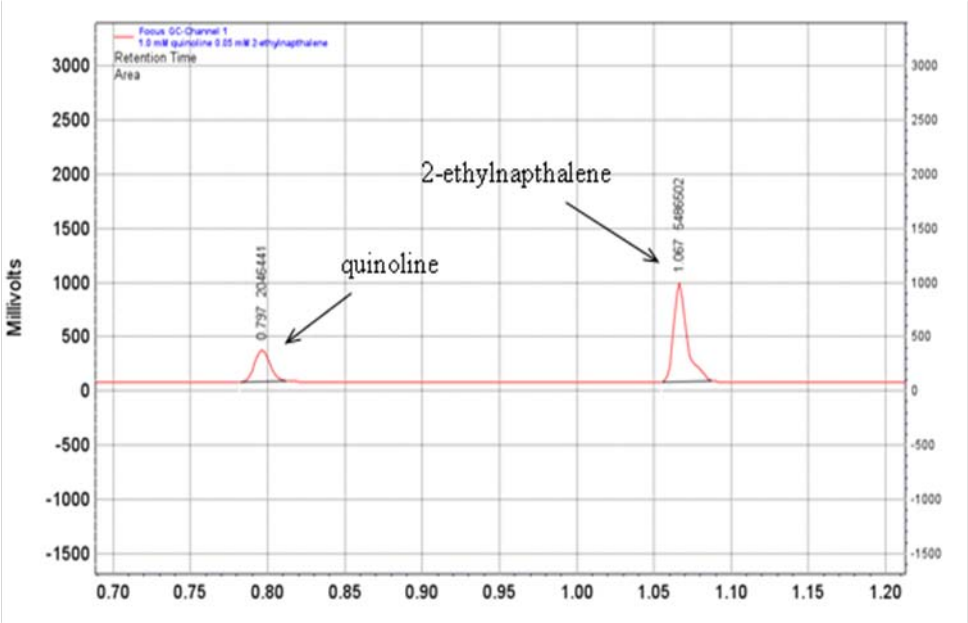

Figure 5-10. Gas chromatograph resulting from thermal desorption from a PDMS SPME fiber that was exposed to an aqueous solution (pH = 8.2) containing 1.0 mM quinoline and 0.05 mM 2-ethylnapthalene for 1.0 min.

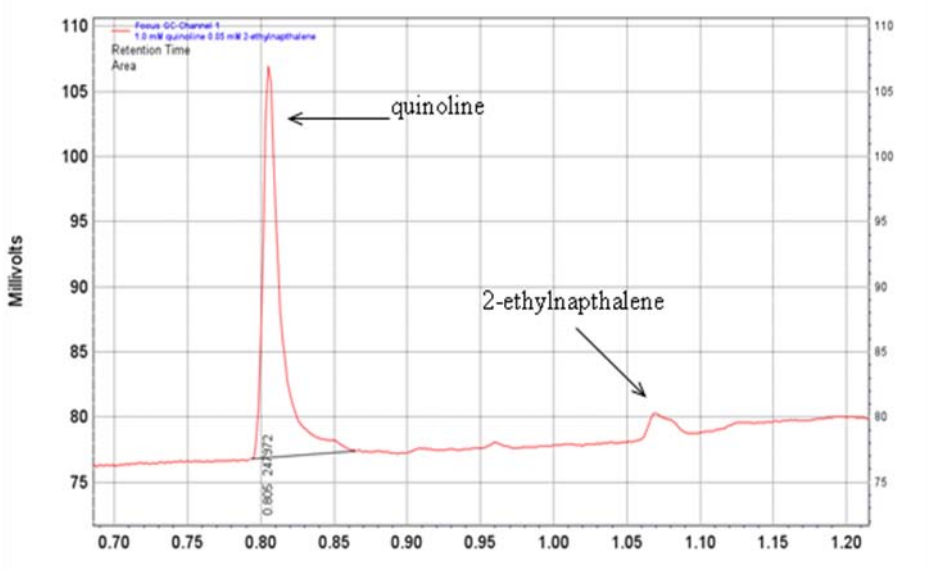

Figure 5-11. Gas chromatograph resulting from thermal desorption from a **2** SPME fiber that was exposed to an aqueous solution (pH = 8.2) containing 1.0 mM quinoline and 0.05 mM 2-ethylnapthalene for 1.0 min.

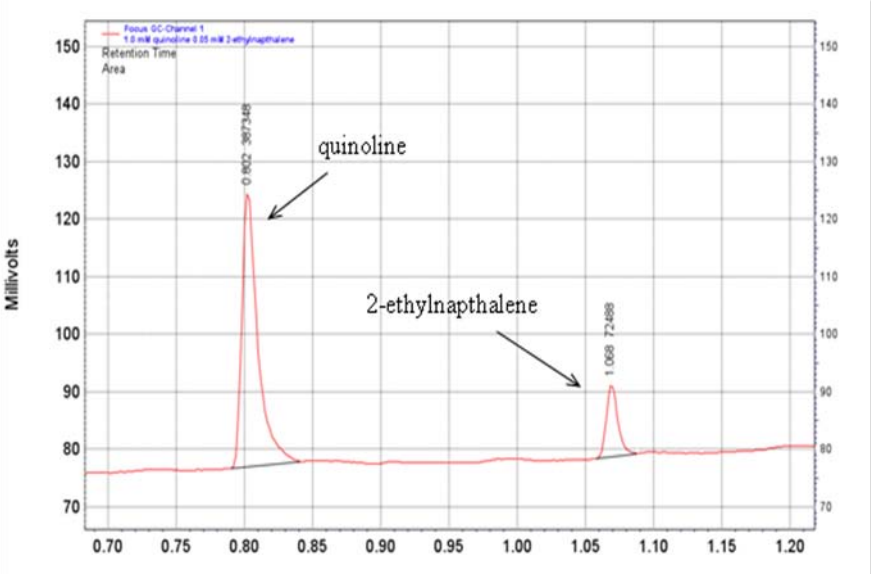

Figure 5-12. Gas chromatograph resulting from thermal desorption from a 35.0% (w/w) 1/2 SPME fiber that was exposed to an aqueous solution (pH = 8.2) containing 1.0 mM quinoline and 0.05 mM 2-ethylnapthalene for 1.0 min.

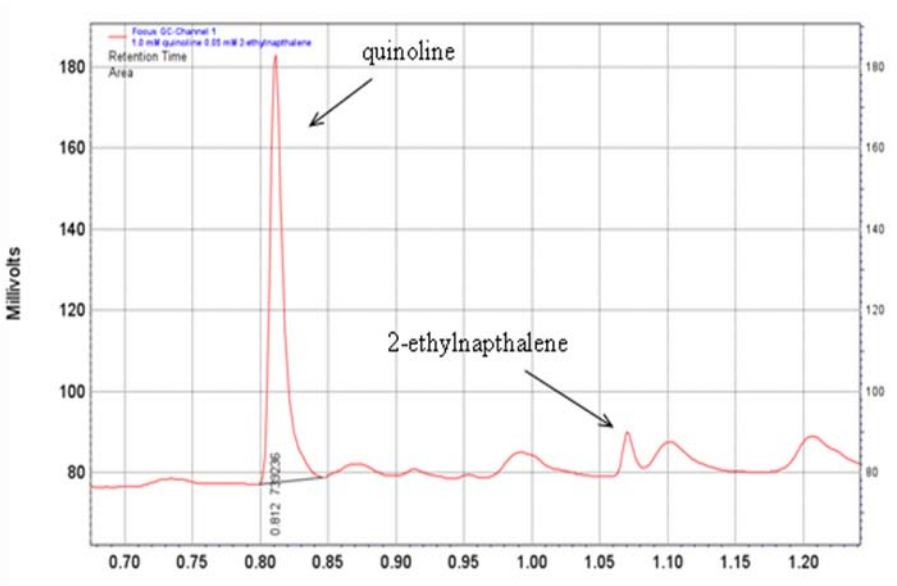

Figure 5-13. Gas chromatograph resulting from thermal desorption from an 85.0% (w/w) 1/2 SPME fiber that was exposed to an aqueous solution (pH = 8.2) containing 1.0 mM quinoline and 0.05 mM 2-ethylnapthalene for 1.0 min.

A comparison of the chromatogram of the 1.0 mM quinoline and 0.05 mM 2-ethylnapthalene stock solution (**Figure 5-9**) to that resulting from the rmal desorption from PDMS fibers exposed to the same solution shows that the nonpolar PDMS coating (**Figure 5-10**) favors adsorption of the more nonpolar 2-ethylnapthalene over quinoline. While a comparison of the chromatogram of the stock solution to that from 0.0% (w/w) **1**/**2** coated fibers shows that **2** films favor quinoline. This is likely a result of the carboxylic acid groups present in **2**. The chromatograms from desorption of 35.0% and 85.0% (w/w) **1**/**2** coated fibers exposed to the same solution show similar results to 0.0% (w/w) **1**/**2** coated fibers but with a slightly increased quinoline peak area. Nonetheless, the receptor-doped F-SPE fibers favors ubstrates with hydrogen bonding groups complimentary to that of the receptor, i.e. heterocyclic nitrogens with carboxylic acids, over those without functional groups to a greater extent than commercially available PDMS fibers.

Lugert, *et. al*[173] have shown that a linear perfluoropolyether (**3**, M_n = 2700 g mol^{-1}) is an effective plasticizer for **2** films and is completely miscible, forming homogenous films. The authors also noted that the ether oxygens did not significantly affect the selectivity of sensing membranes and any coordination with metals or hydrogen bonding was weakened by the large electronegativity of the many fluorine atoms. Addition of a linear perfluoropolyether plasticizer (**3**) to the blend should lower the glass transition temperature (T_g) and allow molecules to move more freely through the film. We repeated similar extraction experiments as above using 25.0 and 50.0% (w/w) **3**/**2** coated fibers and the 25.0 and 50.0% (w/w) **1**/**2** coated fibers. The test sample was an aqueous solution (pH = 8.2) containing 0.5 mM quinoline and 0.25 mM napthalene. The resulting chromatograms are shown below in **Figure 5-14** through **Figure 5-18**.

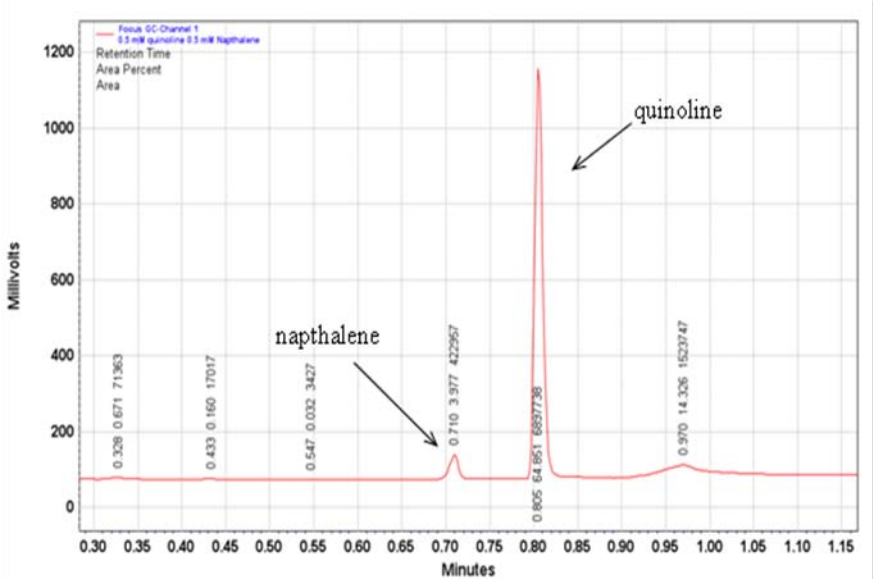

Figure 5-14. Gas chromatograph of a 1.0 µL injection of a 0.5 mM quinoline and 0.25 mM napthalene aqueous solution (pH = 8.2).

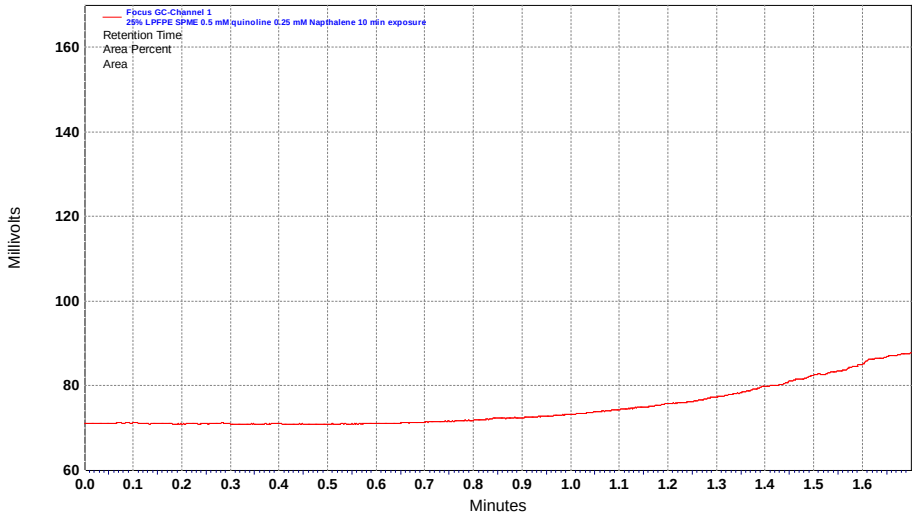

Figure 5-15. Gas chromatograph resulting from thermal desorption from a 25.0% (w/w) 3/2 SPME fiber that was exposed to an aqueous solution (pH = 8.2) containing 0.5 mM quinoline and 0.25 mM napthalene for 10.0 min.

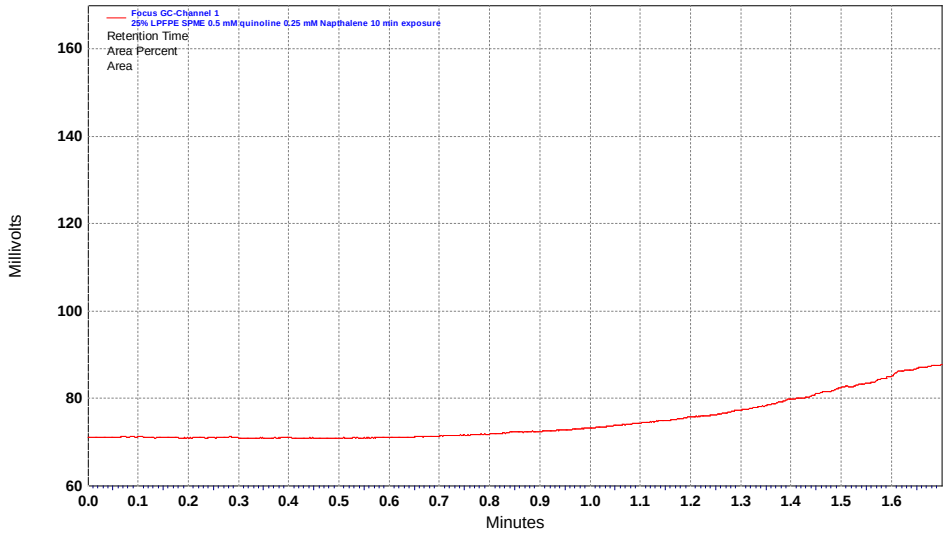

Figure 5-16. Gas chromatograph resulting from thermal desorption from a 50.0% (w/w) 3/2 SPME fiber that was exposed to an aqueous solution (pH = 8.2) containing 0.5 mM quinoline and 0.25 mM napthalene for 10.0 min.

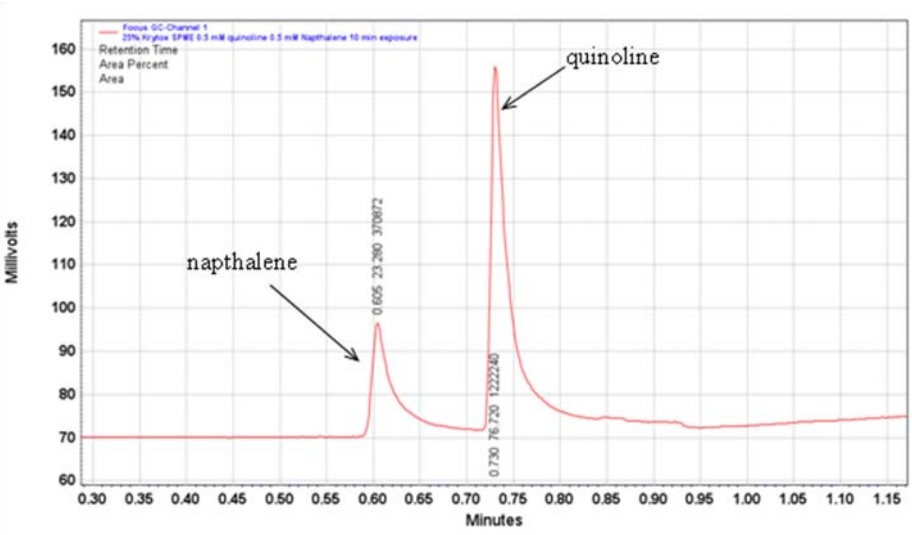

Figure 5-17. Gas chromatograph resulting from thermal desorption from a 25.0% (w/w) 1/2 SPME fiber that was exposed to an aqueous solution (pH = 8.2) containing 0.5 mM quinoline and 0.25 mM napthalene for 10.0 min.

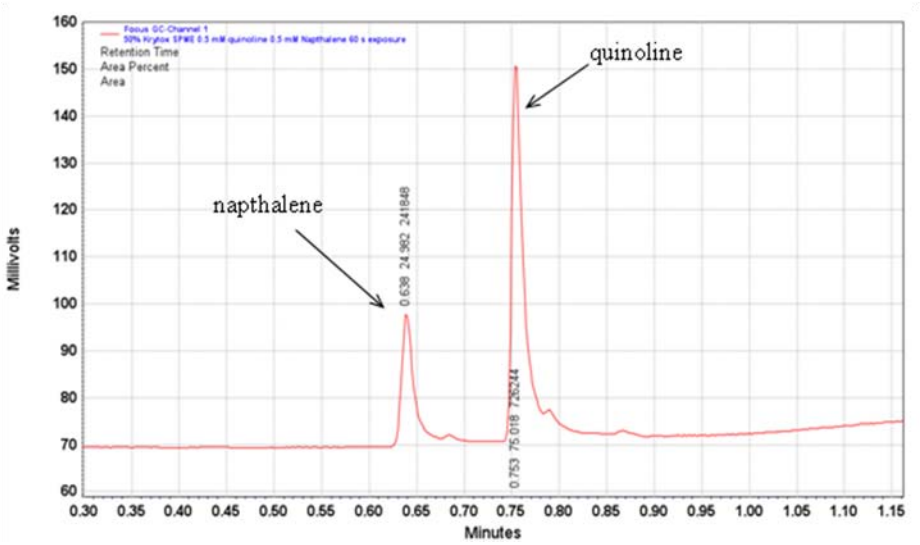

Figure 5-18. Gas chromatograph resulting from thermal desorption from a 50.0% (w/w) **1**/**2** SPME fiber that was exposed to an aqueous solution (pH = 8.2) containing 0.5 mM quinoline and 0.25 mM napthalene for 10.0 min.

The gas chromatograph shows that there was no analyte was present in the 25.0 or 50.0% (w/w) **3**/**2** (receptor-free) fibers, even after 10.0 min of exposure to the solution. The 25.0 and 50.0% (w/w) **1**/**2** fibers show somewhat greater selectivity for quinoline over napthalene. Ideally, we would like to design a film blend that showed definite preference for specific groups (i.e. pyridine-like nitrogens or carboxylic acids) so we could selectively extract a target analyte with a receptor-doped film coating. Although we are not quite to this point, the addition of plasticizer **3** to the mix shows promise for allowing the user more control over the system. We are working on optimizing the film composition for selective extraction using 96-well microplates. When a particular blend shows promise for high selectivity, these compositions will be applied to the F-SPME device for direct thermal desorption in the GC inlet.

5.4 CONCLUSIONS

We have shown that the partitioning of pyridine-like substrates between buffered aqueous solutions into **1**/**2** films depends on the formation of the receptor-substrate complex and the size of the substrate. We expected the distribution of non-fluorous pyridine-like substrates in receptor-free **2** films (0.0% (w/w) **1**/**2**) to be negligible, but this was not observed. We suggested that the high fractional free volume (FFV) of **2** allows partitioning of substrates into receptor-free films. Adding a plasticizer to the blend should reduce the FFV and thus the unintentional extraction of unwanted analytes. It is also quite possible that we are observing the effects of surface adsorption rather than absorption into the film. More work will need to be done to optimize the film composition of receptor (**1**), plasticizer (**3**), and amorphous polymer (**2**). The most efficient way to do this is to use a 96-well microplate. The experimental setup is shown in **Figure 5-19**. From left to right (wells 1-12) the fraction of receptor **1** will decrease while the fraction of plasticizer **3** will increase. The total percentage of polymer added to **2** (**1** + **3**) will remain constant. The absolute amount of **2** in the blend will increase from top to bottom (wells A-H), ranging from 5 mg/mL solutions to 30 mg/mL. The effectiveness of the films will then be evaluated by measuring log *D* of a 1.0 mM aqueous quinoline solution (pH = 8.2) in each film composition, i.e. in each well. Quinoline was chosen as the analyte because it showed significant partitioning into 0.0% (w/w) **1**/**2** films and an increase in log *D* with increasing **1** fraction (see **Figure 5-6**). Thus, a reduction of log *D* (0.0% (w/w) **1**/**2**) with the addition of **3** to the composition of the film should be experimentally straightforward.

Dynamic Mechanical Analysis (DMA) can be used to characterize polymer films and is especially useful for studying the viscoelastic nature of the films. DMA will be used to for

determine the glass transition temperature (T_g) and degree of plasticization for films with varying compositions of **1**, **2**, and **3** Members of the molecular recognition subdivision of the Weber Group will continue this work.

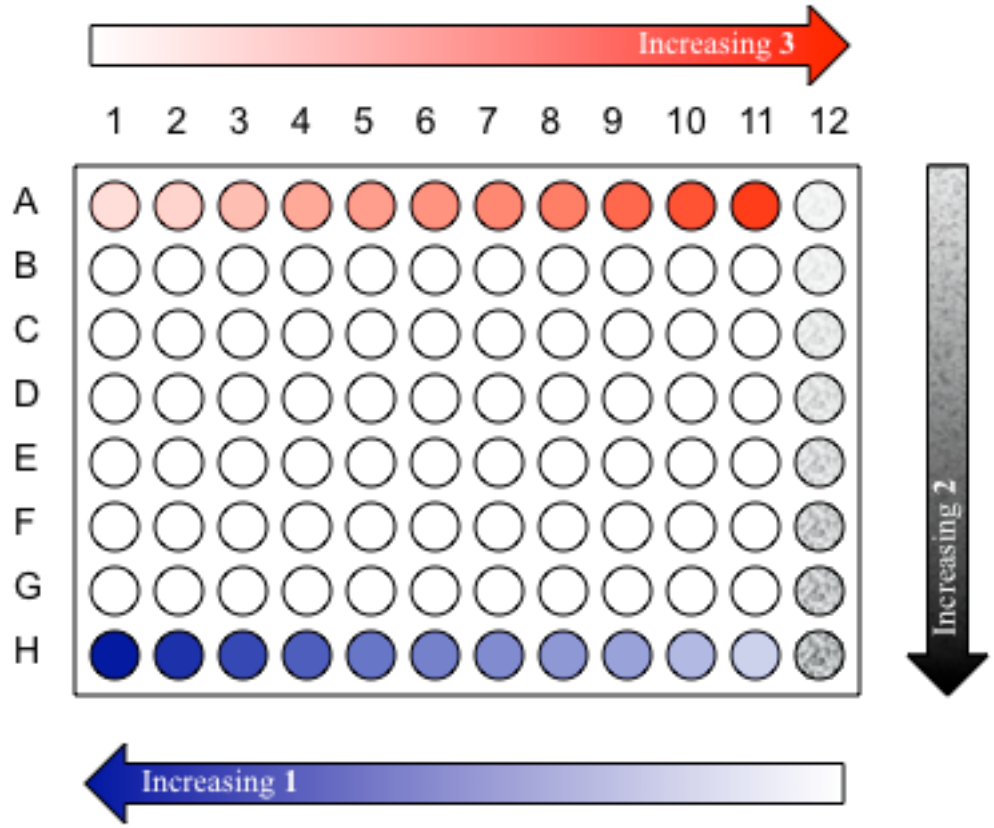

Figure 5-19. The experimental design for optimizing the film composition with three components, receptor (**1**), amorphous film (**2**), and plasticizer (**3**).

We observed that addition of receptor **1** to the film, i.e. the addition of carboxylic acid functional groups, effectively increased the film/aqueous partition coefficient for pyridine-like bases that interact favorably with **1**. Primed optical fibers were dip-coated with such receptor-

doped films to create a fluorous, molecular recognition-based, SPME device for aqueous extractions followed with direct GC thermal desorption. Preliminary results show that, when compared to commercially available polydimethylsiloxane (PDMS) SPME fibers, **1**-doped Teflon AF has greater selectivity for pyridine-like bases over their non-heterocyclic counterparts. The fiber coatings are very thin (< 10 μm). In the future, we hope to apply thicker film coatings (of optimized composition) to the fibers to ensure that we are observing absorption processes. To our knowledge, this is the first report coupling receptor-doped fluorous membrane extraction with SPME.

More long-term goals are to employ receptors with multiple functional groups and geometrical constraints for selective extractions so that a receptor is extracted not only upon functional groups, but also on size and orientation. The ideal analyte, complimentary to the receptor in both functional groups and geometric constraints, should bind very strongly to the receptor. A similar solute with identical functional groups but a different shape and orientation should no longer have a strong interaction with the receptor, even though it will have the same polarity, solubility, etc. This 'inferior' analyte would represent the ideal interferent for determining receptor-based extraction selectivity. Using a less-coordinating, less-solvating receiving phase decreases partition coefficient of both analyte and interferent. However, it also increases receptor-'ideal' analyte affinity, but not receptor-interferent affinity. So, under the assumption that the interferent has no affinity for the receptor, and the same polarity and molar volume as the analyte, a poorer solvent influences selectivity by increasing the role of the receptor, and decreasing the role of the solvent, in the distribution process. The same can be said for thin film extractions: a highly nonpolar flurous thin film should reduce the partitioning of any nonfluorous analyte while strengthening receptor-analyte interactions. We hope to design

fluorous-soluble receptors that have specific geometric constraints for important target analytes and perform similar studies both in solution and thin films.

5.5 ACKNOWLEDGEMENTS

This research was funded by the National Science Foundation (NSF) through grants CHE0315188 and CHE0615952.

APPENDIX A

2.0 HYDROGEN BOND COMPLEX FORMATION AND PROTON TRANSFER BETWEEN CARBOXYLIC ACIDS AND PYRIDINES IN A FLUOROUS SOLVENT: SUPPORTING INFORMATION

This Appendix contains supporting information for section 2.0 Hydrogen Bond Complex Formation and Proton Transfer Between Carboxylic Acids and Pyridines in a Fluorous Solvent. It contains single-crystal X-ray crystallographic data for 1:1 PFDA-pyridine in CIF format (**Table A-1**) as well as Figures showing: (**Figure A-1**) the UV spectroscopic results of titrations of Krytox (**1)** with pyridine in FC-72, **Figure A-2**) spectra showing the IR OH stretching region of **1** with various concentrations of pyridine in FC-72, (**Figure A-3**) spectra showing the IR carbonyl stretching region of pyridine with various concentrations of **1** in the absence of any solvent, (**Figure A-4**) factor analysis (EFA) results on the IR carbonyl stretching region of a titration of **1** with pyridine in FC-72, (**Figure A-5**) EFA results on the IR OH stretching region of a titration of **1** with pyridine in FC-72, and (**Figure A-6**) the IR carbonyl stretching region of PFDA and 1:1 PFDA-pyridine crystal KBr pellets.

Table A-1. Summary of crystallographic data.

1:1 PFDA-Pyridine Crystal	
formula	$C_{15}H_6F_{19}NO_2$ single crystal
formula weight	593.21
temp (K)	150(2)
space group	$P\bar{1}$
a (A)	9.777(2)
b (A)	10.960(2)
c (A)	19.356(4)
α (deg)	96.59(3)
β (deg)	100.37(3)
γ (deg)	91.10(3)
Z	4
R (%)	16.84

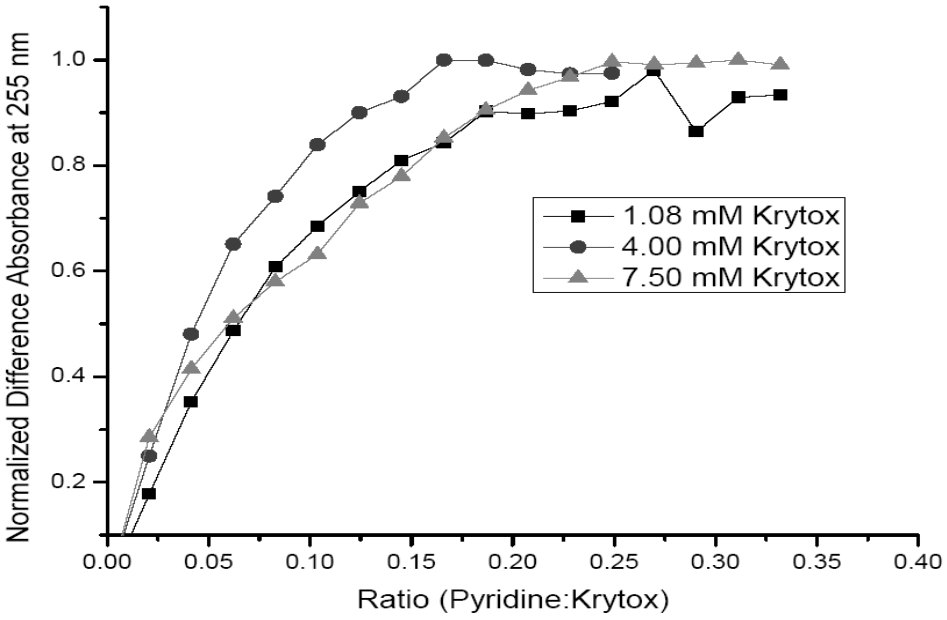

Figure A-1. A titration of 1.08 mM **1** (■), 4.00 mM **1** (●), and 7.50 mM **1** (▲) in FC-72 with a pyridine solution in FC-72. The normalized UV difference absorbance (0.1 cm cell) at 255 nm is

plotted as a function of the pyridine to **1** molar ratio. Each solution is diluted to a constant volume to maintain uniform **1** activity.

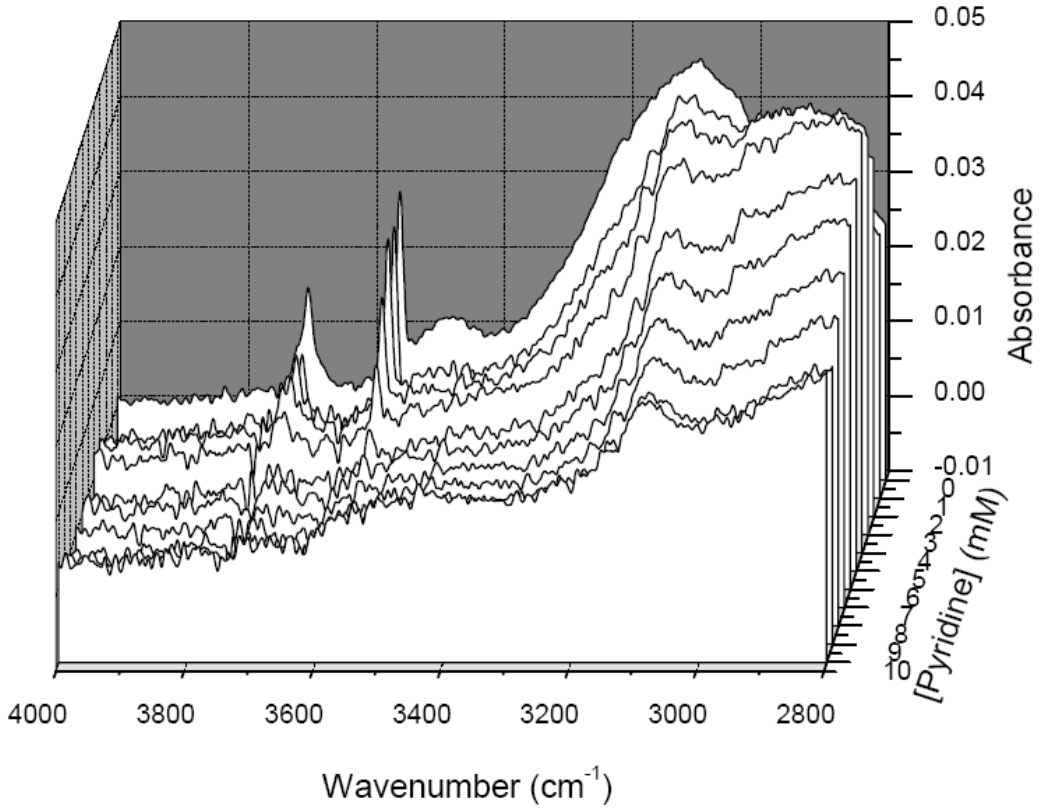

Figure A-2. The IR –OH stretching region of a titration of 10 mM **1** in FC-72 with 0.05 mL increments of 20 mM Pyridine in FC-72 (constant volume). KBr flow cell with 0.05 cm path length, average of 20 scans.

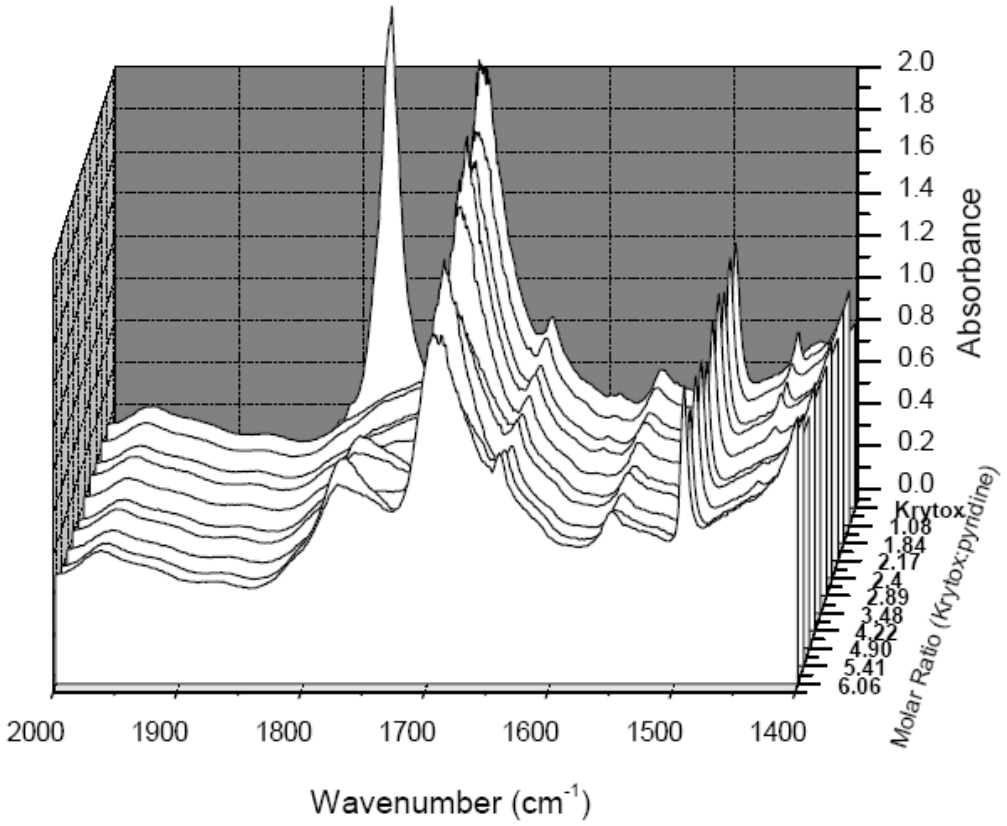

Figure A-3. The IR spectra resulting from a titration of 12.48 mM pyridine (no solvent) with 1-oil (no solvent). Only the carbonyl-stretching region is shown. KBr flow cell with 0.05 cm path length, average of 20 scans.

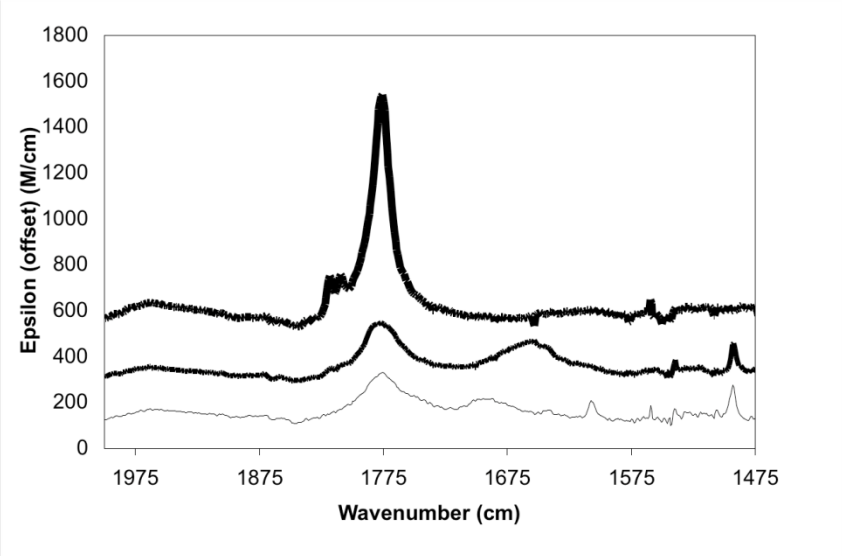

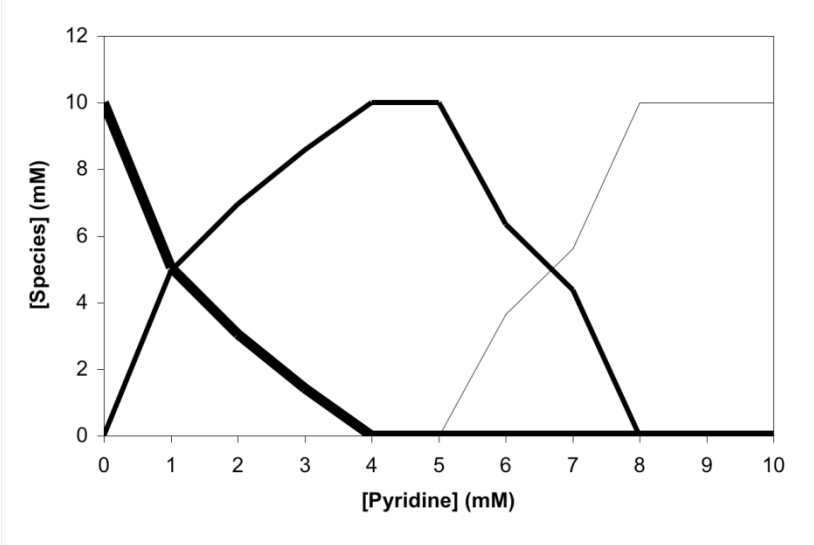

Figure A-4. SpecFit eigenvector factor analysis results from the IR carbonyl region of a titration of 10 mM **1** in FC-72 with 0.05 mL increments of 20 mM Pyridine in FC-72 (constant volume). KBr flow cell with 0.05 cm path length, average of 20 scans. Above: spectra of the resulting species; below: concentration profiles of the resulting species; species 1 (thick line), species 2 (medium line) and species 3 (thin line).

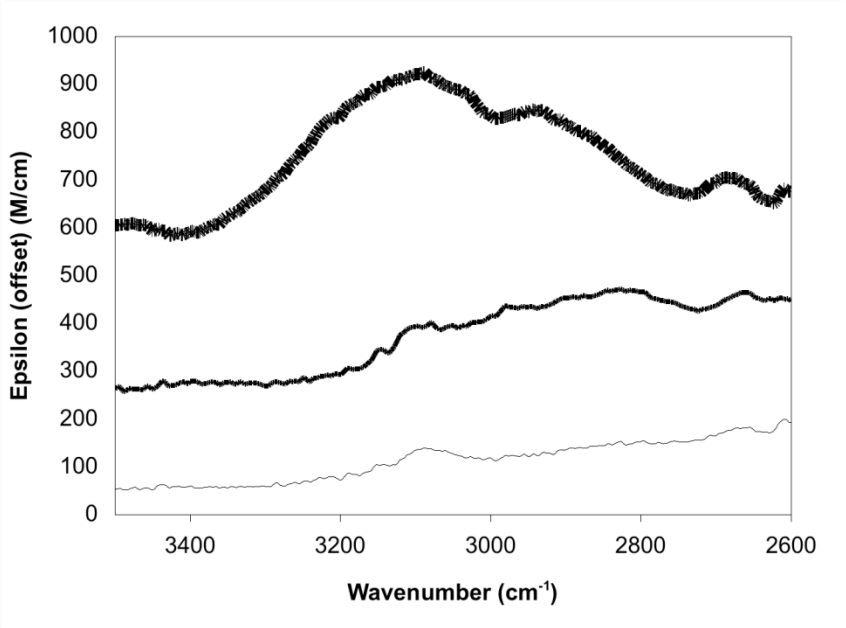

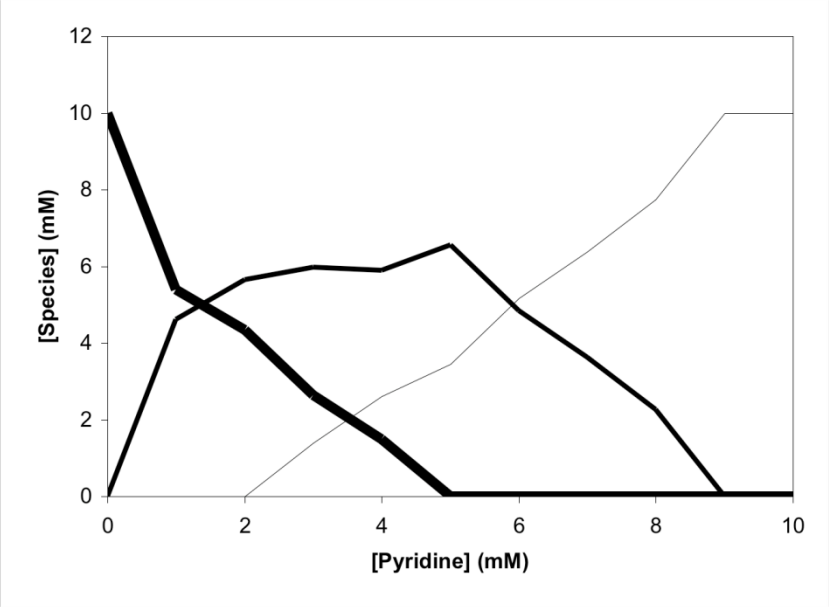

Figure A-5. SpecFit eigenvector factor analysis results from the IR hydroxyl region of a titration of 10 mM **1** in FC-72 with 0.05 mL increments of 20 mM Pyridine in FC-72 (constant volume). KBr cell with 0.05 cm path length, average of 20 scans. Above: spectra of the resulting species; below: concentration profiles of the resulting species; species 1 (thick line), species 2 (medium line) and species 3 (thin line).

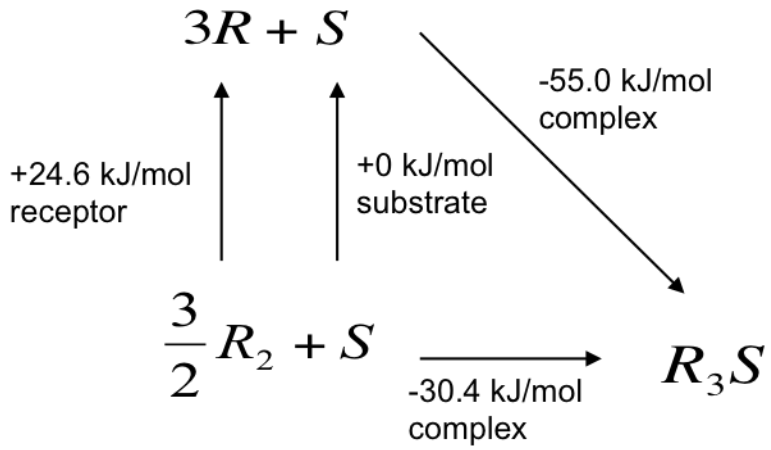

Figure A-6. Thermodynamic cycle for the formation of a 3:1 Krytox:Pyridine complex in FC-72 from a Krytox dimer and free pyridine.

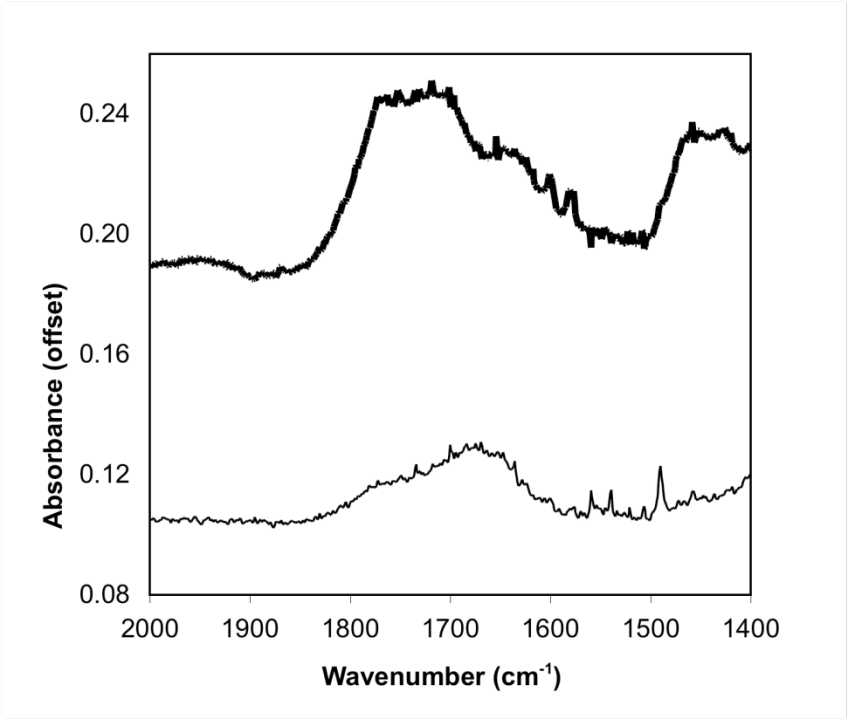

Figure A-7. The IR carbonyl stretching region of PFDA (thick line) and 1:1 PFDA-pyridine crystal (thin line) KBr pellets.

APPENDIX B

3.0 MOLECULAR AND IONIC HYDROGEN BOND FORMATION IN FLUOROUS SOLVENTS: SUPPORTING INFORMATION

This Appendix contains data supporting section 3.0 Molecular and Ionic Hydrogen Bond Formation in Fluorous Solvetns. This includes a derivation of the normalized method of continuous variations as well as Figures showing: (**Figure B-1**) UV spectra from a constant-volume titration of quinoline with **1** in FC-72, (**Figure B-2**) titration curve at 314 nm resulting from a titration of quinoline with **1** in FC-72, (**Figure B-3**) Overlay of predicted concentration profiles from model-free EFA and regression analysis of the UV spectra resulting from a constant-volume titration of isoquinoline with **1** in FC-72, (**Figure B-4**) IR spectra showing carbonyl and quinoline ring vibrational regions from a solvent –free titration of neat quinoline with **1**, (**Figure B-5**) IR spectra showing carbonyl and quinoline ring vibrational regions from a titration of constant 2.5 mM **1** with quinoline in FC-72, (**Figure B-6**) IR spectrum of a perfluorodecanoic acid-quinoline crystal/KBr pellet, (**Table B-1**) a listing of literature and experimental data corresponding to molecular complexes shown in **Figure 3-22**, and (**Table B-2**) a listing of literature and experimental data corresponding to ionic complexes shown in **Figure 3-22**.

B.1 NORMALIZED ABSORBANCE METHOD OF CONTINUOUS VARIATIONS

From equilibrium considerations (**Equation B-1**), between substrate, *S*, receptor, *R*, and complex, R_nS_m it is clear that the stoichiometric coefficients (*m* and *n*) must first be determined before the formation constant, K_f, can be defined.

$$nR + mS \rightleftharpoons R_nS_m$$

Equation B-1

$$K_f = \frac{[R_nS_m]}{[R]^n[S]^m}$$

Equation B-2

The continuous variation method is often used to determine stoichiometry; it requires that a series of solutions be prepared containing both the substrate and receptor in varying proportions so that a range of mole ratios is sampled while the sum of receptor and substrate concentrations remains constant[60,61,68]. The absorbance of each solution is measured and plotted against the mole fraction of receptor (*x*), where *R* and *S* are the receptor and substrate, respectively.

$$x = \frac{[R]}{[R]+[S]}$$

Equation B-3

When a dominant complex is formed, the resulting plot should be triangular and the maximum value is related to *n/m*.

A maximum absorbance, A_{max}, can be obtained by measuring the absorbance of a solution containing excess *R* and a concentration of *S* equal to the concentration at x = *n/(n+m)*,

in other words, were A is maximum; thereby ensuring that all S is in the R_nS_m form. Plotting the ratio of measured absorbance to this new maximum value, $y = A/A_{max}$, against x generates a convenient normalized plot[61,103]. If the path length remains constant, the absorbance term then becomes:

$$y = \frac{A}{A_{max}} = \frac{[R_nS_m]}{[R_nS_m]_{max}}$$

Equation B-4

where A is the absorbance of the sample and all values have been corrected for the contribution of any uncomplexed constituents. By setting $m = 1$, the complex stoichiometry can be normalized to moles of substrate and the maximum complex contributing to A_{max} is given by equation S5.

$$[R_nS]_{max} = (1 - x)[S]_{max}$$

Equation B-5

Therefore, the concentration of complex at any point in the series of solutions can be determined using the following equation.

$$[R_nS] = y(1 - x)[S]_{max}$$

Equation B-6

where $[S]_{max}$ = [S] at $x = 0$. The formation constant for the complex, K_f, is then most accurately defined by using the equilibrium concentrations of complex at the stoichiometric ratio of the complex where the plot is maximum.

$$K_f = \frac{y_{max}(1-x)[S]_{max}}{[(1-y_{max})(1-x)[S]_{max}][x[S]_{max} - ny_{max}(1-x)[R]_{max}]^n}$$

Equation B-7

where $[R]_{max}$ = [R] at $x = 1$ and y_{max} is the value of y at $x = n/(n+m)$.

B.2 MOLECULAR VS. IONIC COMPLEX FORMATION

B.2.1 Ultraviolet Spectroscopy

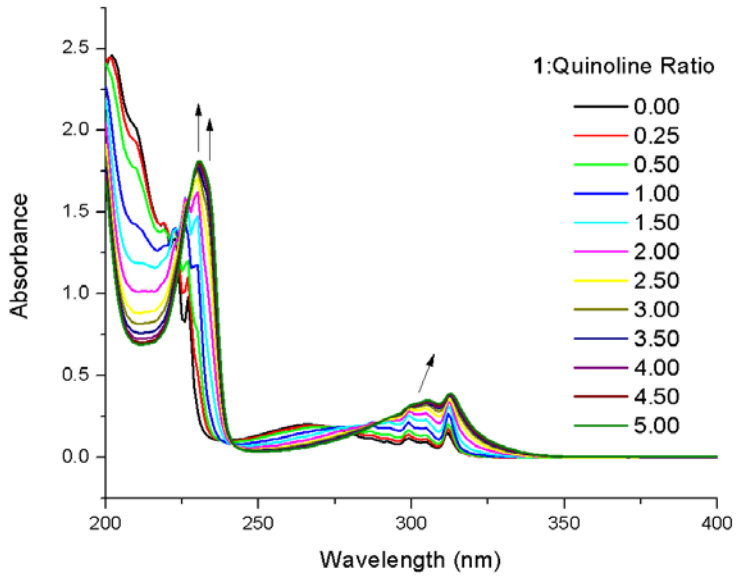

Figure B -1. Representative UV spectra from a constant-volume titration of 1.0 mM quinoline with **1** (non-absorbing from 200-400 nm) in FC-72, path length = 0.1 cm. Arrows indicate increasing [**1**].

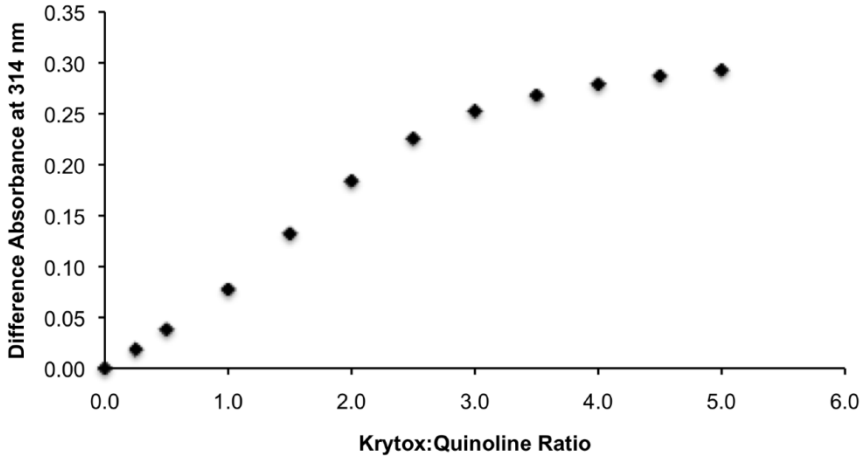

Figure B-2. Difference absorbance at 314 nm from a constant volume titration of quinoline with **1** in FC-72.

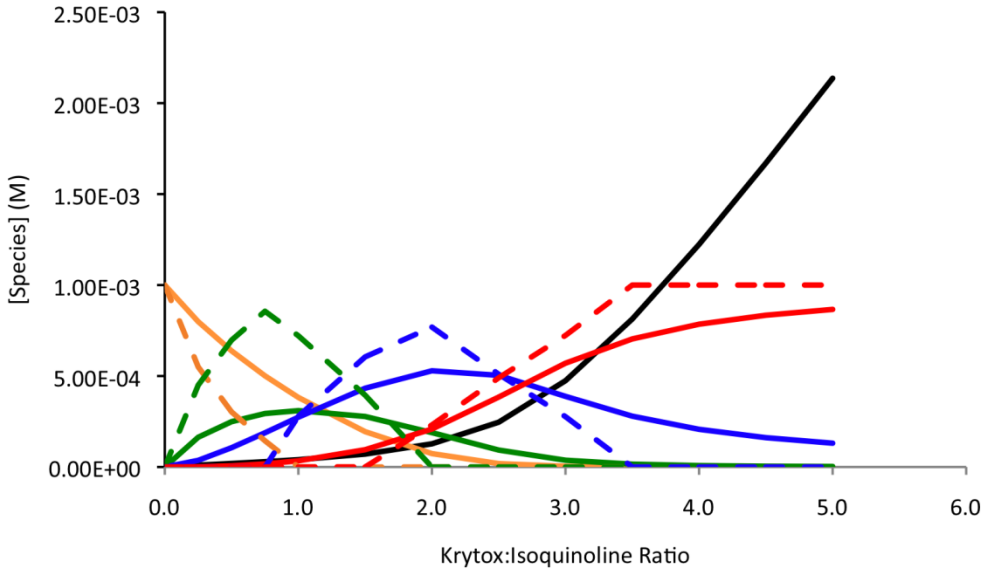

Figure B-3. Overlay of predicted concentration profiles from model-free EFA (---) and regression analysis (—) of the ultraviolet spectra resulting from a titration of isoquinoline with **1** in FC-72 for free isoquinoline (orange), a 1:1 (green), 2:1 (blue), and 3:1 (red) isoquinoline:**1** complex, and free **1** (black), respectfully.

B.2.2 Infrared Spectroscopy

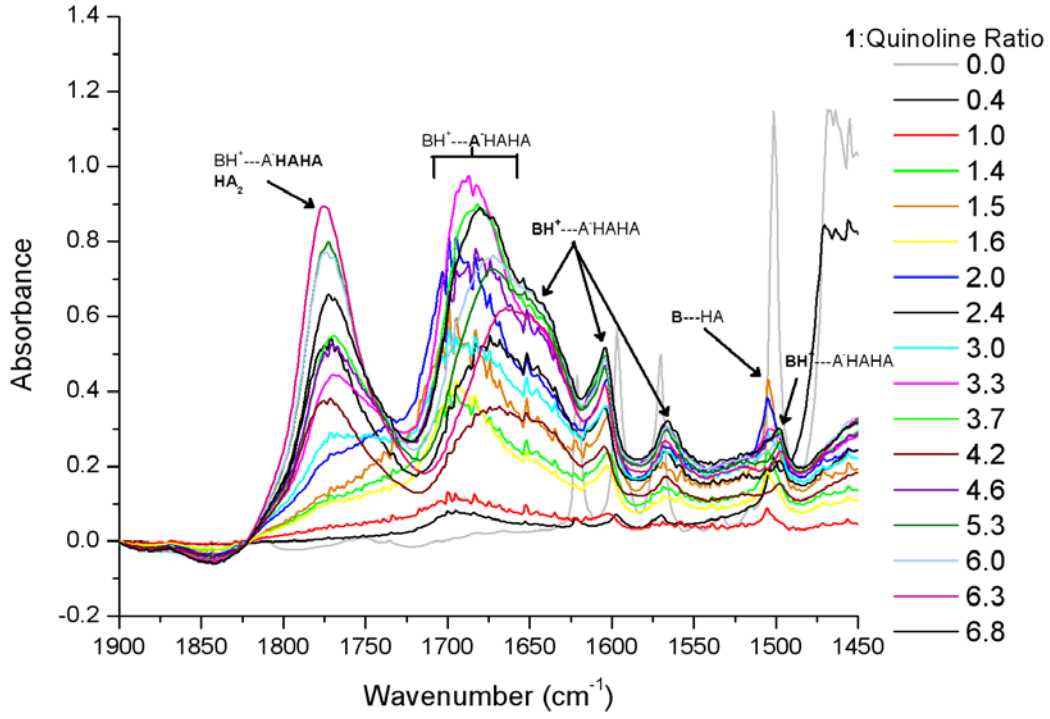

Figure B-4. IR spectra showing carbonyl and quinoline ring vibrational regions from a solvent – free titration of neat quinoline with **1**. B, quinoline; HA, **1**; B---HA; quinoline-**1** molecular complex; BH^+---A^-HAHA, quinolinium-**1**-carboxylate ionic complex. The portion of the complex shown in bold is responsible for the vibration. Path length = 0.1 mm, resolution = 2 cm^{-1}, 50 scans co-added, spectra were baseline-corrected and smoothed to 5 points using the boxcar method.

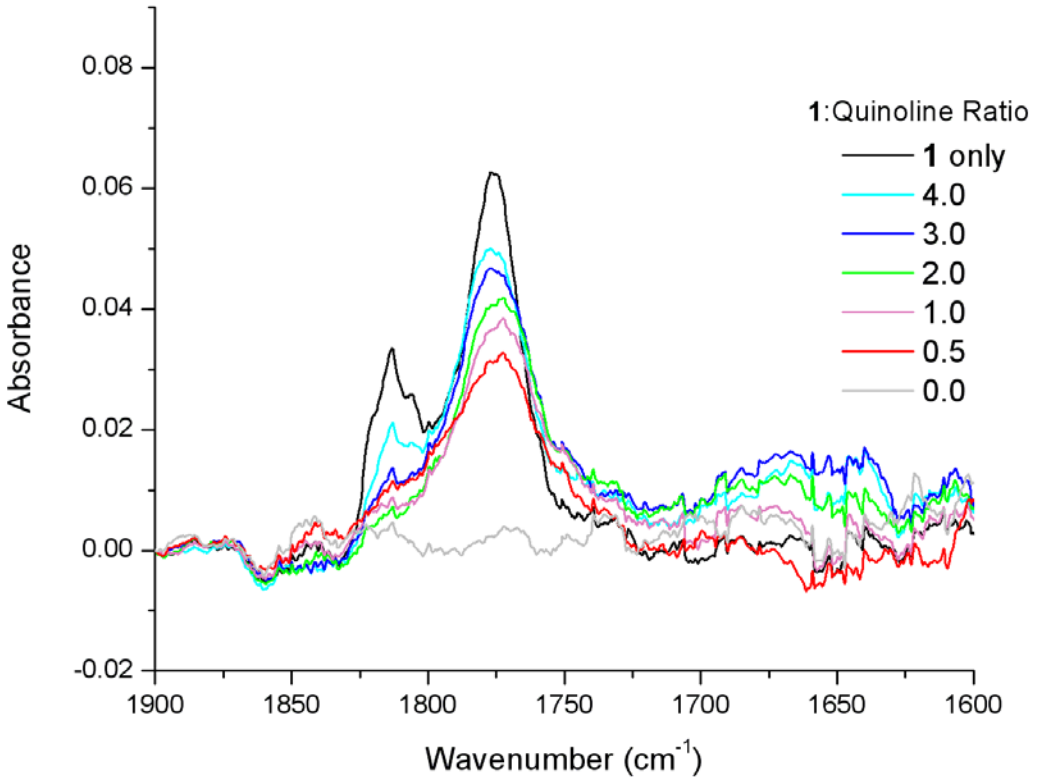

Figure B-5. IR spectra showing carbonyl and quinoline ring vibrational regions from a titration of constant 2.5 mM **1** with quinoline in FC-72; shown as the **1**:quinoline ratio. Path length = 0.1 mm, resolution = 0.25 cm^{-1}, 500 scans co-added, spectra were baseline-corrected and smoothed to 49 points using the boxcar method.

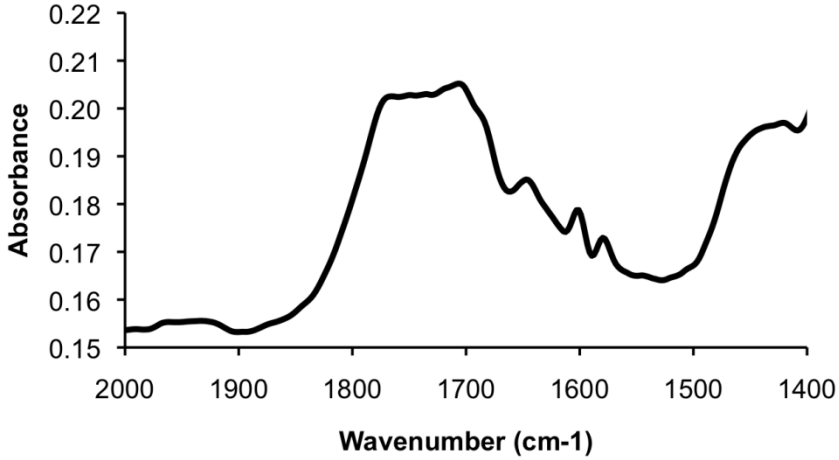

Figure B -6. IR s pectrum of a p erfluorodecanoic aci d-quinoline c rystal/KBr pe llet. Resolution = 2 cm^{-1}, 20 scans co-added, spectra were baseline-corrected and smoothed to 5 points using the boxcar method. Heterogeneous broadening leads to overlapping of the carboxylated and quinolinium peaks spanning 1800-1600 cm^{-1}. Sharp quinolinium peaks can be seen at 1638 cm^{-1} as well as hydrogen-bonded quinoline at 1602 cm^{-1}.

B.2.3 Solvent Effects in Hydrogen-Bonding and Proton Transfer

Table B-1. Literature and experimental data corresponding to molecular complexes shown in **Figure 3-22**. $\Delta pK_a = pK_{aBH+} - pK_{aAH}$; π^* = Kamlet-Taft dipolarity/polarizability parameter.

Solvent	π^*	Acid	Base	ΔpKa	Stoichiometry (base:acid)
water[174]	1.17	water	pyridine	-10.54	-----
carbontetrachloride[92]	0.28	phenol	pyrazine	-9.28	1:1, 1:2
carbontetrachloride[92]	0.28	phenol	pyrimidine	-8.72	1:1, 1:2
carbontetrachloride[92]	0.28	phenol	3-cyanopyridine	-8.59	1:1
carbontetrachloride[92]	0.28	phenol	4-cyanopyridine	-8.05	1:1
carbontetrachloride[92]	0.28	phenol	pyridazine	-7.65	1:1, 1:2
carbontetrachloride[92]	0.28	phenol	3-bromopyridine	-7.11	1:1
carbontetrachloride[92]	0.28	phenol	pyridine	-4.78	1:1
cyclohexane[100]	0.00	4-fluorophenol	pyridine	-4.75	1:1
chlorobenzene[100]	0.71	4-fluorophenol	pyridine	-4.75	1:1
o-dichlorobenzene[100]	0.75	4-fluorophenol	pyridine	-4.75	1:1
carbontetrachloride[92]	0.28	phenol	3-methylpyridine	-4.27	1:1
carbontetrachloride[92]	0.28	phenol	4-methylpyridine	-3.97	1:1
carbontetrachloride[92]	0.28	phenol	3,5-dimethylpyridine	-3.80	1:1
dichloromethane[175]	0.82	acetic acid	pyrazole	-2.25	1:1
carbontetrachloride[176]	0.28	formic acid	pyrazole	-1.24	-----
acetonitrile[97]	0.75	picric Acid	2-cyanopyridine	-0.50	1:1
FC-72	-0.41	**1**	pyrazine	0.44	1:1
chloroform	0.58	perfluorodecanoic acid	pyrazine	0.44	NC
cyclohexane	0.00	acetic acid	pyridine	0.45	1:1
hexane[96]	-0.04	acetic acid	pyridine	0.45	1:1
carbontetrachloride[72]	0.28	acetic acid	pyridine	0.45	1:1
chloroform[72,94]	0.58	acetic acid	pyridine	0.45	1:1
FC-72	-0.41	**1**	pyrimidine	0.94	1:1
chloroform	0.58	perfluorodecanoic acid	pyrimidine	0.94	NC
chloroform[94]	0.58	benzoic acid	pyridine	1.00	1:1
acetonitrile[97]	0.75	picric Acid	3-cyanopyridine	1.06	1:1
acetonitrile[97]	0.75	picric Acid	4-cyanopyridine	1.60	1:1
chloroform[72,94]	0.58	iodoacetic acid	pyridine	2.02	1:1
chloroform[94]	0.58	bromoacetic acid	pyridine	2.30	1:1
cyclohexane	0.00	chloroacetic acid	pyridine	2.35	1:1
HFE-7100	0.23[177]	chloroacetic acid	pyridine	2.35	1:1
carbontetrachloride[72]	0.28	chloroacetic acid	pyridine	2.35	1:1
chloroform	0.58	chloroacetic acid	pyridine	2.35	1:1
chloroform[72]	0.58	chloropropionic acid	pyridine	2.37	1:1
acetonitrile[97]	0.75	picric Acid	2-Bromopyridine	2.54	1:1
FC-72	-0.41	**1**	quinazoline	3.14	1:1
chloroform	0.58	perfluorodecanoic acid	quinazoline	3.14	1:1

-----, stoichiometry is not reported; NC, no complexation

Table B-2. Literature and experimental data corresponding to ionic complexes shown in **Figure 3-22**. $\Delta pK_a = pK_{aBH+} - pK_{aAH}$; π* = Kamlet-Taft dipolarity/polarizability parameter.

Solvent	π	Acid*	Base	Δp*K*a	Stoichiometry (base:acid)
1,2-dichloroethane[100]	0.81	4-fluorophenol	pyridine	-4.75	1:1
dichloromethane[100]	0.82	4-fluorophenol	pyridine	-4.75	1:1
dichloromethane[178]	0.82	acetic acid	pyridine	0.45	1:1, 1:2
dichloromethane[175]	0.82	trichloroacetic acid	pyrazole	2.24	1:1, 1:2
dichloromethane[175]	0.82	trifluoroacetic acid	pyrazole	2.24	1:1, 1:2
chloroform[72]	0.58	chloroacetic acid	pyridine	2.35	1:1, 1:2
dichloromethane[73,179]	0.82	chloroacetic acid	pyridine	2.35	1:1, 1:2
acetonitrile[97]	0.75	picric acid	3-bromopyridine	2.54	1:1
chloroform[94]	0.58	cyanoacetic acid	pyridine	2.74	1:1
chloroform[72,94]	0.58	dichloroacetic acid	pyridine	3.95	1:1
dichloromethane[73,93]	0.82	dichloroacetic acid	pyridine	3.95	1:1
chloroform[94]	0.58	difluoroacetic acid	pyridine	3.96	-----
FC-72	-0.41	trichloroacetic acid	pyridine	4.50	1:3
cyclohexane	0.00	trichloroacetic acid	pyridine	4.50	1:1
HFE-7100	0.23	trichloroacetic acid	pyridine	4.50	1:3
chloroform[72]	0.58	trichloroacetic acid	pyridine	4.50	1:2
dichloromethane[93]	0.82	trichloroacetic acid	pyridine	4.50	1:1
FC-72	-0.41	**1**	quinoline	4.64	1:3
chloroform	0.58	perfluorodecanoic acid	quinoline	4.64	1:3
carbontetrachloride[180]	0.28	trifluoroacetic acid	isoquinoline	4.76	-----
butylchloroide[180]	0.39	trifluoroacetic acid	isoquinoline	4.76	-----
toluene[180]	0.54	trifluoroacetic acid	isoquinoline	4.76	1:1, 1:2
benzene[180]	0.59	trifluoroacetic acid	isoquinoline	4.76	-----
chlorobenzene[180]	0.71	trifluoroacetic acid	isoquinoline	4.76	-----
FC-72	-0.41	**1**	pyridine	4.94	1:3
cyclohexane	0.00	trifluoroacetic acid	pyridine	4.94	-----
cyclohexane	0.00	perfluorodecanoic acid	pyridine	4.94	1:1
HFE-7100	0.23	perfluorodecanoic acid	pyridine	4.94	1:1, 1:2
chloroform	0.58	perfluorodecanoic acid	pyridine	4.94	1:1
chloroform[72,94]	0.58	trifluoroacetic acid	pyridine	4.94	1:2
dichloromethane[73,175]	0.82	trifluoroacetic acid	pyridine	4.94	1:1
FC-72	-0.41	trifluoroacetic acid	pyridine	4.94	1:1
FC-72	-0.41	**1**	isoquinoline	5.14	1:3
acetonitrile[181]	0.75	trifluoroacetic acid	quinoline	5.24	1:2

-----, stoichiometry is not reported

BIBLIOGRAPHY

(1) Chen, Z.; Weber, S. G. *Anal. Chem.* **2007**, *79*, 1043-1049.

(2) Platts, J. A.; Abraham, M. H.; Butina, D.; Hersey, A. *J. Chem. Inf. Comput. Sci.* **2000**, *40*, 71-80.

(3) Platts, J. A.; Butina, D.; Abraham, M. H.; Hersey, A. *J. Chem. Inf. Comput. Sci.* **1999**, *39*, 835-845.

(4) Smith, R. M. *J. Chromatogr., A.* **2003**, *1000*, 3-27.

(5) Cantwell, F. F.; Losier, M. In *Sampling and Sample Preparation for Field and Laboratory*; Pawliszyn, J., Ed.; Elsevier: New York, NY, 2002.

(6) Poole, C. F. In *Sampling and Sample Praparation for Field and Laboratory*; Pawliszyn, J., Ed.; Elsevier: New York, NY, 2002, p 341-477.

(7) Arthur, C. L.; Pawliszyn, J. *Anal. Chem.* **1990**, *62*, 2145-2148.

(8) Pawliszyn, J. *Solid Phase Microextraction, Theory and Practice*; Wiley-VCH: New York, NY, 1997.

(9) Henry, M. *SPE Technology - Principles and Practical Consequences*; Marcel Dekker, Inc.: New York, NY, 2000.

(10) Fritz, J. S. *Analytical Solid-Phase Extraction*; Wiley-VCH: New York, NY, 1999.

(11) Mitra, S. *Sample Preparation Techniques in Analytical Chemistry*; John Wiley & Sons: Hoboken, NJ, 2003; Vol. 162.

(12) Raynie, D. E. *Anal. Chem.* **2004**, *76*, 4659-4664.

(13) Valenta, J. N.; Weber, S. G. *J. Chromatogr., A.* **1996**, *722*, 47-57.

(14) Li, S.; Sun, L.; Chung, Y.; Weber, S. G. *Anal. Chem.* **1999**, *71*, 2146-2151.

(15) Stillinger, F. H.; Wasserman, Z. *J. Phys. Chem.* **1978**, *82*, 929-940.

(16) Lehn, J. M. *Science* **1993**, *260*, 1762-3.

(17) Yin, H.; Lee, G.-i.; Sedey, K. A.; Rodriguez, J. M.; Wang, H.-G.; Sebti, S. M.; Hamilton, A. D. *J. Am. Chem. Soc.* **2005**, *127*.

(18) Valenta, J. N.; Dixon, R. P.; Hamilton, A. D.; Weber, S. G. *Anal. Chem.* **1994**, *66*, 2397-2403.

(19) Hunter, C. A. *Angew. Chem., Int. Ed.* **2004**, *43*, 5310-5324.

(20) O'Neal, K.; Geib, S.; Weber, S. G. *Anal. Chem.* **2007**, *79*, 3117-3125.

(21) Hildebrand, J. H.; Scott, R. L. *The Solubility of Nonelectrolytes*; Third ed.; Reinhold Publishing Corporation: New York, 1950.

(22) Gladysz, J. A.; Curran, D. P.; Horvath, I. T. *Handbook of Fluorous Chemistry*; Wiley-VCH: Weinheim, Germany, 2004.

(23) Horvath, I. T.; Rabai, J. *Science* **1994**, *266*, 72.

(24) Curran, D. P.; Lee, Z. *Green Chem.* **2001**, *3*, G3-G7.

(25) Curran, D. P. *Angew. Chem., Int. Ed.* **1998**, *37*, 1175.

(26) Curran, D. P.; Hadida, S.; Kim, S.-Y.; Luo, Z. *J. Am. Chem. Soc.* **1999**, *121*.

(27) Wipf, P.; Reeves, J. T. *Tetrahedron Lett.* **1999**, *40*.

(28) Nakamura, H.; Linclau, B.; Curran, D. P. *J. Am. Chem. Soc.* **2001**, *123*, 10119-10120.

(29) Curran, D. P. *Science* **2008**, *321*, 1645-1646.

(30) Chen, H.; Weiner, W. S.; Hamilton, A. D. *Curr Opin Chem Biol* **1997**, *1*, 458-466.

(31) Vishweshwar, P.; Nangia, A.; Lynch, V. M. *J. Org. Chem.* **2002**, *67*, 556-565.

(32) Doan, V.; Koppe, R.; Kasai, P. H. *J. Am. Chem. Soc.* **1997**, *119*, 9810-9815.

(33) Yu, M. S.; Curran, D. P.; Nagashima, T. *Org. Lett.* **2005**, *7*, 3677-3680.

(34) 3M In *Product Information*; 3M, Ed. 2003.

(35) Pinnau, I.; Toy, L. G. *J. Membr. Sci.* **1996**, *109*, 125-133.

(36) Alentiev, A. Y.; Shantarovich, V. P.; Merkel, T. C.; Bondar, V. I.; Freeman, B. D.; Yampolskii, Y. P. *Macromolecules* **2002**, *35*, 9513-9522.

(37) Polyakov, A. M.; Starannikova, L. E.; Yampolskii, Y. P. *J. Membr. Sci.* **2003**, *216*, 241-256.

(38) Lai, C.-Z.; Koseoglu, S. S.; Lugert, E. C.; Boswell, P. G.; Rábai, J.; Lodge, T. P.; Bu□hlmann, P. *J. Am. Chem. Soc.* **2009**, *in press*.

(39) Zhao, H.; Zhang, J.; Wu, N.; Zhang, X.; Crowley, K.; Weber, S. G. *J. Am. Chem. Soc.* **2005**, *127*, 15112-15119.

(40) Zhao, H.; Ismail, K.; Weber, S. G. *J. Am. Chem. Soc.* **2004**, *126*, 13184-13185.

(41) Pawliszyn, J. *Anal. Chem.* **2003**, *75*, 2543-2558.

(42) Buhlmann, P.; Badertscher, M.; Simon, W. *Tetrahedron* **1993**, *49*, 595-8.

(43) Jin, Z. M.; Fu, W.; Pan, Y. J.; Zou, J. W.; Hu, M. L. *J. Inclusion Phenom. Mol. Recognit. Chem.* **2005**, *51*, 225-229.

(44) Lipkowitz, K. B.; Raghothama, S.; Yang, J. A. *J. Am. Chem. Soc.* **1992**, *114*, 1554-62.

(45) Meindersma, G. W.; van Schoonhoven, T.; Kuzmanovic, B.; de Haan, A. B. *Chem. Eng. Process.* **2006**, *45*, 175-183.

(46) Pietraszkiewicz, O.; Brzozka, Z.; Pietraszkiewicz, M. *Mater. Sci. Eng., C* **2001**, *C18*, 117-120.

(47) Potluri, V. K.; Maitra, U. *J. Org. Chem.* **2000**, *65*, 7764-7769.

(48) Shinkai, S.; Tsukagoshi, K.; Ishikawa, Y.; Kunitake, T. *J. Chem. Soc., Chem. Comm.* **1991**, 1039-41.

(49) Shoji, Y.; Tashiro, K.; Aida, T. *J. Am. Chem. Soc.* **2004**, *126*, 6570-6571.

(50) Oshima, T.; Higuchi, H.; Ohto, K.; Inoue, K.; Goto, M. *Langmuir* **2005**, *21*, 7280-7284.

(51) Palomo, C.; Aizpurua, J. M.; Loinaz, I.; Fernandez-Berridi, M. J.; Irusta, L. *Org. Lett.* **2001**, *3*, 2361-2364.

(52) Loiseau, J.; Fouquet, E.; Fish, R. H.; Vincent, J. M.; Verlhac, J. B. *J. Fluorine Chem.* **2001**, *108*.

(53) Hope, E. G.; Kemmitt, R. D. W.; Stuart, A. M. *J. Am. Chem. Soc., Dalt. Trans.* **1998**, 3765-3770.

(54) Contel, M.; Villuendas, P. R.; Fernandez-Gallardo, J.; Alonso, P. J.; Vincent, J.-M.; Fish, R. H. *Inorg. Chem.* **2005**, *44*, 9771-9778.

(55) Vincent, J.-M.; Contel, M.; Laguna, M.; Fish, R. H. In *Handbook of Fluorous Chemistry* Weinheim, Germany, 2004, p 395-397.

(56) El Bakkari, M.; McClenaghan, N.; Vincent, J.-M. *J. Am. Chem. Soc.* **2002**, *124*, 12942-12943.

(57) Boswell, P. G.; Lugert, E. C.; Rabai, J.; Amin, E. A.; Buehlmann, P. *J. Am. Chem. Soc.* **2005**, *127*, 16976-16984.

(58) Boswell, P. G.; Buhlmann, P. *J. Am. Chem. Soc.* **2005**, *127*, 8958-8959.

(59) Riess, J. G. *Tetrahedron* **2002**, *58*, 4113-4131.

(60) Connors, K. A. *Binding Constants* 411 ed.; John Wiley & Sons: New York, 1987.

(61) Likussar, W.; Boltz, D. F. *Anal. Chem.* **1971**, *43*, 1265-1273.

(62) Klingsberg, E. *Pyridine and Its Derivatives Part One*; Interscience Publishers, Inc.: New York, 1960; Vol. Fourteen.

(63) Alkorta, I.; Elguero, J. *J. Org. Chem.* **2002**, *67*, 1515-1519.

(64) Marechal, Y. *Vib. Spectrosc.* **1987**, *16*, 311-56.

(65) Kojima, I.; Yoshida, M.; Tanaka, M. *J. Inorg. Nucl. Chem.* **1970**, *32*, 987-995.

(66) Remko, M. *Advances in Molecular Relaxation and Interaction Processes* **1979**, *15*, 193-206.

(67) Steiner, T. *Acta Crystallographica Section B* **2001**, *57*, 103-106.

(68) Vosburgh, W. C.; Cooper, G. R. *J. Am. Chem. Soc.* **1941**, *63*, 437-442.

(69) Meyer, A. S. J.; Ayres, G. H. *J. Am. Chem. Soc.* **1957**, *79*, 49-53.

(70) Golubev, N. S.; Smirnov, S. N.; Gindin, V. A.; Denisov, G. S.; Benedict, H.; Limbach, H.-H. *J. Am. Chem. Soc.* **1994**, *116*, 12055-12056.

(71) Nibu, Y.; Marui, R.; Shimada, H. *J. Phys. Chem. A* **2006**, *110*, 9627-9632.

(72) Barrow, G. M. *J. Am. Chem. Soc.* **1956**, *78*, 5802-5806.

(73) Dega-Szafran, Z.; Grundwald-Wyspianska, M.; Szafran, M. *Spectrochimica Acta, Part A* **1991**, *47*, 543-550.

(74) Lee, J. Y.; Painter, P. C.; Coleman, M. M. *Macromolecules* **1988**, *21*, 954-960.

(75) Gill, N. S.; Nuttall, R. H.; Scaife, D. E.; Sharp, D. W. A. *J. Inorg. Nucl. Chem.* **1961**, *18*, 79-87.

(76) Fernandez-Berridi, M. J.; Iruin, J. J.; Irusta, L.; Mercero, J. M.; Ugalde, J. M. *J. Phys. Chem. A* **2002**, *106*, 4187-4191.

(77) Johnson, S. L.; Rumon, K. A. *J. Phys. Chem.* **1964**, *69*, 74-86.

(78) Binstead, R. A.; Jung, B.; Zuberbuhle, A. D.; 3.0 ed.; Spectrum Software Associates: 200-2004.

(79) Bulmer, J. T.; Shurvell, H. F. *J. Phys. Chem.* **1973**, *77*, 256-262.

(80) Gonzalez, A.; Irusta, L.; Fernandez-Berridi, M. J.; Iruin, J. J.; Sierra, T.; Oriol, L. *Vib. Spectrosc.* **2006**, *41*, 21-27.

(81) Rocaboy, C.; Rutherford, D.; Bennett, B. L.; Gladysz, J. A. *J. Phys. Org. Chem.* **2000**, *13*, 596-603.

(82) Taylor, R.; Kennard, O.; Versichel, W. *J. Am. Chem. Soc.* **1983**, *105*.

(83) Lehn, J.-M. *Macrocyclic Chemistry - Aspects of Organic and Inorganic Supramolecular Chemistry*, Wiley-VCH: Weinheim, 1993.

(84) Schrader, T.; Hamilton, A. D. *Functional Synthetic Receptors*; Wiley-VCH: Weinhelm, 2005.

(85) Ansyln, E. V.; Dougherty, D. A. *Modern Physical Organic Chemistry*; University Science Books Sausalito, CA, 2006.

(86) Vincent, J.-M. *J. Fluorine Chem.* **2008**, *129*, 903-909.

(87) El Bakkari, M.; Vincent, J.-M. *Org. Lett.* **2004**, *6*, 2765-2767.

(88) Boswell, P. G.; Szıjjarto, C.; Jurisch, M.; Gladysz, J. A.; Rabai, J.; Buhlmann, P. *Anal. Chem.* **2008**, *80*, 2084-2090.

(89) Boenigk, D.; Mootz, D. *J. Am. Chem. Soc.* **1988**, *110*, 2135-2139.

(90) Odinokov, S. E.; Mashkovsky, A. A.; Glazunov, V. P. *Spectrochimica Acta* **1976**, *32A*, 1355-1363.

(91) Dawa, B. A.; Gowland, J. A. *Can. J. Chem.* **1978**, *56*, 2567-3833.

(92) Kasende, O.; Zeegers-Huyskens, T. *J. Phys. Chem.* **1984**, *88*, 2132-2137.

(93) Denisov, G. S.; Gindin, V. A.; Golubev, N. S.; Ligay, S. S.; Shchepkin, D. N.; Smirnov, S. N. *J. Mol. Liq.* **1995**, *67*, 217-234.

(94) Langner, R.; Zundel, G. *J. Am. Chem. Soc., Far. Trans.* **1995**, *91*, 3831-3838.

(95) Golubev, N. S.; Denisov, G. S.; Smirnov, S. N.; Shchepkin, D. N. *Zeitschrift fur Physikalishche Chemie* **1996**, *196*, 73-84.

(96) Drichko, N. V.; Kerenskaia, G. Y.; Schreiber, V. M. *J. Mol. Struct.* **1999**, *477*, 127-141.

(97) Magonski, J. *J. Phys. Org. Chem.* **2002**, *15*, 204-210.

(98) Berg, E. R.; Freeman, S. A.; Green, D. D.; Ulness, D. J. *J. Phys. Chem.* **2006**, *110*, 13434-13446.

(99) Berg, E. R.; Green, D. D.; Moliva A, D. C.; Bjerke, B. T.; Gealy, M. W.; Ulness, D. J. *J. Phys. Chem. A* **2008**, *112*, 833-838.

(100) Joris, L.; Mitsky, J.; Taft, R. W. *J. Am. Chem. Soc.* **1972**, *94*, 3438-3442.

(101) Denisov, G. S.; Kulbida, A. I.; Micheev, V. A.; Rumynskaja, I. G.; Schreiber, V. M. *J. Mol. Liq.* **1983**, *26*, 159-168.

(102) Jeffrey, G. A. *An Introduction to Hydrogen Bonding*; Oxford University Press: New York, 1997.

(103) Momoki, K.; Sekino, J.; Sato, H.; Yamaguchi, N. *Anal. Chem.* **1969**, *41*, 1286-1299.

(104) Peral, F.; Gallego, E. *J. Mol. Struct.* **1995**, *372*, 101-112.

(105) Peral, F.; Gallego, E. *Spectrochimica Acta Part A: Molecular and Biomolecular Spectroscopy* **2003**, *59*, 1223-1237.

(106) Albert, A.; Armarego, W. L. F.; Spinner, E. *Journal of the Chemical Society* **1961**, 2689-96.

(107) Peral, F.; Gallego, E. *J. Mol. Struct.* **1994**, *326*, 59-68.

(108) Denisov, G. S.; Mikheev, V. A.; Sorkornov, A. B.; Sorkornov, T. V.; Terushkin, B. S.; Shraiber, V. M. *Zh. Prikl. Spektrosk.* **1985**, *66*.

(109) Harris, D. C.; Bertolucci, M. D. *Symmetry and Spectroscopy: An Introduction to Vibrational and Electronic Spectroscopy*; Dover Publications: New York, NY, 1978.

(110) Dines, T. J.; MacGregor, L. D.; Rochester, C. H. *Langmuir* **2002**, *18*, 2300-2308.

(111) Kamlet, M. J.; Abboud, J. L.; Taft, R. W. *J. Am. Chem. Soc.* **1977**, *99*, 6027-6038.

(112) Sokornova, T. V.; Shraiber, V. M. *Zh. Prikl. Spektrosk.* **1992**, *56*, 200-4.

(113) Zhang, X.-B.; Guo, C.-C.; Li, Z.-Z.; Shen, G.-L.; Yu, R.-Q. *Anal. Chem.* **2002**, *74*, 821-825.

(114) Papkovsky, D.; Uskova, M. A.; Ponomarev, G. V.; Korpela, T.; Kulmala, S.; Guilbault, G. G. *Anal. Chim. Acta* **1998**, *374*, 1-9.

(115) Czolk, R. *Sens. Actuators, B* **1996**, *30*, 61-63.

(116) Malinowska, E.; Gorski, L.; Meyerhoff, M. E. *Anal. Chim. Acta* **2002**, *468*, 133-141.

(117) Malinski, T.; Patton, S.; Kubaszewski, E. *Monitoring Molecules in Neuroscience, Proceedings of the International Conference on In Vivo Methods, 6th, Seignosse, Fr., Sept. 17-20, 1994* **1994**, 11-12.

(118) Nakagawa, K.; Sadaoka, Y.; Supriyatno, H.; Kubo, A.; Tsutsumi, C.; Tabuchi, K. *Sens. Actuators, B* **2001**, *76*, 42-46.

(119) Pedrosa, J. M.; Dooling, C. M.; Richardson, T. H.; Hyde, R. K.; Hunter, C. A.; Martin, M. T.; Camacho, L. *Mater. Sci. Eng., C* **2002**, *C22*, 433-438.

(120) Pedrosa, J. M.; Dooling, C. M.; Richardson, T. H.; Hyde, R. K.; Hunter, C. A.; Martin, M. T.; Camacho, L. *J. Mater. Chem.* **2002**, *12*, 2659-2664.

(121) Worsford, O.; Dooling, C. M.; Richardson, T. H.; Vysotsky, M. O.; Tregonning, R.; Hunter, C. A.; Malins, C. *J. Mater. Chem.* **2001**, *11*, 399-403.

(122) Dooling, C. M.; Worsfold, O.; Richardson, T. H.; Tregonning, R.; Vysotsky, M. O.; Hunter, C. A.; Kato, K.; Shinbo, K.; Kaneko, F. *J. Mater. Chem.* **2001**, *11*, 392-398.

(123) O'Riordan, T. C.; Buckley, D.; Ogurtsov, V.; O'Connor, R.; Papkovsky, D. B. *Anal Biochem* **2000**, *278*, 221-227.

(124) Furuto, T.; Lee, S. K.; Amao, Y.; Asai, K.; Okura, I. *J. Photochem. Photobiol., A* **2000**, *132*, 81-86.

(125) Ashkenasy, G.; Ivanisevic, A.; Cohen, R.; Felder, C. E.; Cahen, D.; Ellis, A. B.; Shanzer, A. *J. Am. Chem. Soc.* **2000**, *122*, 1116-1122.

(126) Amao, Y.; Okura, I. *Analyst (Cambridge, U. K.)* **2000**, *125*, 1601-1604.

(127) Amao, Y.; Asai, K.; Okura, I. *J. Porphyrins Phthalocyanines* **2000**, *4*, 292-299.

(128) Qin, W.; Parzuchowski, P.; Zhang, W.; Meyerhoff, M. E. *Anal. Chem.* **2003**, *75*, 332-340.

(129) Delmarre, D.; Bied-Charreton, C. *Sens. Actuators, B* **2000**, *62*, 136-142.

(130) Leray, I.; VerniËres, M.-C.; Bied-Charreton, C. *Sens. Actuators, B* **1999**, *54*, 243-251.

(131) Nakazawa, J.; Mizuki, M.; Shimazaki, Y.; Tani, F.; Naruta, Y. *Org. Lett.* **2006**, *8*, 4275-4278.

(132) D'Souza, F.; Deviprasad, G. R. *J. Org. Chem.* **2001**, *66*, 4601-4609.

(133) Weiss, J. *J. Inclusion Phenom. Mol. Recognit. Chem.* **2001**, *40*, 1-22.

(134) Kim, Y.-H.; Hong, J.-I. *Chem. Commun.* **2002**, 512-513.

(135) Imahori, H.; Fukuzumi, S. *Adv. Funct. Mater.* **2004**, *14*, 525-536.

(136) Harima, Y.; Miyatake, M.; Price, P.; Yamashita, K. *Chem. Phys. Lett.* **1996**, *262*, 274-278.

(137) Hu, J.-S.; Guo, Y.-G.; Liang, H.-P.; Wan, L.-J.; Jiang, L. *J. Am. Chem. Soc.* **2005**, *127*, 17090-17095.

(138) Ring, D. J.; Aragoni, M. C.; Champness, N. R.; Wilson, C. *Crystal Engineering Communications* **2005**, *7*, 621-623.

(139) Malinowska, E.; Meyerhoff, M. E. *Anal. Chim. Acta* **1995**, *300*, 33-43.

(140) Bakker, E.; Buehlmann, P.; Pretsch, E. *Chem. Rev.* **1997**, *97*, 3083-3132.

(141) Buhlmann, P.; Pretsch, E.; Bakker, E. *Chem. Rev.* **1998**, *98*, 1593-1688.

(142) Amemiya, S.; Buhlmann, P.; Umezawa, Y.; Jagessar, R. C.; Burns, D. H. *Anal. Chem.* **1999**, *71*, 1049-1054.

(143) Steinle, E. D.; Amemiya, S.; Buhlmann, P.; Meyerhoff, M. E. *Anal. Chem.* **2000**, *72*, 5766-73.

(144) Malinowska, E.; Niedziolka, J.; Meyerhoff, M. E. *Anal. Chim. Acta* **2001**, *432*, 67-78.

(145) Malinski, T.; Taha, Z. *Nature* **1992**, *358*, 676-678.

(146) Paolesse, R.; Mandoj, F.; Marini, A.; Di Natale, C. *Encyclopedia of Nanoscience and Nanotechnology* **2004**, *9*, 21-42.

(147) DiMagno, S. G.; Dussault, P. H.; Schultz, J. A. *J. Am. Chem. Soc.* **1996**, *118*, 5312-5313.

(148) Pozzi, G.; Montanari, F.; Quici, S. *Chemical Communications (Cambridge)* **1997**, 69-70.

(149) Liu, C.; Shen, D.-M.; Chen, Q.-Y. *Eur. J. Org. Chem.* **2006**, 2703-2706.

(150) Tamiaki, H.; Nishiyama, T.; Shibata, R. *Bioorg. Med. Chem. Lett.* **2007**, *17*, 1920-1923.

(151) Korotchenko, V. N.; Severin, K.; Gagne, M. R. *Org. Biomol. Chem.* **2008**, *6*, 1961-1965.

(152) Vasil'ev, V. V.; Borisov, S. M. *Sens. Actuators, B* **2002**, *82*, 272-276.

(153) O'Neal, K.; Weber, S. G. *J. Phys. Chem. B* **2008**, *113*, 149-158.

(154) Buhlmann, P.; Boswell, P. G.; (Regents of the University of Minnesota, USA). Application: WO

WO, 2006, p 68pp.

(155) El Bakkari, M.; Fronton, B.; Luguya, R.; Vincent, J.-M. *J. Fluorine Chem.* **2006**, *127*, 558-564.

(156) El Bakkari, M.; Luguya, R.; Correa da Costa, R.; Vincent, J.-M. *New J. Chem.* **2008**, *32*, 193-196.

(157) Schumacher, H. J.; Wolff, K. *Z. physik. Chem.* **1934**, *B26*, 453-62.

(158) Schumacher, H. J.; Sundhoff, D. *Z. physik. Chem.* **1936**, *B34*, 300-8.

(159) Adler, A. D.; Longo, F. R.; Kampas, F.; Kim, J. *J. Inorg. Nucl. Chem.* **1970**, *32*, 2443-2445.

(160) Akins, D. L.; Zhu, H.-R.; Guo, C. *J. Phys. Chem.* **1996**, *100*, 5420-5425.

(161) Fleischer, E. B. *Inorg. Chem.* **1962**, *1*, 493-495.

(162) Nguyen, K. A.; Day, P. N.; Pachter, R.; Tretiak, S.; Chernyak, V.; Mukamel, S. *J. Phys. Chem. A* **2002**, *106*, 10285-10293.

(163) Kalyanasundaram, K. *Inorg. Chem.* **1984**, *23*, 2453-2459.

(164) Hambright, P. In *Porphyrins and Metalloporphyrins*; Smith, K. M., Ed.; Elsevier: Oxford, 1975, p 233-278.

(165) Hildebrand, J. H.; Cochran, D. R. F. *J. Am. Chem. Soc.* **1949**, *71*, 22-5.

(166) Anastas, P. T.; Warner, J. C. *Green Chemistry, Theory and Practice*; Oxford University Press: Oxford, NY, 1998.

(167) Li, S.; Weber, S. G. In *Applications of Solid Phase Microextraction*; Pawliszyn, J., Ed.; Royal Society of Chemistry: Letchworth, Hertfordshire, UK, 1999.

(168) Valenta, J. N.; Sun, L.; Ren, Y.; Weber, S. G. *Anal. Chem.* **1997**, *69*, 3490-3495.

(169) Sun, L.; Weber, S. G. *J Mol Recognit* **1998**, *11*, 28-31.

(170) Zhang, X.; Zhao, H.; Chen, Z.; Nims, R.; Weber, S. G. *Anal. Chem.* **2003**, *75*, 4257-4264.

(171) StataCorp; 9.2 ed. College Station, TX, 2007.

(172) Lai, C.-Z.; Koseoglu, S. S.; Lugert, E. C.; Boswell, P. G.; Rabai, J.; Lodge, T. P.; Buhlmann, P. *J. Am. Chem. Soc.* **2009**, *131*, 1598-1606.

(173) Lugert, E. C.; Lodge, T. P.; Buhlmann, P. *J. Polym. Sci., Part B: Polym. Phys.* **2008**, *46*, 516-525.

(174) Zoidis, E.; Yarwood, J.; Danten, Y.; Besnard, M. *Mol. Phys.* **1995**, *85*, 373 - 383.

(175) Castaneda, J. P.; Denisov, G. S.; Kucherov, S. Y.; Schreiber, V. M.; Shurukhina, A. V. *J. Mol. Struct.* **2003**, *660*, 25-40.

(176) Bureiko, S. F.; Denisov, G. S. *J. Mol. Struct.* **2004**, *700*, 49-53.

(177) Kho, Y. W.; Conrad, D. C.; Shick, R. A.; Knutson, B. L. *Indian Engineering Chemical Research* **2003**, *42*, 6511-6517.

(178) Dega-Szafran, Z.; Hrynio, A.; Szafran, M. *J. Mol. Struct.* **1990**, *240*, 159-174.

(179) Denisov, G. S.; Kuzina, L. A.; Furin, G. G. *Zhurnal Obshchei Khimii* **1995**, *65*, 1721-1725.

(180) Denisov, G. S.; Mikheev, V. A.; Sokornova, T. V.; Shraiber, V. M. *Khim. Fiz.* **1984**, *3*, 1109-1113.

(181) Denisov, G. S.; Golubev, N. S. *J. Mol. Struct.* **1981**, *75*, 1981.